Final Report

CORROSION RESISTANT ALLOYS FOR REINFORCED CONCRETE

(Contract Number BD 228)

submitted to

Florida Department of Transportation Research Center
605 Suwannee Street
Tallahassee, Florida 32399

submitted by

Francisco Presuel-Moreno
Department of Ocean Engineering
Florida Atlantic University – SeaTech Campus
101 North Beach Road
Dania Beach, Florida 33004

Rodney G. Powers (retired)
Florida Department of Transportation – State Materials Office
5007 NE 39th Avenue
Gainesville, Florida 32609

and

William H. Hartt
Hartt and Associates, Inc.
20914 Morada Court
Boca Raton, Florida 33433

September 1, 2008

Disclaimer

The opinions, findings, and conclusions expressed in this publication are those of the authors and not necessarily those of the State of Florida Department of Transportation.

SI* (MODERN METRIC) CONVERSION FACTORS

APPROXIMATE CONVERSIONS TO SI UNITS

Symbol	When You Know	Multiply By	To Find	Symbol
		LENGTH		
in	inches	25.4	millimeters	mm
ft	feet	0.305	meters	m
yd	yards	0.914	meters	m
mi	miles	1.61	kilometers	km
		AREA		
in^2	square inches	645.2	square millimeters	mm^2
ft^2	square feet	0.093	square meters	m^2
yd^2	square yard	0.836	square meters	m^2
ac	acres	0.405	hectares	ha
mi^2	square miles	2.59	square kilometers	km^2
		VOLUME		
fl oz	fluid ounces	29.57	milliliters	mL
gal	gallons	3.785	liters	L
ft^3	cubic feet	0.028	cubic meters	m^3
yd^3	cubic yards	0.765	cubic meters	m^3
	NOTE: volumes greater than 1000 L shall be shown in m^3			
		MASS		
oz	ounces	28.35	grams	g
lb	pounds	0.454	kilograms	kg
T	short tons (2000 lb)	0.907	megagrams (or "metric ton")	Mg (or "t")
		TEMPERATURE (exact degrees)		
^oF	Fahrenheit	5 (F-32)/9 or (F-32)/1.8	Celsius	^oC
		ILLUMINATION		
fc	foot-candles	10.76	lux	lx
fl	foot-Lamberts	3.426	$candela/m^2$	cd/m^2
		FORCE and PRESSURE or STRESS		
lbf	poundforce	4.45	newtons	N
lbf/in^2	poundforce per square inch	6.89	kilopascals	kPa

APPROXIMATE CONVERSIONS FROM SI UNITS

Symbol	When You Know	Multiply By	To Find	Symbol
		LENGTH		
mm	millimeters	0.039	inches	in
m	meters	3.28	feet	ft
m	meters	1.09	yards	yd
km	kilometers	0.621	miles	mi
		AREA		
mm^2	square millimeters	0.0016	square inches	in^2
m^2	square meters	10.764	square feet	ft^2
m^2	square meters	1.195	square yards	yd^2
ha	hectares	2.47	acres	ac
km^2	square kilometers	0.386	square miles	mi^2
		VOLUME		
mL	milliliters	0.034	fluid ounces	fl oz
L	liters	0.264	gallons	gal
m^3	cubic meters	35.314	cubic feet	ft^3
m^3	cubic meters	1.307	cubic yards	yd^3
		MASS		
g	grams	0.035	ounces	oz
kg	kilograms	2.202	pounds	lb
Mg (or "t")	megagrams (or "metric ton")	1.103	short tons (2000 lb)	T
		TEMPERATURE (exact degrees)		
^oC	Celsius	1.8C+32	Fahrenheit	^oF
		ILLUMINATION		
lx	lux	0.0929	foot-candles	fc
cd/m^2	$candela/m^2$	0.2919	foot-Lamberts	fl
		FORCE and PRESSURE or STRESS		
N	newtons	0.225	poundforce	lbf
kPa	kilopascals	0.145	poundforce per square inch	lbf/in^2

*SI is the symbol for the International System of Units. Appropriate rounding should be made to comply with Section 4 of ASTM E380.
(Revised March 2003)

Technical Report Documentation Page

1. Report No.	2. Government Accession No.	3. Recipient's Catalog No.
4. Title and Subtitle Corrosion Resistant Alloys for Reinforced Concrete		5. Report Date September 1, 2008 6. Performing Organization Code
7. Author(s) William H. Hartt,* Rodney G. Powers,** Francisco Presuel Moreno,* Mario Paredes,** Ronald Simmons,** Hui Yu,* Rodrigo Himiob* (See Box 9)		8. Performing Organization Report No. FAU-OE-CMM-0801
9. Performing Organization Name and Address *Florida Atlantic University – Sea Tech Campus 101 North Beach Road Dania Beach, FL 33004 **Florida Department of Transportation – State Materials Office, 5007 NE 39th Street Gainesville, FL 32609		10. Work Unit No. (TRAIS) 11. Contract or Grant No. BD 228
12. Sponsoring Agency Name and Address ***Office of Infrastructure Research and Development Federal Highway Administration 6300 Georgetown Pike McLean, VA 22012		13. Type of Report and Period Covered Final Report 14. Sponsoring Agency Code

15. Supplementary Notes
Contracting Officer's Technical Representative (COTR): Y.P. Virmani, HRDI-10

16. Abstract

Deterioration of concrete bridges because of reinforcing steel corrosion has been recognized for four-plus decades as a major technical and economic challenge for the United States. As an option for addressing this problem, renewed interest has focused on corrosion resistant reinforcements, stainless steels in particular. The present research study was performed jointly by Florida Atlantic University and the Florida Department of Transportation to evaluate reinforcements of this type. These reinforcements included solid stainless steels 3Cr12 (UNS-S41003), 2101LDX (ASTM A955-98), 2304 (UNS-S32304), 2205 (UNS 31803), two 316L (UNS S31603) alloys, and two 316 stainless steel clad black bar products, and MMFX-2 (ASTM A1035). Black bar (ASTM A615) reinforcement provided a baseline for comparison purposes. Results from short term tests and preliminary results from long-term exposure of reinforced concrete slabs were presented in the first Interim Report (FHWA-HRT-07-039) for this project. This report provides longer-term data and analyses of four different types of reinforced concrete specimens, two of which were intended to simulate northern bridge decks exposed to deicing salts and the remaining two to substructure elements undergoing seawater exposure. Three different concrete mix designs were employed, and specimen types included variables such as a 1) simulated concrete crack, 2) bent top bar, 3) corrosion resistant upper bar(s) and black steel lower bars, and 4) intentional clad defects such that the carbon steel substrate was exposed. Cyclic wet-dry ponding with a sodium chloride (NaCl) solution was employed for the former two specimen types, and continuous partial submergence in either a NaCl solution or at a coastal marine site in Florida for the latter two. The exposures were for periods in excess of four years. The candidate alloys were ranked according to performance, and an analysis is provided that projects performance in actual concrete structures. A subsequent final report is to be issued at a later time.

17. Key Word	18. Distribution Statement
Reinforced concrete, bridges, corrosion resistance, corrosion testing, high performance reinforcement, stainless steel, MMFX-2 steel	No restrictions. This document is available to the public through NTIS, Springfield, VA 22161

19. Security Classif. (of this report)	20. Security Classif. (of this page)	21. No. of Pages	22. Price
Unclassified	Unclassified	131	

Form DOT F 1700.7 (8-72) Reproduction of completed page authorized

EXECUTIVE SUMMARY

Deterioration of concrete bridges because of reinforcing steel corrosion has been recognized for four-plus decades as a major technical and economic challenge both for the United States and for Florida. As an option for addressing this problem, renewed interest has focused recently on corrosion resistant reinforcements, stainless steels in particular. The present research study was performed jointly by Florida Atlantic University and the Florida Department of Transportation to evaluate such reinforcements. Candidate alloys were solid stainless steels 3Cr12 (UNS-S41003), 2101LDX (ASTM A955-98), 2304 (UNS-S31803), 2205 (UNS 31803), two 316L (UNS S31603) alloys, and two 316 stainless steel clad black bar products, and MMFX 2 (ASTM A1035). Black bar (ASTM A615) reinforcement provided a baseline for comparison purposes. Results from short term tests and preliminary results from long-term exposures of reinforced concrete slabs were presented in an Interim Report for this project published by the Federal Highway Administration as Report No. FHWA-HRT-07-039. This final report provides longer-term data and analyses of chloride exposures that involved four different types of reinforced concrete specimens, two of which were intended to simulate northern bridge decks exposed to deicing salts and the remaining two to substructure elements undergoing seawater exposure. Three different concrete mix designs were employed, and specimen types included combinations with a 1) simulated concrete crack, 2) bent top bar, 3) corrosion resistant upper bar(s) and black steel lower bars, and 4) intentional clad defects or crevices between bars (or both) such that the carbon steel substrate was exposed (clad bars only), in addition to the standard condition where none of the above modifications were present. Cyclic wet-dry ponding with a sodium chloride (NaCl) solution was employed for the former two specimen types and continuous partial submergence in either a NaCl solution or at a coastal marine site in Florida for the latter two. The reinforcements were classified into two groups as either improved or high performers, where alloys in the former category initiated corrosion during the project time frame, albeit at times greater than for black bar, and ones in the latter did not, at least in cases for specimens of the standard configuration. Improved performers were 3Cr12, MMFX-2, and 2101, and the remaining were high performers. The critical Cl^- concentration, C_T, required to initiate corrosion on improved performance and black reinforcement was determined; and the ratio of the former to the latter was calculated. A lower limit for this ratio was calculated in the case of the high performance reinforcements. The C_T results serve as input to analyses for calculation of maintenance free service life of structures that utilize these reinforcements. This, in turn, facilitates determination of the benefit that can be derived from utilization of corrosion resistant reinforcements.

TABLE OF CONTENTS

TABLE OF CONTENTS (continued)

LIST OF FIGURES

LIST OF FIGURES (continued)

LIST OF FIGURES (continued)

page no.

LIST OF FIGURES (continued)

page no.

LIST OF FIGURES (continued)

page no.

LIST OF FIGURES (continued)

page no.

LIST OF FIGURES (continued)

page no.

LIST OF TABLES

LIST OF TABLES (continued)

LIST OF TABLES (continued)

LIST OF TABLES (continued)

1.0. INTRODUCTION

1.1. General

The United States has a major investment in its highway system, the operational performance of which, in conjunction with that of other transportation modes, is critical to economic strength and societal well being. While deterioration of structures with time is a normal and expected occurrence, the rate at which this has occurred for highway bridges since advent in the 1960's of a clear roads policy and application during wintertime of deicing salts in northern locations has been abnormally advanced and posed significant maintenance challenges. Also important is similar advanced deterioration of reinforced concrete bridges in coastal locations, both northern and southern, as a consequence of sea water and spray exposure. In both cases (deicing salt or marine exposure), the deterioration is a consequence of the aggressive nature of the chloride ion in combination with moisture and oxygen.[1] Over half of the total bridge inventory in the United States is of the reinforced concrete type, and these structures have been particularly affected. A recent study[2] indicated that the annual direct cost of corrosion to bridges is $5.9-9.7B. If indirect factors are included also, this cost can be as much as ten times higher.[3]

As this problem has manifested itself during the past 40-plus years, technical efforts have been directed towards, first, understanding the deterioration mechanism and, second, developing prevention and intervention strategies. With regard to the former, steel and concrete are in most aspects mutually compatible, as exemplified by the fact that, in the absence of chlorides, the relatively high pH of concrete pore solution (pH ≈ 13.0-13.8) promotes formation of a protective oxide (passive) film such that corrosion rate is negligible and decades of relatively low maintenance result. However, in the presence of chlorides, even at concentrations at the steel depth as low as 0.6 kg/m^3 (1.0 pcy) on a concrete weight basis,[4] the passive film may become locally disrupted and active corrosion may commence. Once this occurs, solid corrosion products form progressively near the steel-concrete interface and lead ultimately to concrete cracking and spalling. Figure 1-1 shows a photograph illustrating such damage for the case of a coastal bridge piling. Because corrosion induced deterioration is progressive, inspections for damage assessment must be routinely performed; and present Federal guidelines require a visual inspection every two years.[5] If indicators of deterioration are not addressed, then public safety is at risk. As an example, corrosion induced concrete spalls occur as potholes in a bridge deck and contribute to unsafe driving conditions. In the extreme, structural failure and collapse result.

1.2. Modeling of Reinforced Concrete Structure Deterioration and Service Life Projection.

Corrosion induced deterioration of reinforced concrete can be modeled in terms of three sequential component steps or periods: 1) time for corrosion initiation, T_i, 2) time, subsequent to corrosion initiation, for appearance of cracking on the external concrete surface (crack propagation), T_c, and 3) time for

Figure 1-1: Photograph of a cracked and spalled marine bridge piling.

surface cracks to evolve into spalls which progress to the point where maintenance beyond what is routine is required, T_s. The sum $T_c + T_s$ is termed the corrosion propagation period, T_p; and maintenance-free service life, T_{mf}, is then $T_i + T_p$. As defined, maintenance-free service life is not intended to include occasional minor or routine repairs, as are likely to be required for any structure of significant size prior to T_{mf} or even T_i being reached. Figure 1-2 illustrates these parameters schematically in conjunction with a plot of cumulative damage versus time (adapted from Tutti).[6] Thus, the critical challenge for T_{mf}

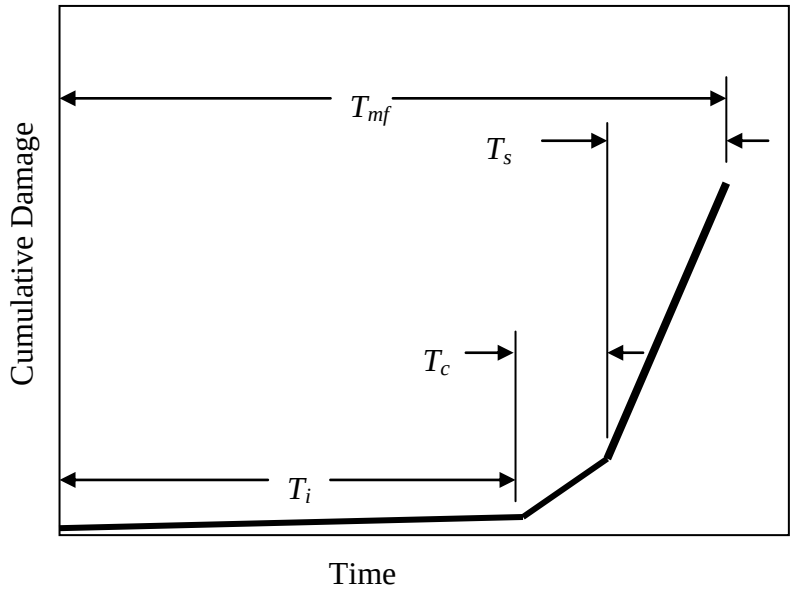

Figure 1-2: Schematic illustration of the various steps in deterioration of reinforced concrete due to chloride induced corrosion.

determinations is to develop data from either laboratory and test yard experiments or service experience (or both) that facilitate projection of T_i and T_p. Of course, T_i for actual structures cannot be determined directly from laboratory experimentation, since T_i for laboratory specimens is necessarily much briefer than for structures. However, it is generally recognized that passive film breakdown and initiation of active corrosion for reinforcing steel in concrete commence once a critical Cl^- concentration, C_T, is achieved at the reinforcement depth.[7] Consequently, if C_T is known from test yard exposures and the same value applies to actual structures, then T_i for the latter can be calculated using the solution to Fick's second law of diffusion, assuming that diffusion is the predominant Cl^- transport mechanism in both cases (test yard specimens and structure). Stating Fick's second law for one-dimensional diffusion as,

$$\frac{\partial^2 C(x,T)}{\partial T^2} = D_e \frac{\partial^2 C(x,T)}{\partial x^2} \qquad (1\text{-}1$$

where C(x,T) is $[Cl^-]$ after time T at distance x into the concrete in the direction of diffusion measured from the exposed surface and D_e is the effective diffusion coefficient which, as Eq. 1-1 is written, is assumed to be independent of x and T, then its solution is,

$$C(x,T) = C_s \cdot \mathrm{ERF}\left(\frac{x}{2 \cdot (D_e \cdot T)^{0.5}}\right), \qquad (1\text{-}2$$

where, C_s is $[Cl^-]$ at the concrete surface and ERF is the Gaussian error function. Further, at corrosion initiation C(x,T) is C_T, x is the rebar cover, and $T = T_i$. Thus,

$$C_T = C_s \cdot \mathrm{ERF}\left(\frac{x}{2 \cdot (D_e \cdot T_i)^{0.5}}\right). \qquad (1\text{-}3$$

This solution assumes that C_T, C_s, x, and D_e are spatially and chronologically constant, whereas they are, in fact, distributed parameters with the range for C_T varying by more than an order of magnitude.[8,9] Also, C_s and D_e may vary with exposure time and concrete age. Equation 1-3, as written, also considers that initial $[Cl^-]$ in the concrete is zero. Also implicit in this expression is that the diffusion media (concrete) is homogeneous and without cracks. Nonetheless, analyses based on Eq. 1-3 are generally accepted as a viable engineering tool for projection of T_i.

Less focus has been placed upon T_c; however, some authors have developed sophisticated models that consider the tendency for solid corrosion products about corroding reinforcement to develop tensile

hoop stresses and ultimately concrete cracking.[10] Variables that influence T_c include: 1) corrosion rate, 2) specific volume of solid corrosion products and rate at which these form, 3) concrete microstructure and strength, and 4) ratio of concrete cover to rebar diameter. Alternatively, T_c can be assumed as a specific time, for example, five years for surface cracks to appear in the case of black bar.[9] Less attention has focused upon T_s and any subsequent period that might lapse before maintenance intervention commences.

Based upon the corrosion deterioration model represented by Figure 1-2, methods of Life-Cycle Cost Analysis (LCCA) are now commonly employed to evaluate and compare different materials selection and design alternatives. This approach considers both initial cost and the projected life history of maintenance, repair, and rehabilitation expenses that are required to achieve the design life (synonymous with T_{mf}). These are evaluated in terms of the time value of money, from which Present Worth is determined; and comparisons between different options can then be made on a cost normalized basis. Thus, materials selection choices define C_T which, in combination with design parameters, allow calculation of T_i; and with estimation of T_c and T_s, T_{mf} can be projected. Iterations may be required depending upon cost and design life considerations. Figure 1-3 schematically illustrates this progression.

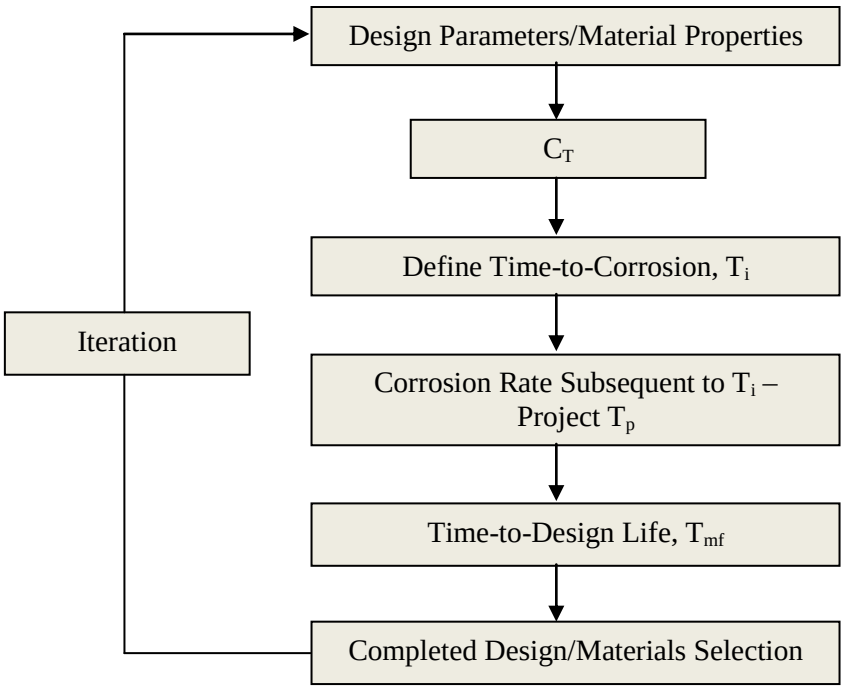

Figure 1-3: Representation of the sequential steps involved in the design process.

1.3. Epoxy-Coated Reinforcing (ECR) Steel

In the early 1970's, research studies were performed that qualified ECR as an alternative to black bar for reinforced concrete bridge construction;[11,12] and for the past 30 years ECR has been specified by most state Departments of Transportation (DOTs) for bridge decks and substructures exposed to chlorides. At the same time, concrete mix designs were improved by specification of low water-to-cement ratio (w/c), possibly admixed with pozzolans or corrosion inhibitors (or both), and covers over reinforcement of 65 mm or more.[13] However, premature corrosion induced cracking of marine bridge substructures in Florida[14,15,16,17] indicated that ECR is of little benefit for this type of exposure; and while performance of ECR in northern bridge decks has been generally good to-date (30-plus years), still the degree of corrosion resistance afforded in the long-term for major structures with design lives of 75-100 years is uncertain.

2.0. PROJECT OBJECTIVE

In response to the above concerns regarding ECR, interest has focused during the past 15 years upon more corrosion resistant alternatives to ECR, stainless steels in particular. Such alloys may become competitive on a life-cycle cost basis, since the higher initial expense of the steel per se may be recovered over the life of the structure via reduced maintenance expenses arising from corrosion induced damage.

Corrosion resistant reinforcements (CRR) may be advantageous beyond the considerations discussed above. This is illustrated by the flow diagram in Figure 1-4, where the obvious, explicit benefit of reduced corrosion rate and extended service life is indicated to the left. However, CRR can also impact design by possibly allowing concrete cover to be reduced which, in turn, should result in lower superstructure weight and potentially smaller substructure size and weight. Further, lower cover can lead to reduced width of concrete cracks and, hence, less corrosion at these which translates to lower maintenance costs.

This research was performed jointly by Florida Atlantic University and the Florida Department of Transportation as a six year effort to evaluate the suitability of various corrosion resistant reinforcements for concrete bridges exposed to chlorides. An initial phase of the study provided a critical literature review of corrosion resistant reinforcements,[18] and an initial Interim Report[19] was subsequently published. The present report updates results from this Interim Report and provides findings for the subsequent three years of the project.

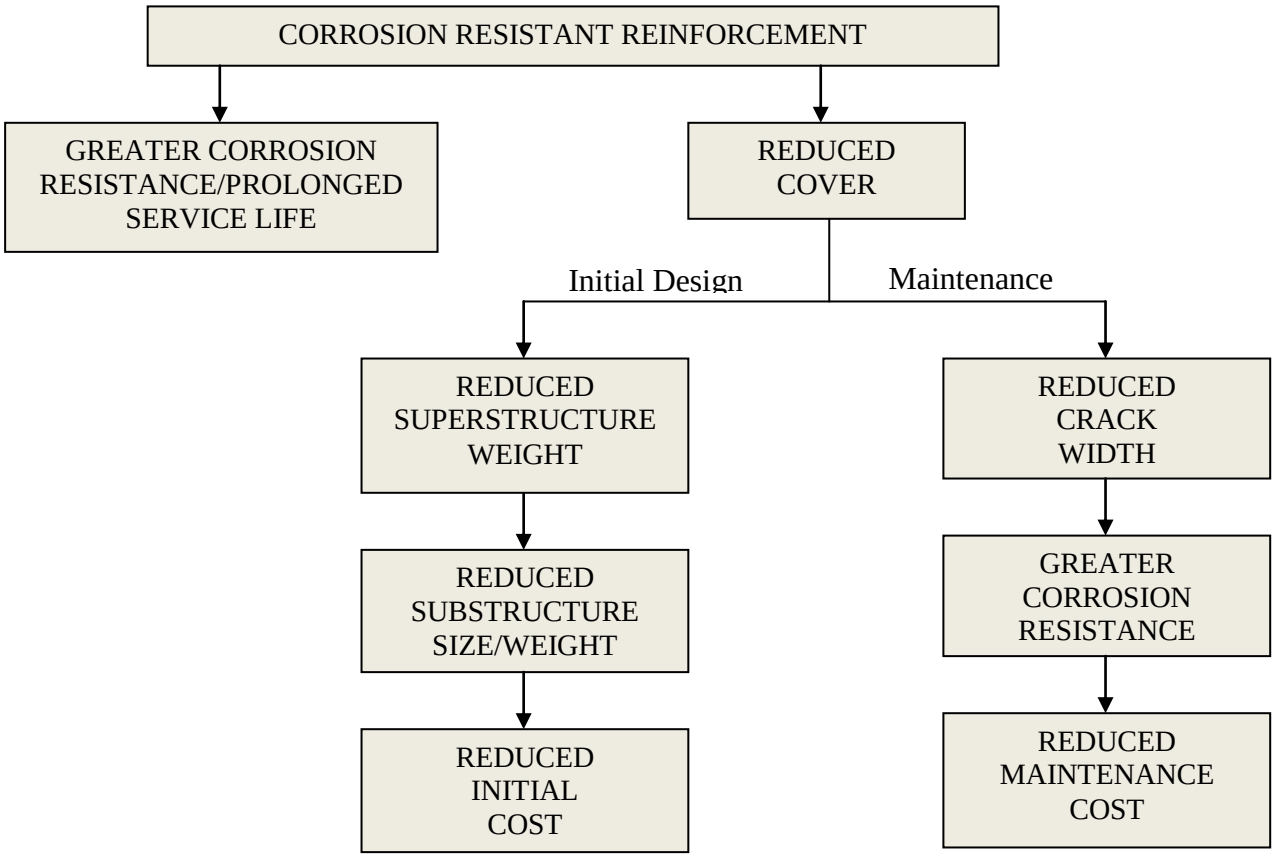

Figure 1-4: Schematic representation of benefits that can be derived from corrosion resistant reinforcements.

3.0. MATERIALS AND EXPERIMENTAL PROCEDURES

3.1. Reinforcing Steels

Table 3-1 lists the various steels that were employed in this study. These are the same as addressed in the initial Interim Report[19] for this project except that Types 304 and 2304SS were acquired in the meantime and added to the test matrix. Composition for all bars is shown in Table 3-2. Bar size in all cases was #5 (nominally 16 mm diameter) except for Type 304 SS which was #4 (12.7 mm diameter). The two types of clad bars (designated as STAX and SMI) were fabricated by two distinct processes, the former by packing a stainless steel tube with steel scrap followed by rolling and the latter by plasma spray application of stainless steel to a carbon steel billet and then rolling. Unless noted otherwise, bars were tested in the as-received surface condition.

3.2. Concrete Mix Designs

Three concrete mix designs, designated STD1 (5 bags cement and 0.50 water-to-cement ratio (w/c)) which yields a high permeability concrete, STD2 (7 bags of cement and 0.41 w/c) which results in

Table 3-1: Listing of reinforcements that were investigated.

Designation./Spec.	Common Design.	As-Rec'd. Cond.	Microstructure	PREN[1]	Supplier
UNS-S31603	Type 316LSS	Pickled[2]	Austenite	26.4 [3]	Slater Steels Corporation
				25.1 [4]	Dunkirk Specialty Steel
UNS-S30400	Type 304SS	Pickled[2]	Austenite	19.6	Dunkirk Specialty Steel
UNS-S32304	Type 2304SS	Pickled	Duplex (Austenite plus Ferrite)	24.9	UGITECH
ASTM A955-98	Type 2101LDXSS	As-Rolled	Lean Duplex (Austenite plus Ferrite)	25.1	Gerdau AmeriSteel Corp.
ASTM A1035	MMFX 2	As-Rolled	Microcomposite austenite-martensite	9.4	MMFX Corporation
AASHTO MP 13M/MP 13-04	Nouvinox	Pickled	316 Clad/Carbon Steel Core	-	Stelax Industries, Ltd.
	SMI	Pickled	316 Clad/Carbon Steel Core	-	CMC Steel Group
UNS-S41003	Type 3Cr12SS	Pickled	Ferritic	12	American Utility Metals
ASTM A615	Black Bar	As-Rolled	Ferrite/Pearlite	0.3	Gerdau AmeriSteel Corp.

[1] PREN (Pitting Resistance Equivalent Number) where PREN = %Cr + 3.3·%Mo + 16·%N

[2] Pickled with HF and nitric acid per ASTM A380.

[3] Subsequently designated as 316.16.

[4] Subsequently designated as 316.18.

Table 3-2: Composition of the reinforcements.

Alloy	C	Mn	P	S	Si	Cr	Ni	Mo	Cu	N	Fe
Type 316.16	0.03	1.55	0.025	0.001	0.59	18.43	10.06	2.08	0.42	0.068	Bal.
Type 316.18	0.03	1.66	0.026	0.005	0.42	16.97	10.07	2.15	0.85	0.065	Bal.
Type 304SS	0.07	0.94	0.020	0.001	0.58	18.25	8.12	0.40	0.30	-	Bal.
Type 2205SS	0.029	1.68	0.028	0.004	0.63	21.58	4.80	2.64	-	0.15	Bal.
Type 2304SS	0.03	1.16	0.026	0.002	0.45	22.33	4.16	0.25	0.30	0.11	Bal.
Type 2101SS	0.04	4.70	0.019	0.001	0.80	22.47	1.68	0.24	0.38	0.117	Bal.
A1035	0.05	0.45	0.012	0.015	0.23	9.30	0.10	0.03	0.12	-	Bal.
Type 3Cr12SS	0.04	0.38	0.018	0.024	0.71	11.69	0.50	0.09	0.02	-	Bal.
A615	0.30	1.22	0.013	0.032	0.26	0.21	0.19	0.04	-	-	Bal.

moderate permeability, and STD3 (7 bags of cement and 0.50 w/c), which is of improved permeability between that of STD1 and STD2, were employed. Target mix designs for each of these are listed in Table 3-3. The various corrosion resistant alloy types, in addition to black bar (Table 3-1), were used as reinforcement.

Table 3-3: Concrete batch mix design.

Material	STD1	STD2	STD3
Cement (Bags)	5	7	7
Cement, kg	213	300	300
Water, kg	107	122	149
Water/Cement	0.50	0.41	0.50
Fine Aggregate (silica sand), kg	652	540	489
Coarse Aggregate (limestone), kg	753	753	747

3.3. Specimen Types, Design, and Fabrication

3.3.1. General

Four different types of reinforced concrete specimens, designated 1) simulated deck slabs (SDS), 2) macro-cell slabs (MS), 3) 3-bar tombstone columns (3BTC), and 4) field columns (FC), were fabricated by the Florida Department of Transportation State Materials Office (FDOT-SMO) in Gainesville, FL. The first two specimen designs were intended to simulate a northern bridge deck or slab exposed to chlorides from either deicing salts or sea water, whereas the latter two represent a marine substructure element. The SDS specimens underwent exposure at FAU, the MS and 3BTC at the FDOT-SMO Corrosion Laboratory in Gainesville, FL, and the FC at an inter-coastal waterway site at Crescent Beach, FL. The standard specimen (STD) consisted of all straight bars in the as-received condition in concrete

compacted according to ASTM C192.[20] However, other specimens employed variations of this according to the description and nomenclature listed in Table 3-4.

Prior to casting, the reinforcement was degreased by cleaning with hexane, followed by the application of heat shrink tubing at the bar ends to provide an electrical barrier at the concrete-reinforcement interface leaving only the center portion of the reinforcement to within approximately 25 mm of the concrete surface exposed. The casting procedure was similar for all specimen types. This involved placement of freshly mixed concrete in the specimen molds in two lifts followed by consolidation of each lift for 20 to 30 seconds on a vibration table. The first lift filled the specimen mold approximately half full, and the second lift completely filled the mold. The surface of the specimens was troweled smooth using a wooden or metal float. After 24 hours, the molds were dissembled; and the specimens were removed, placed in sealed plastic bags, and stored for six months. The design of each of the four specimen types is provided below.

3.3.2. Simulated Deck Slab (SDS) Specimens.

The simulated deck slab (SDS) specimens were fabricated with six bars, three of which comprised a top and three a bottom layer, as illustrated schematically in Figure 3-1. Concrete cover for all bars was 25 mm, and triplicate specimens were prepared for each bar type and specimen variable (described below). Because of the large inventory of specimens, fabrication and delivery to FAU occurred at six different times. The Interim Report[19] provided results for exposure of the initial three specimens lots (Lots 1-3), and data for these has been updated in this report. In addition, data acquired from the final three lots (Lots 4-6) are presented and discussed. Lots 4-6 specimens are listed in Table 3-5. A distinction between the initial and final three lots is that heat shrink end sleeves were not installed on bar ends of Lots 1-3 specimens. Because of concern that absence of sleeves on bars of the initial three lots may have resulted in premature corrosion initiation where rebars exited the concrete, replicates of black bar (BB), 3Cr12, MMFX-2, and 2101 reinforced specimens (these were the only STD type specimens that initiated corrosion) were included in Lot 5. Otherwise, specimens of Lots 4-6 consisted of reinforcement types/specimen configurations that were not present in Lots 1-3. The following example illustrates the nomenclature that was adapted to identify a standard specimen:

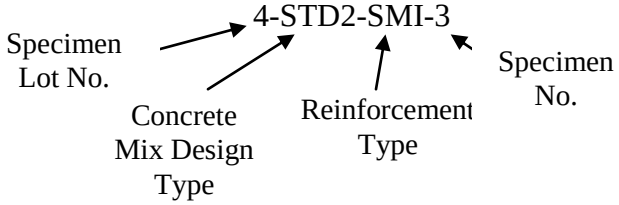

Table 3-4: Listing of the various specimen types, variables, and the nomenclature for each.

Specimen Designation	Description	Specimen Type
STD1	STD1 concrete mix.	SDS, FC
STD2	STD2 concrete mix.	SDS, 3BTC
STD3	STD3 concrete mix.	3BTC
BCAT	STD1 concrete, bottom mat black steel.	SDS, MS
CCON	STD1 concrete mix, simulated concrete crack.	SDS, MS
CCNB	STD1 concrete mix, bottom mat (cathode) black bars, simulated concrete crack.	SDS, MS
CREV	STD1 concrete mix, top bar crevice.	SDS
CCRV	STD1 concrete mix, simulated concrete crack, top bar crevice.	SDS
BENT	STD1 concrete mix, top bar bent	MS
	STD3 concrete mix, top bar bent	3BTC
BNTB	STD1 concrete mix, top bar bent, bottom bars black steel.	MS
CBNT	STD1 concrete mix, simulated concrete crack, top bar bent.	MS
CBNB	STD1 concrete mix, simulated concrete crack, bottom bars black steel, top bar bent.	MS
ELEV	STD3 concrete mix, one bar elevated.	3BTC
WB	STD1 concrete mix, top bars wire brushed.	SDS
ARWB	STD1 concrete mix, top bars as received.	MS
USDB	STD1 concrete mix, 3 mm diameter clad holes 25 mm apart on top bars.	SDS, MS
UBDB	STD1 concrete mix, 3 mm diameter clad holes 25 mm apart on top bars, top bar bent.	MS
CSDB	STD1 concrete mix, simulated concrete crack, 3 mm diameter clad holes 25 mm apart.	SDS, MS
CBDB	STD1 concrete, cracked concrete, 3 mm diameter clad holes 25 mm apart on top bars, top bar bent.	MS
BCCD	STD1 concrete mix, 3 mm diameter clad holes 25 mm apart on top bars, bottom bars black steel.	SDS. MS
ACID	STD1 concrete mix, top bars lab pickled, cathode as received.	SDS
ABRD	STD1 concrete mix, blasted/abraded top bars, bottom bars as received.	SDS
CVNC	STD1 concrete mix, top bar crevice, no end caps.	SDS

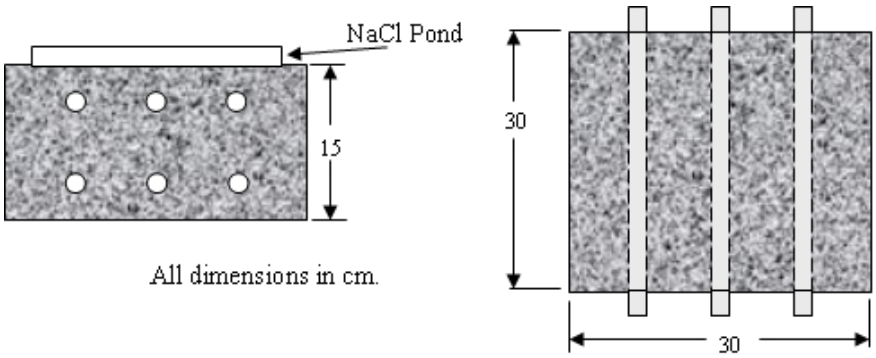

Figure 3-1: Schematic illustration of the standard simulated deck slab specimens (heat shrink tubing at bar ends not shown).

Table 3-5: Listing of Lots 4-6 SDS specimens.

Lot 4 Specimens	Lot 5 Specimens	Lot 6 Specimens
4-STD2-SMI-1	5-STD1-2304-1	6-CCRV-304-1
4-STD2-SMI-2	5-STD1-2304-2	6-CCRV-304-2
4-STD2-SMI-3	5-STD1-2304-3	6-CCRV-304-3
4-STD1-SMI-1	5-STD1-MMFX-1	6-CCON-304-1
4-STD1-SMI-2	5-STD1-MMFX-2	6-CCON-304-2
4-STD1-SMI-3	5-STD1-MMFX-3	6-CCON-304-3
4-CCON-SMI-1	5-STD1-BB-1	6-WB-304-1
4-CCON-SMI-2	5-STD1-BB-2	6-WB-304-2
4-CCON-SMI-3	5-STD1-BB-3	6-WB-304-3
4-CREV-SMI-1	5-STD1-2201-1	6-CVNC-SMI-1
4-CREV-SMI-2	5-STD1-2201-2	6-CVNC-SMI-2
4-CREV-SMI-3	5-STD1-2201-3	6-CVNC-SMI-3
4-BCCD-SMI-1	5-STD1-3Cr12-1	6-CCNB-304-1
4-BCCD-SMI-2	5-STD1-3Cr12-2	6-CCNB-304-2
4-BCCD-SMI-3	5-STD1-3Cr12-3	6-CCNB-304-3
4-CCRV-SMI-1	5-USDB-MMFX-1	6-CREV-304-1
4-CCRV-SMI-2	5-USDB-MMFX-2	6-CREV-304-2
4-CCRV-SMI-3	5-USDB-MMFX-3	6-CREV-304-3
4-USDB-SMI-1	-	6-STD1-304-1
4-USDB-SMI-2	-	6-STD1-304-2
4-USDB-SMI-3	-	6-STD1-304-3
4-CCRV-3Cr12-1	-	6-STD2-304-1
4-CCRV-3Cr12-2	-	6-STD2-304-2
4-CCRV-3Cr12-3	-	6-STD2-304-3
4-CSDB-SMI-1	-	6-BCAT-304-1
4-CSDB-SMI-2	-	6-BCAT-304-2
4-CSDB-SMI-3	-	6-BCAT-304-3

There were six specimen lots, and these correspond to the order in which they were fabricated and delivered to FAU by FDOT. Likewise, designation of specimens that were non-standard (BCAT, CCON, …, see Table 3-4) is illustrated by the example below:

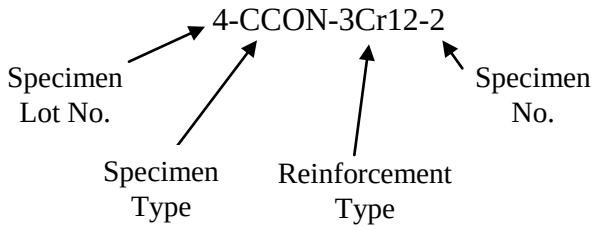

Thus, the last digit identifies this as simulated deck slab specimen no. 2. The reinforcement is 3Cr12 with a simulated crack from Lot 4. The default mix design (no indication) is STD1. Concrete mix designs STD1 and STD2 were employed for Type 304SS and SMI bars but with most specimens being prepared using the former. Eight different modifications to the above standard SDS specimen configuration were prepared and exposed, as listed and described below.

1. Slabs with a corrosion resistant bar type for the top layer and black bars in the bottom (designated BCAT). All specimens of this type, except for those reinforced with Type 304SS, were included in the first three lots; and results were provided in the Interim Report.[19] Results for Type 304SS BCAT specimens are presented here.

2. Slabs with a simulated concrete crack (designated CCON). In fabrication of these specimens, a 1.6 mm thick stainless steel shim was placed vertically in the form on top of and perpendicular to the upper bars at the mid span. The shim was removed subsequent to initial concrete set. Reinforcement types in Lots 4-6 SDS specimens that employed this configuration were Type 304SS and SMI.

3. Slabs with a bar splice that formed a crevice (designated CREV). In this case, two bars that overlapped for a portion of their embedded length replaced each of the three single top bars in the standard specimen. Hence, the top reinforcement layer consisted of six rebars instead of three, as was the case for the other specimen types. Cover for each of the bar pairs was maintained at 25 mm. Figure 3-2 illustrates this specimen type schematically. Reinforcement types in Lots 4-6 SDS specimens that employed this configuration were Type 304SS and SMI.

4. Slabs with a bar crevice (splice) per the above configuration but also with a simulated concrete crack (designated CCRV). Reinforcement types in Lots 4-6 SDS specimens that employed this configuration were 3Cr12, Type 304SS, and SMI.

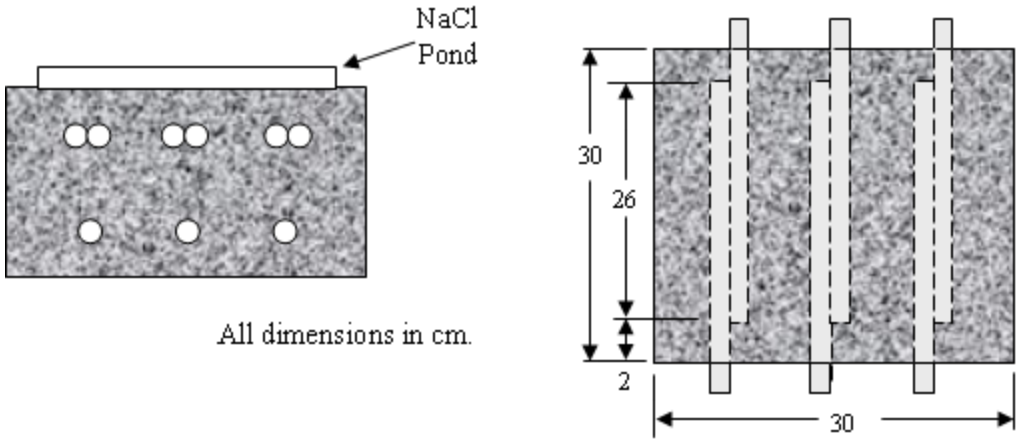

Figure 3-2: Schematic illustration of the CREV type simulated deck slab specimens.

5. Slabs with a simulated concrete crack and black bar cathode (designated CCNB). The only reinforcement type in Lots 4-6 SDS specimens that employed this configuration was Type 304SS.
6. Slabs with wire brushed bars (designated WB). Only specimens with Type 304SS bars in Lot 6 employed this condition.
7. Slabs with a simulated concrete crack and 3 mm holes drilled through the cladding on the top of upper bars at 25 mm spacing (designated CSDB). Only specimens with SMI bars were employed in this condition.
8. Slabs with 3 mm holes drilled through the cladding or surface layer on the top of upper bars at 25 mm spacing (USDB). Reinforcement types in Lots 4-6 SDS specimens that employed this configuration were SMI and MMFX-2.

Upon delivery to FAU, an electrical connection was established between bars in each of the two layers of each slab using a stainless steel wire in conjunction with a drilled hole and connection screw at one end of each bar. Periodically, a 10 Ω resistor was temporarily inserted in the circuit between the two bar layers; and voltage drop across this was then measured, from which macro-cell current was calculated. The specimen sides were coated with a UV resistant paint, inverted relative to their orientation at casting, and a plastic bath with a vented lid was mounted on what was the bottom formed face. Prior to ponding, the specimens were stored outdoors in a covered location for two months at the FAU Sea Tech Campus which is approximately 300 m inland from the Atlantic Ocean southeast of Ft. Lauderdale. The initial week of ponding was with potable water to promote saturation or a high humidity pore structure so that, upon ponding, diffusion and not sorption would be the primary Cl^- ingress

mechanism. This was followed by cyclic one week wet – one week dry ponding with 15 wt% NaCl. The salt water pondings commenced on July 26, 2005, August 10, 2005, and December 11, 2006, respectively, for Lots 4, 5, and 6. Figure 3-3 is a photograph of a mold with CCRV-SMI reinforcement prior to concrete pouring. Figure 3-4 shows two specimens under test, and Figure 3-5 is a perspective view of the test site.

Figure 3-3: View of a mold for a CCRV-SMI specimen prior to concrete pouring.

Figure 3-4: Photograph of two SDS specimens under exposure.

Figure 3-5: Photograph of SDS specimens under exposure in the outdoor test yard.

Monitoring of potential of electrically connected bars of individual specimens and of voltage drop between bar layers was performed weekly. The onset of active corrosion was defined as having occurred if a measureable voltage drop was detected for two consecutive measurement periods. This detection limit corresponded to a current of 0.1 μA. Subsequent to the BB specimens becoming active (the first specimens to do so), the potential and voltage drop measurement procedure was modified, as follows:

1. Once corrosion activity was detected according to the voltage drop criterion (see above), each of the top bars was electrically isolated temporarily from all other bars.
2. Individually, each of the three top bars was then connected through a 10 Ω resistor to the three bottom bars and voltage drop measured. By this, the top bar(s) that was active was identified.
3. The top bar(s) for which voltage drop was zero were reconnected to the three bottom bars, leaving the top bar(s) that did show corrosion activity isolated; and exposure and monitoring of the remaining connected bars continued.
4. Steps 1-3 were repeated as successive bars became active. Once corrosion activity was detected for the last of the three top bars, testing of that slab was discontinued and the specimen dissected.

3.3.3. Macro-cell Slab (MS) Specimens

The design for these specimens is a modification of the standard G109 geometry and consisted of either a single straight or bent top bar and four straight bottom bars, the latter being positioned at two elevations

beneath the top bar. This geometry is illustrated by Figure 3-6. The standard condition was with the reinforcement wire brushed, but one set was prepared with bars as-received (ARWB). The STD1

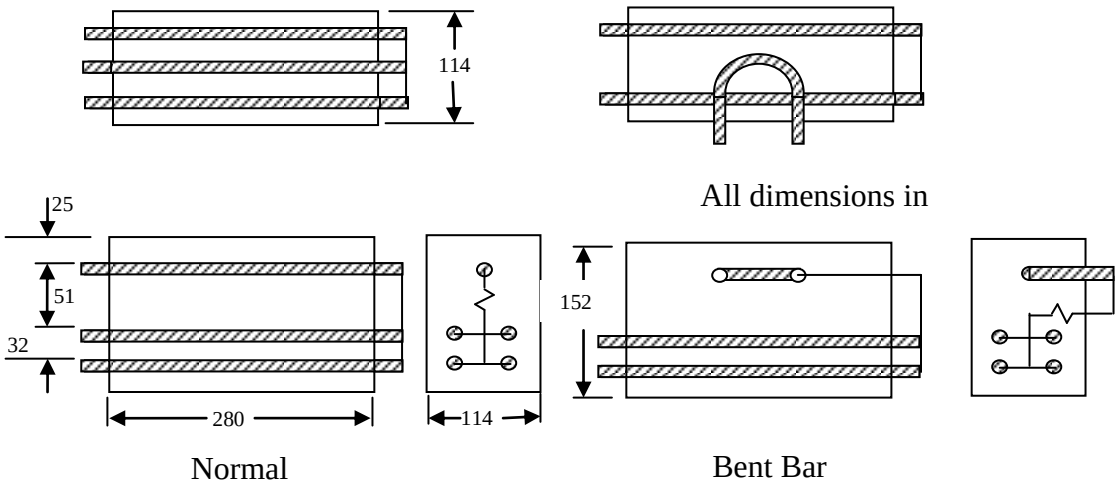

Figure 3-6: Geometry of the macro-cell slab type specimen with both bent and straight bars (all dimensions in mm).

specimens were fabricated with and without a simulated crack, but specimens based upon the STD2 concrete mix were of the standard type only (no crack). The types of specimens that were fabricated are indicated in Table 3-4 with individual specimens identified according to the same convention that was explained above for SDS specimens except that "MS" is included in the nomenclature. Subsequent to curing, the specimens were inverted relative to the orientation at casting; and a 76x152 mm plastic container for ponding was attached to what had been the bottom cast face. The top bar was wired to the four lower bars through a one Ohm resistor via 16 gauge multi-strand wire and solder eyelet connectors, the latter being attached to bar ends using a stainless steel screw mounted into a hole drilled into the end of each bar. The specimens were subjected to a 14 days wet – 14 days dry cyclic ponding with a 3.0 wt% NaCl solution until corrosion induced cracking occurred. Duplicate sets of three STD1 specimens were prepared with one set being exposed in a screened, covered outdoor location and the second (designated STD1G) in a constant temperature (25^{o}C) and relative humidity (50 percent) room. In addition, a single set of three other reinforcement/specimen types (see Table 3-4) and of STD2 specimens were prepared and exposed in the same outdoor location noted above. Figure 3-7 shows a photograph of three specimens, and Figure 3-8 is a perspective view of the outdoor exposure. For both the controlled and ambient outdoor exposures, potential was recorded monthly, and current was recorded daily via an Agilent 34970A data acquisition system.

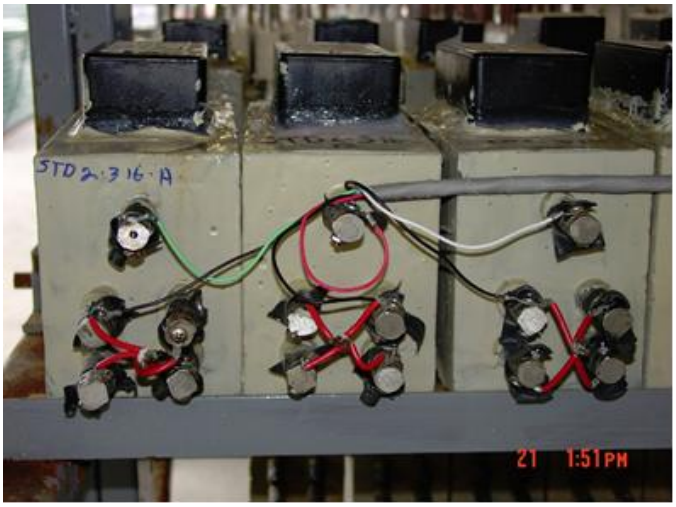

Figure 3-7: Photograph of three MS specimens under exposure.

Figure 3-8: Photograph of macro-cell slab specimens under exposure.

3.3.4. 3-Bar Tombstone Column (3BTC) Specimens

As noted above, the 3BTC specimens were intended to simulate a marine bridge substructure element. Three bar configurations, normal (STD), bent (BENT), and elevated (ELEV), were prepared, as illustrated schematically in Figures 3-9; and concrete mixes STD2 and STD3 (Table 3-3) were employed. Figure 3-10 shows a photograph of bars of the bent configuration in a mold prior to concrete placement. The bar clamping and alignment method that is illustrated here served to maintain the intended cover (24 mm) to within close tolerance. The normal reinforcement configuration has been employed by the FDOT for more than ten years and is intended to provide baseline data that can be compared to results from previous studies. On the other hand, the bent bar configuration was considered particularly relevant in the case of stainless clad and possibly MMFX-2 reinforcements because of the possibility of clad or surface layer cracking. Reinforcements that were employed were BB, 3Cr12, MMFX-2, 2101, Types 316 and 304 SS,

and SMI. Six specimens with each rebar type were prepared for the STD2 and STD3 BB type specimens. Otherwise, the number of specimens was three. Figure 3-11 is a photograph of a specimen after casting. Prior to exposure, a one Ohm resistor was wired between each long bar and the other two bars using the procedure described above for the MS specimens. Subsequent to curing, specimens were positioned vertically in a plastic tank and submerged in a 3.5 wt% NaCl solution to a depth of 152 mm for the purpose of facilitating formation of an electrochemical macro-cell on each of the longer bars. Figure 3-12 shows specimens under exposure in the outdoor screened room at the FDOT-SMO Corrosion Laboratory.

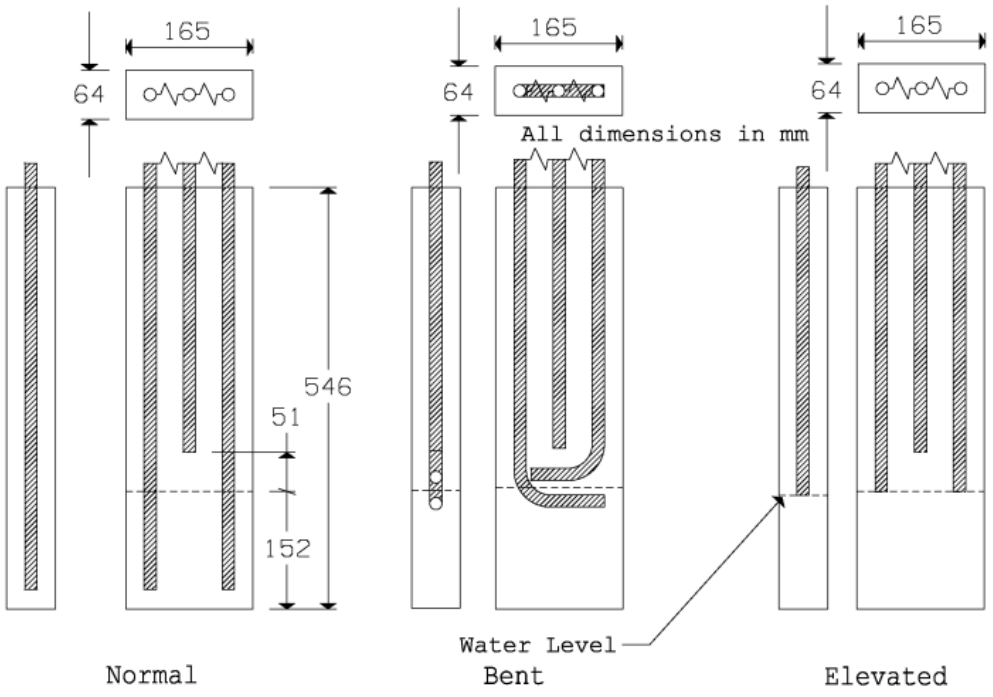

Figure 3-9: Schematic illustration of the tombstone type 3-bar column specimen for each of the three bar configurations.

Once exposure was initiated, potential of all three bars coupled and voltage drop across the two resistors was measured daily for each specimen utilizing a pair of Agilent 34970A data acquisition systems. Exposure of individual specimens was terminated upon concrete cracking or appearance of visible corrosion product bleed-out.

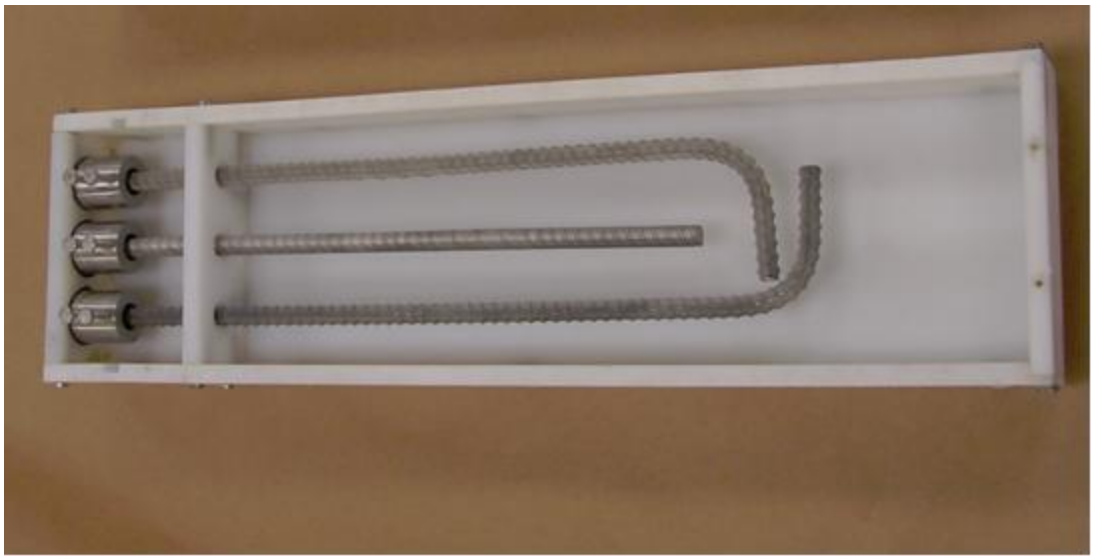

Figure 3-10: Photograph of Type 304 rebars of the bent configuration in a mold prior to concrete placement.

Figure 3-11: Photograph of a 3BTC specimen.

Figure 3-12: Photograph of 3BTC specimens under exposure.

3.3.5. Field Column (FC) Specimens

All specimens of this type were based upon the STD1 concrete mix design only and with bars in the as-received condition. Figure 3-13 is a schematic drawing that illustrates the specimen geometry. Reinforcements that were employed were black bar, 3Cr12, MMFX-2, 2101, 316.16SS, 304SS, and SMI with end caps. Each bar was electrically isolated from the others while exposed and during potential measurements. The columns were exposed in the inter-coastal waterway at Crescent Beach, Florida by jetting the lower 1.2 m in sand such that mean high water was approximately 1.8 m from the specimen bottom. Placement was delayed because of environmental permitting issues but commenced in September, 2005. Figure 3-14 is a photograph of the specimens installed at the exposure site. A single potential was measured for each of the four bars by placing a copper-copper sulfate electrode in the moist sand near the base of the column. Polarization resistance, R_p, of one bar in each column was determined using an embedded Ti electrode as reference and one of the other three bars as a counter electrode. A cyclic polarization scan was performed to calculate total resistance, R_t; and solution resistance, R_s, was determined using a 3-point resistance test. Finally, R_p was calculated as $R_t - R_s$. These measurements were performed at the time of initial exposure and at approximately six month intervals subsequently until corrosion induced cracking or visible corrosion product bleed out was observed.

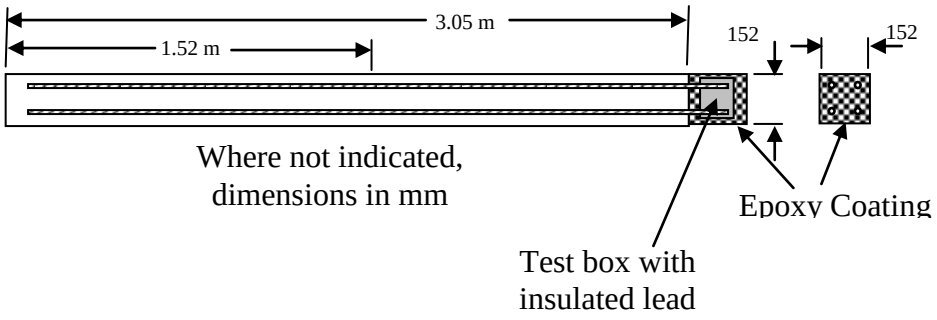

Figure 3-13: Geometry of the field column type specimen.

Figure 3-14: Photograph of field column specimens under exposure at the Intracoastal Waterway site in Crescent Beach, Florida.

Tables 3-8 to 3-13 of the Interim Report[19] list all specimens of each of the four designs that had been deployed as of that submission, and these are reproduced here as Tables 3-6 to 3-11. Shaded cells in these tables indicate specimens that had not been fabricated at the time the earlier report was prepared, but these were included in the Lots 4-6 inventory (see Table 3-1).

Table 3-6: Listing of specimens reinforced with 316.18 and 3Cr12 (Table 3-8 from the first Interim Report for this project).

Description	SDS	S3BC	3BTC	MS	FC
STD1 mix design, standard specimen.	3	6	-	6	3
STD3 mix design, standard specimen.	3	3	3	3	-
STD2 mix design, standard specimen.	-	-	6	-	-
STD1-BCAT.	3	-	-	3	-
STD1-CCON.	3	-	-	3	-
STD1-CCNB.	3	-	-	3	-
STD1-CREV.	3	-	-	-	-
STD1-CCRV.	3	-	-	-	-
STD1-BENT.	-	3	-	3	-
STD3-BENT.	-	-	3	-	-
STD1-BNTB.	-	-	-	3	-
STD1-CBNT.	-	-	-	3	-
STD1-CBNB.	-	-	-	3	-
STD1-ELEV.	-	3	-	-	-
STD3-ELEV.	-	-	3	-	-
STD1-WB.	3	-	-	-	-
STD1-ARWB.	-	-	-	3	-
Total	24	15	15	33	3
				TOTAL	90

Table 3-7: Listing of specimens with 2101 rebar (Table 3-9 from the first Interim Report for this project).

Description	SDS	S3BC	3BTC	MS	FC
STD1 mix design, standard specimen.	3	6	-	6	3
STD3 mix design, standard specimen.	3	3	3	3	-
STD2 mix design, standard specimen.	-	-	6	-	-
STD1-BCAT.	3	-	-	3	-
STD1-CCON.	3	-	-	3	-
STD1-CCNB.	3	-	-	3	-
STD1-CREV.	3	-	-	-	-
STD1-CCRV.	3	-	-	-	-
STD1-BENT.	-	3	3	3	-
STD3-BENT.	-	-	3	-	-
STD1-BNTB.	-	-	-	3	-
STD1-CBNT.	-	-	-	3	-
STD1-CBNB.	-	-	-	3	-
STD1-ELEV.	-	3	3	-	-
STD3-ELEV.	-	-	3	-	-
STD1-WB.	3	-	-	-	-
STD1-ARWB.	-	-	-	3	-
STD1-ACID.	3	-	-	-	
STD1-ABRD.	3				
	30	15	15	33	3
				TOTAL:	96

Table 3-8: Listing of specimens reinforced with MMFX-2 (Table 3-10 from the first Interim Report for this project).

Description	SDS	S3BC	3BTC	MS	FC
STD1 mix design, standard specimen.	3	6	-	6	3
STD2 mix design, standard specimen.	3	3	3	3	-
STD3 mix design, standard specimen.	-	-	6	-	-
STD1-BCAT.	3	-	-	3	-
STD1-CCON.	3	-	-	3	-
STD1-CCNB.	3	-	-	3	-
STD1-CREV.	3	-	-	-	-
STD1-CCRV.	3	-	-	-	-
STD1-BENT.	-	3	-	3	-
STD3-BENT .	-	-	3	-	-
STD1-BNTB.	-	-	-	3	-
STD1-CBNT.	-	-	-	3	-
STD1-CBNB.	-	-	-	3	-
STD1-ELEV.	-	3	-	-	-
STD3-ELEV.	-	-	3	-	-
STD1-WB.	3	-	-	-	-
STD1-ARWB.	-	-	-	3	-
STD1-USDB.	3	-	-	3	-
STD1-ACID.	3	-	-	-	-
STD1-ABRD.	3	-	-	-	-
	33	15	15	36	3
				TOTAL:	102

Table 3-9: Listing of specimens reinforced with Stelax (Table 3-11 from the first Interim Report for this project).

Description	SDS	S3BC	3BTC	MS	FC
STD1 mix design, standard specimen.	3	6	-	6	3
STD2 mix design, standard specimen.	3	3	3	3	-
STD3 mix design, standard specimen.	-	-	6	-	-
STD1-CCON.	3	-	-	3	-
STD1-CREV.	3	-	-	-	-
STD1-CCRV.	3	-	-	-	-
STD1-BENT.	-	3	3	3	-
STD3-BENT .	-	-	3	-	-
STD1-CBNT.	-	-	-	3	-
STD1-ELEV.	-	3	3	-	-
STD3-ELEV.	-	-	3	-	-
STD1-WB.	3	-	-	-	-
STD1-ARWB.	-	-	-	3	-
STD1-USDB.	3	-	-	3	-
STD1-UBDB.	-	-	-	3	-
STD1-CSDB.	3	-	-	3	-
STD1-CBDB.	-	-	-	3	-
STD1-BCCD.	3	-	-	3	-
STD1-ACID.	3	-	-	-	-
STD1-ABRD.	3	-	-	-	-
STD1-CVNC .	3	-	-	-	-
	36	15	15	36	3
				TOTAL:	105

Table 3-10: Listing of specimens reinforced with SMI (Table 3-12 from the first Interim Report for this project).

Description	SDS	S3BC	3BTC	MS	FC
STD1 mix design, standard specimen.	3	-	-	6	3
STD2 mix design, standard specimen.	3	-	3	3	-
STD3 mix design, standard specimen.	-	-	6	-	-
STD1-CCON.	3	-	-	3	-
STD1-CREV.	3	-	-	-	-
STD1-CCRV.	3	-	-	-	-
STD1-BENT.	-	-	-	3	-
STD3-BENT .	-	-	3	-	-
STD1-CBNT.	-	-	-	3	-
STD1-ELEV.	-	-	-	-	-
STD3-ELEV.	-	-	3	-	-
STD1-WB.	3	-	-	-	-
STD1-ARWB.	-	-	-	3	-
STD1-USDB.	3	-	-	3	-
STD1-UBDB.	-	-	-	3	-
STD1-CSDB.	3	-	-	3	-
STD1-CBDB.	-	-	-	3	-
STD1-BCCD.	3	-	-	3	-
STD1-ABRD.	3	-	-	-	-
STD1-CVNC .	3	-	-	-	-
	33	0	15	36	3
				TOTAL:	87

Table 3-11: Listing of specimens reinforced with black bar (Table 3-13 from the first Interim Report for this project).

Description	SDS	S3BC	3BTC	MS	FC
STD1 mix design, standard specimen.	3	6	-	9	3
STD2 mix design, standard specimen.	3	6	6	3	-
STD3 mix design, standard specimen.	-	-	6	-	-
CCON - STD1, Cracked concrete.	3	-	-	3	-
	9	12	12	15	3
				TOTAL:	51

3.4. Specimen Terminations and Dissections

3.4.1. Simulated Deck Slab (SDS) Specimens

Specimens that became active and were designated for dissection were opened and evaluated according to the following procedure:

1. Testing/exposure was terminated and the ponding bath removed,
2. Two saw cuts were then made, each of which was perpendicular to the top surface and parallel to and at mid-spacing between the center and each of the two outer bars of each layer.
3. For each of the three resultant specimen parts, a further saw cut was made on each of the previous saw cut faces and on what had been the two specimen side faces opposite and parallel to the top rebars to a depth approximately 10 mm from each rebar. In some cases where corrosion of bottom layer black bars was thought to have occurred, this procedure was performed at the level of these bars also.
4. Each specimen section was split open by placing a chisel in one of the saw cuts from step 3 and tapping gently with a hammer until fracture occurred. This exposed both the rebar and its trace, which were then examined for corrosion and photographed.

Figure 3-15 schematically illustrates the location of concrete cuts as listed in steps 2 and 3 above.

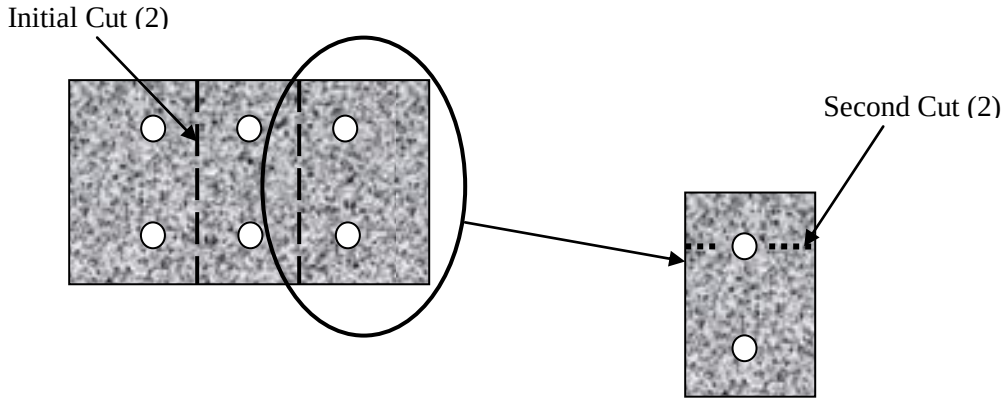

Figure 3-15: Schematic illustration of the concrete sectioning for SDS specimens as listed in dissection steps 2 and 3 above.

3.4.2. Macro-cell Slab (MS) Specimens

Dissection procedure for these specimens was essentially the same as for the SDS ones, as described above.

3.4.3. 3-Bar Tombstone Column (3BTC) Specimens

Dissection of these specimens was performed by making a saw cut to steel depth on the front and back faces along both longer bars starting at the bottom of the specimen and extending up about 0.25 m or more if visual cracking was apparent beyond this. A cut to the steel depth was then made on the front and back faces perpendicular to the reinforcement bars at the 0.25 m elevation across the width of the specimen or just above the highest reaching crack. Once all the cuts were made, a hammer and chisel

were used to split off the cut portion of concrete and expose the reinforcement. Figure 3-16 provides a schematic illustration of these cuts on a specimen.

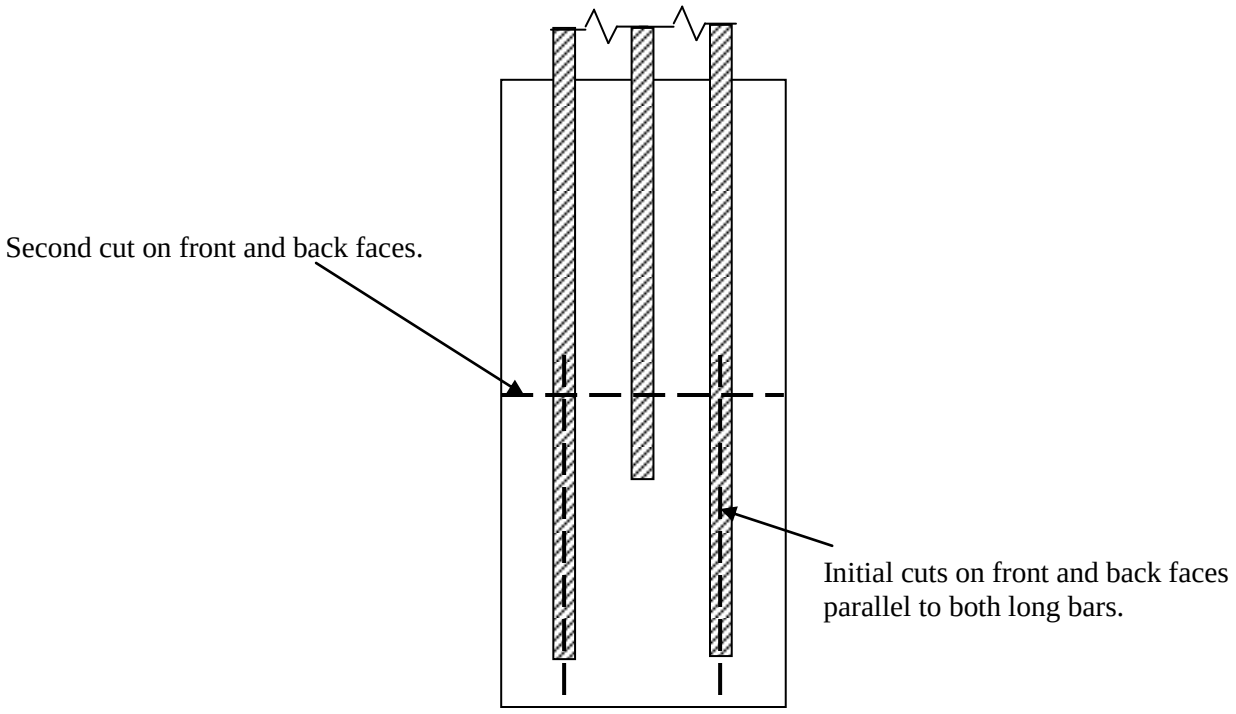

Figure 3-16: Schematic illustration of the concrete sectioning for 3BTC specimens.

3.4.4. Field Column Specimens

No dissections have been made on these specimens due to a lack of an environmental permit to remove them from the test site.

3.5. Chloride Analyses

Concrete samples for [Cl^-] determinations were acquired from SDS specimens according to two methods. Both were performed as soon as feasible once all top layer bars had initiated corrosion, as explained above. The first method involved acquiring a 75 mm diameter core from the top concrete surface at the mid spacing between two adjacent top layer bars. This was then dry sliced parallel to the top surface at 6.4 mm intervals and separately grinding the individual slices to powder. The second involved individually mounting the concrete sections from the top portion of each specimen on a mill and milling a cut approximately 0.6 mm deep along that portion of the rebar trace that was void of corrosion products using a 10 mm diameter square end cutter. Figure 3-17 illustrates this process schematically. For both methods (coring and milling), the powder samples were analyzed for [Cl^-] using the FDOT wet chemistry method.

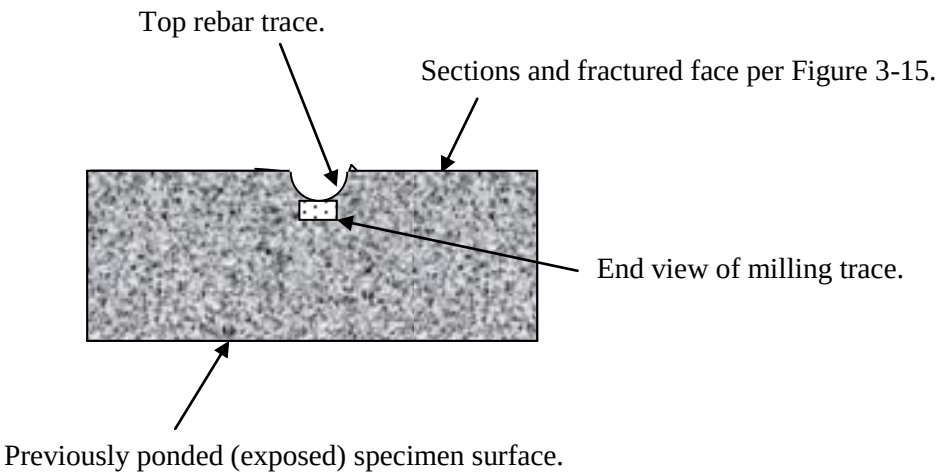

Figure 3-17: Schematic illustration of SDS specimen milling along rebar trace to acquire powdered concrete for chloride analysis.

4.0. RESULTS AND DISCUSSION

4.1. Time-to-Corrosion

4.1.1. Simulated Deck Slab Specimens

4.1.1.1. General

Results and discussion of the corrosion exposures are presented in two subdivisions, the first of which includes black bar, 3Cr12, MMFX-2, and 2101 and is termed improved performance reinforcements and a second termed high performance reinforcements (316, 304, 2304, SMI, and STAX). This distinction was made because the former group of reinforcements initiated corrosion within the project time frame, whereas most of the latter did not. Data for each of these are presented and discussed below.

4.1.1.2. Improved Performance Reinforcements

Data for improved performance reinforced Lot 5 specimens (ones that initiated corrosion) were employed for defining the respective time-to-corrosion, T_i, values. Figure 4-1 shows a typical plot of potential (a) and macro-cell current (b) versus exposure time, in this case for MMFX-2 reinforced specimens. In general, the somewhat abrupt potential shift from relatively positive to more negative (Figure 4-1(a)) was accompanied by occurrence of measureable macro-cell current (Figure 4-1(b)), the latter serving as the criterion for defining T_i for the bar in question and for its being isolation from other bars, as explained in the previous section. In all cases, a positive current indicates that the top layer of bars was anodic to the bottom layer. Time-to-corrosion results for Lot 5 specimens are listed in Table 4-1. However, the procedure whereby individual bars were isolated was employed only after the 5-STD-BB slabs had become active and removed from testing. For these, all three bars in 5-STD-BB-1 and two in 5-STD-BB-

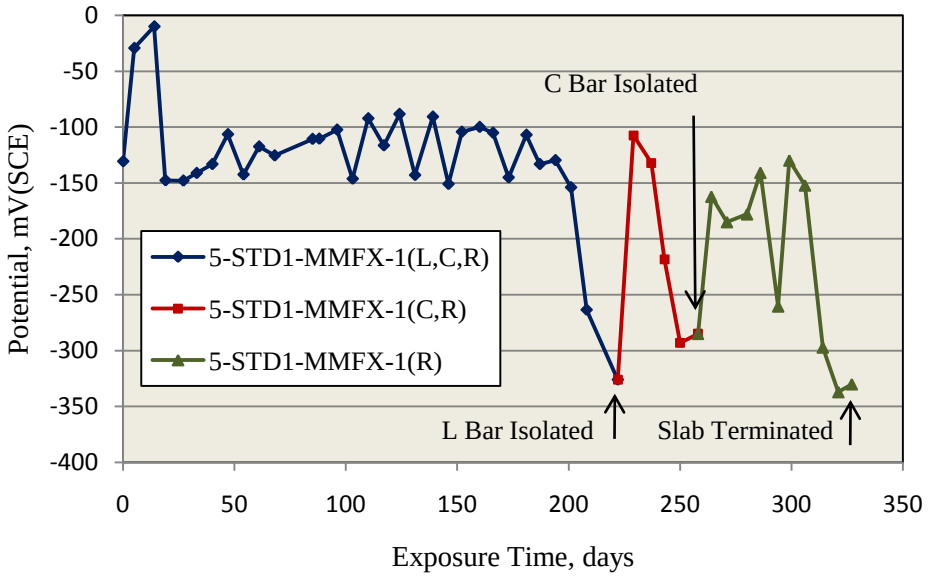

(a)

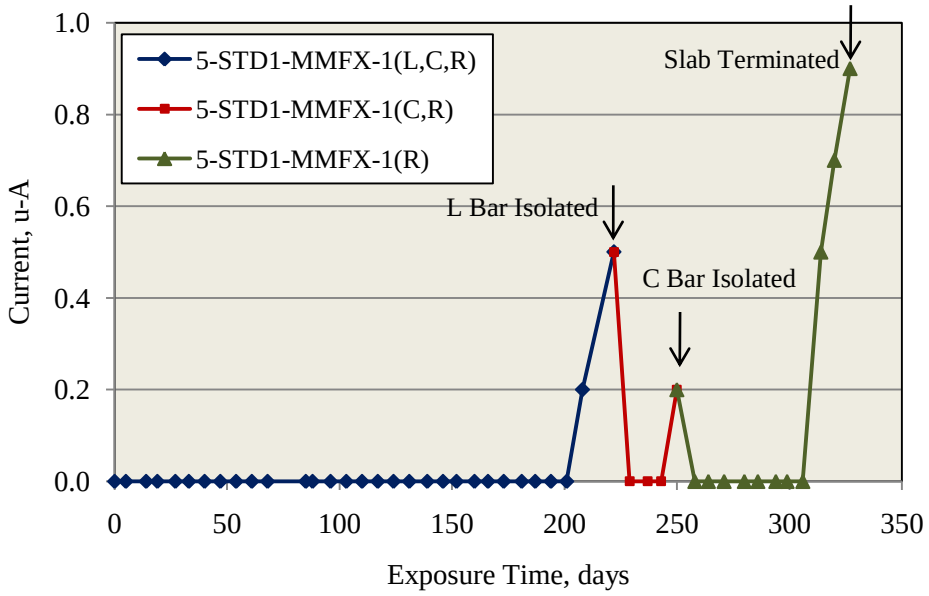

(b)

Figure 4-1: Plot of potential (a) and macro-cell current (b) versus time for specimens reinforced with MMFX-2 steel indicating times at which individual bars became active and were isolated (L – left bar; C – center bar; R – right bar).

2 and 5-STD-BB-3 where found upon dissection to have locations of active corrosion. Bars without corrosion were treated as runouts. Also, if the extent of corrosion on a given bar was 25 mm or more wide, T_i was taken as eight days earlier than the time at termination. For example, specimen 5-STD-BB-1 was removed for exposure after 68 days; and upon dissection the left (L) and center (C) bars where found to have corrosion products less broad than 25 mm, whereas for the right (R) bar corrosion products were

Table 4-1: Time-to-corrosion data for SDS/STD1 specimens with improved performance reinforcements (see Table 3-4 for specimen designation nomenclature).

SDS Specimen	Bar	T_i, days	SDS Specimen	Bar	T_i, days
5-STD1-BB-1	L	68	5-USDB-MMFX-2-2	L	>749
	C	68		C	749
	R	60		R	>749
5-STD1-BB-2	L	60	5-USDB-MMFX-2-3	L	>342
	C	60		C	>343
	R	>68		R	>344
5-STD1-BB-3	L	80	5-STD1-2101-1	L	250
	C	>88		C	264
	R	88		R	152
5-STD1-3Cr12-1	L	404	5-STD1-2101-2	L	124
	C	404		C	>124
	R	314		R	124
5-STD1-3Cr12-2	L	124	5-STD1-2101-3	L	314
	C	>124		C	628
	R	>124		R	250
5-STD1-3Cr12-3	L	342			
	C	>342			
	R	635			
5-STD1-MMFX-2-1	L	264			
	C	299			
	R	327			
5-STD1-MMFX-2-2	L	327			
	C	222			
	R	327			
5-STD1-MMFX-2-3	L	>124			
	C	124			
	R	>124			
5-USDB-MMFX-2-1	L	173			
	C	299			
	R	299			

more extensive (width or length > 25 mm). While somewhat arbitrary, this data modification was thought to provide a more realistic representation of what occurred than if T_i for all bars had simply been taken as the slab termination time.

Figure 4-2 shows a cumulative distribution function (CDF) plot for the STD1 type specimen T_i data in Table 4-1. Weibull statistics were employed because this takes runouts into account in generating the best fit line, although the runout data per se are excluded from the plot. The mean T_i for these four

reinforcements (the mean in Weibull statistics occurs at a CDF of 62.5 percent) is 76 days for BB, 459 days for 3Cr12, 306 days for MMFX-2, and 296 days for 2101. Table 4-2 lists T_i and the ratio of T_i for individual improved performance bars to that for BB at 2, 10, and 20 percent active, these percentages being selected as covering a range of values from damage first occurring to when intervention may be required.

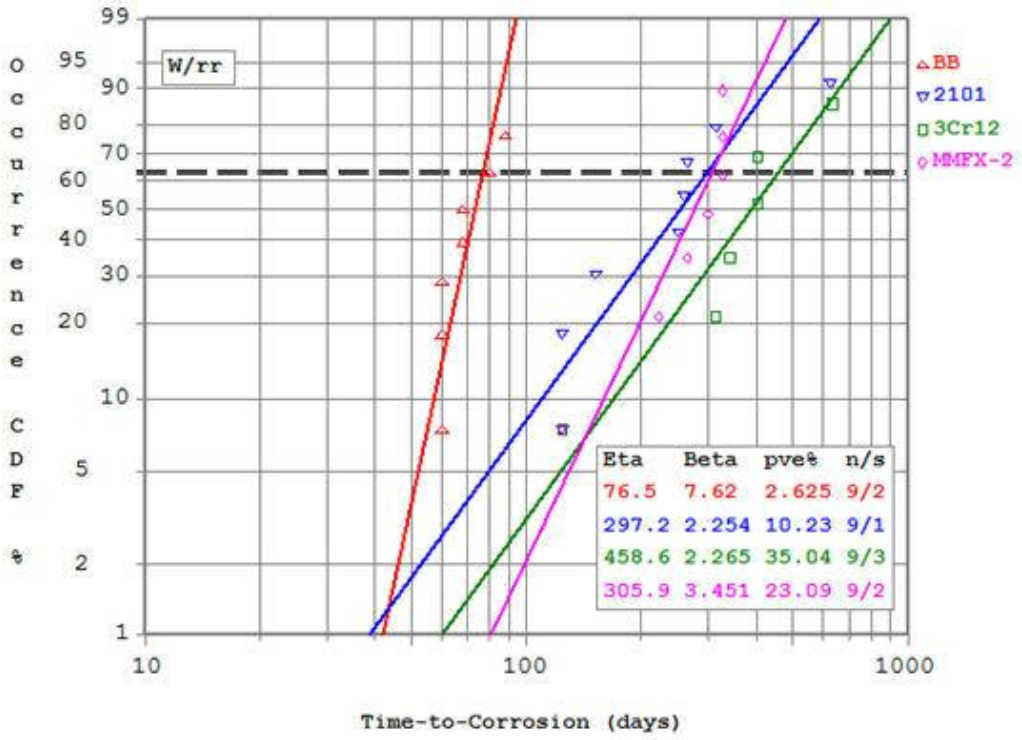

Figure 4-2: Weibull cumulative distribution plot of T_i for the four indicated reinforcements (key: Eta is the mean (dashed horizontal line), Beta is a measure of data spread or slope of the best fit line, pve% is a measure of the line fit to data, n is the total number of specimens, and s the number of runouts).

Table 4-2: Listing of T_i for improved performance reinforcements and T_i ratio to BB for SDS-STD 1 specimens at 2, 10, and 20 percent active.

	T_i, days				T_i(alloy)/T_i(BB)		
Percent Active	BB	3Cr12	MMFX-2	2101	3Cr12	MMFX-2	2101
2	44	81	91	52	1.8	2.1	1.2
10	55	160	175	108	2.9	3.2	2.0
20	62	225	225	140	3.6	3.6	2.3

Figure 4-3 shows a CDF plot of T_i for the two types of specimens reinforced with MMFX-2 (STD and USDB (3mm diameter holes drilled through the surface layer on the upper side of the top bars at 25 mm spacing)). Here, the mean T_i for the STD specimens is 306 days and for the USDB 809 days. It is

unclear if this distinction is simply specimen-to-specimen scatter or reflects actual differences; however, no reason is apparent why surface damaged bars of this alloy should exhibit greater resistance to corrosion initiation than undamaged ones. Figure 4-4 reproduces Figure 4-2 but with both the STD and USDB MMFX-2 specimens included as a common data set. This transposes the MMFX-2 mean T_i from 306 to 435 days, which is essentially the same as for 3Cr12 and at the upper bound for the alloys shown here.

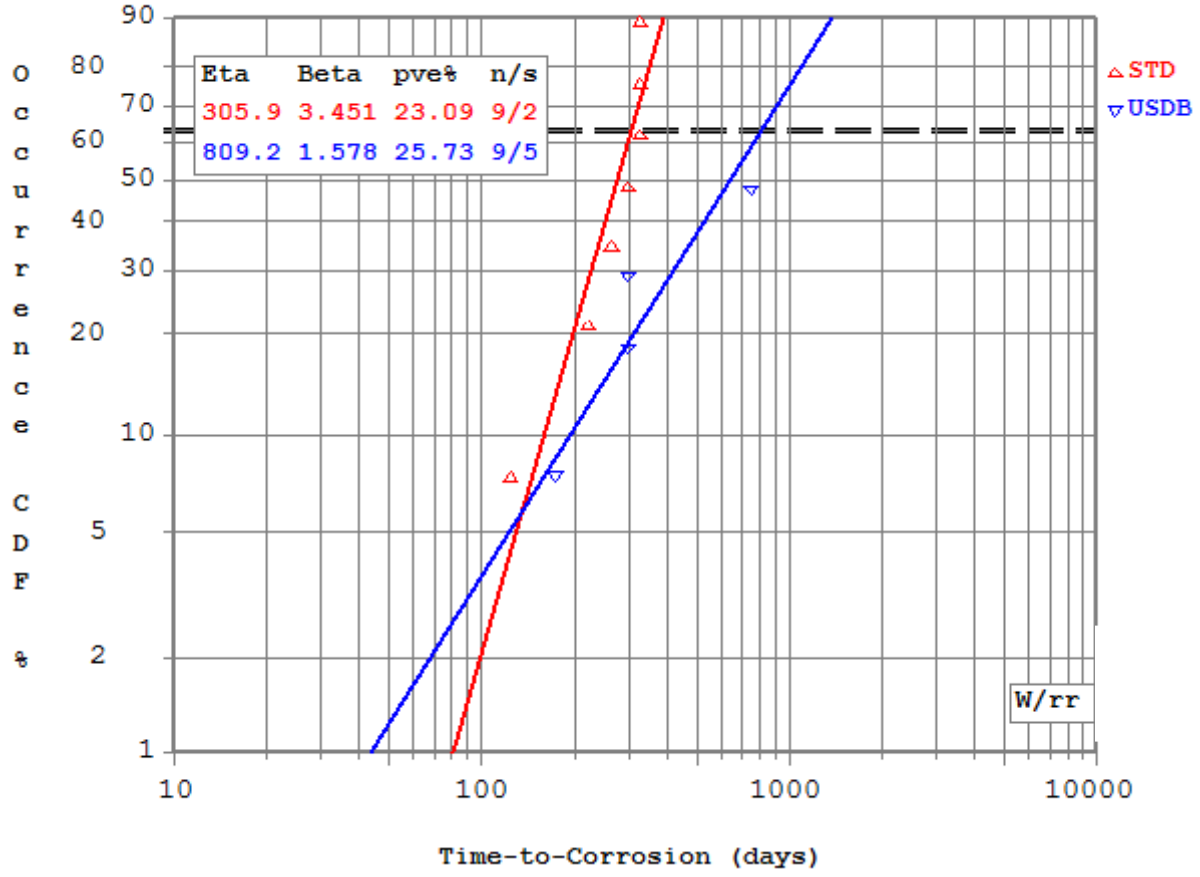

Figure 4-3: Weibull cumulative distribution plot of T_i for STD and USDB MMFX-2 reinforcements.

Referencing T_i data to the mean value has little practical significance, since this corresponds to widespread corrosion having occurred. For this reason, Table 4-3 lists T_i values from Figure 4-4 corresponding to 2, 10, and 20 percent probability of corrosion initiation, as well as the ratio of T_i for each alloy to that for black bar. Consistent with the large Beta (less T_i scatter) in Figure 4-4 for BB specimens compared to the three more corrosion resistant reinforcements, the T_i ratio for each increased with increasing percent active. Thus, 3Cr12 and MMFX-2 were the better performers with T_i(alloy)/T_i(BB) near two at two percent active and 3.6 at 20 percent.

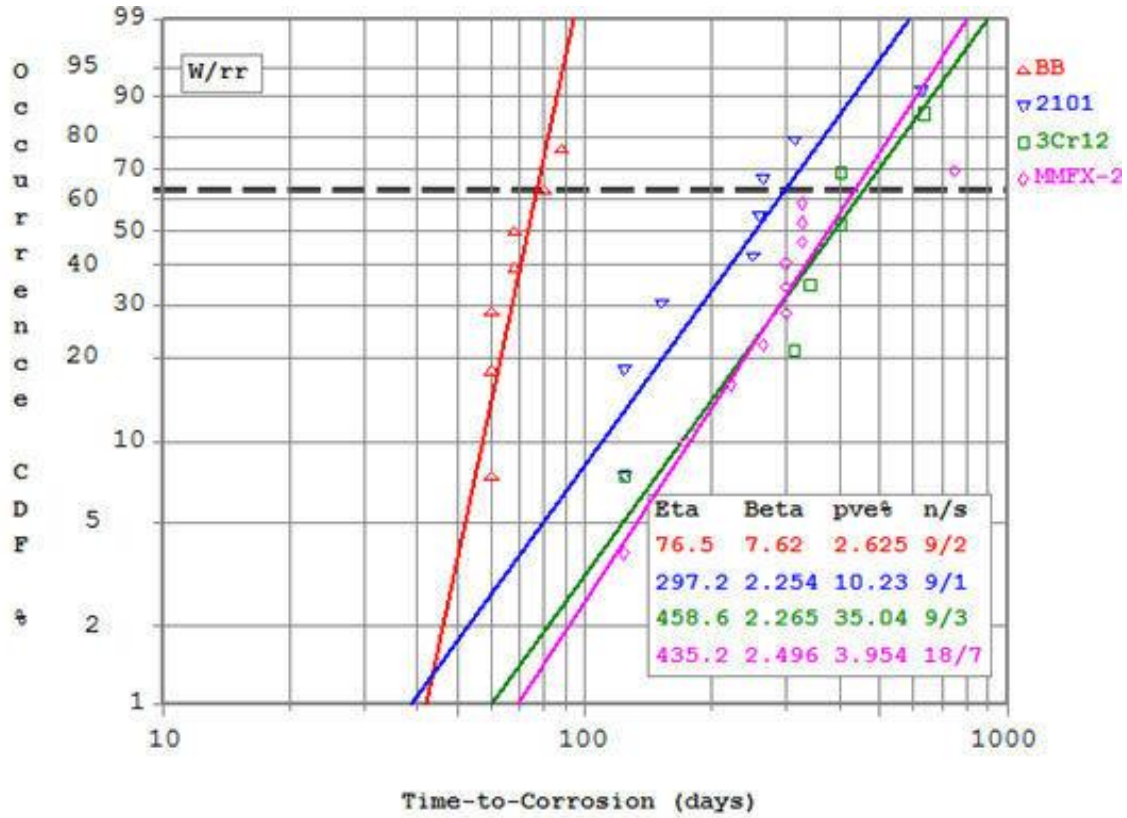

Figure 4-4: Weibull cumulative distribution plot of T_i treating all STD and USDB-MMFX-2 reinforced specimens as a single population.

Table 4-3: Listing of T_i for improved performance reinforcements and T_i ratio to BB for SDS-STD 1 specimens at 2, 10, and 20 percent active based on all MMFX-2 specimens.

	T_i, days				T_i(alloy)/T_i(BB)		
Percent Active	BB	3Cr12	MMFX-2	2101	3Cr12	MMFX-2	2101
2	44	81	91	52	1.8	2.1	1.2
10	55	160	177	108	2.9	4.0	2.0
20	62	225	239	140	3.6	3.9	2.3

4.1.1.3. High Performance Reinforcements.

Table 4-4 lists exposure duration and macro-cell current measurement results for the two types of 316SS (316.16 and 316.18 (see Table 3-1)) reinforced SDS specimens that either did not initiate corrosion or that eventually did initiate corrosion on lower layer BB, as indicated by negative macro-cell current. Figure 4-5 shows a plot of macro-cell current versus exposure time for specimens with a bottom black bar mat. Table 4-5 lists data for Type 304SS reinforced slabs and indicates the same response as for the 316 (no macro-cell current except for specimens fabricated with lower mat black bars which did eventually initiate corrosion).

Table 4-6 lists parameters and macro-cell current measurement results for SDS slabs reinforced with STAX. The data indicate that isolated instances of measurable current occurred on occasion, but for

Table 4-4: Listing of exposure times and macro-cell current data for Type 316SS SDS reinforced slabs.

Specimen No.	Exposure Time, days	No. of Current Measurements	No. of Zero Current Readings	No.of Non-Zero Current Readings	Maximum Negative Current Recorded, μA
1-STD1-316.16-1	1726	178	178	0	-
1-STD1-316.16-2	1726	178	178	0	-
1-STD1-316.16-3	1726	178	178	0	-
1-STD2-316.16-1	1726	178	178	0	-
1-STD2-316.16-2	1726	178	178	0	-
1-STD2-316.16-3	1726	178	178	0	-
3-STD1-316.18-1	1585	1585	1585	0	-
3-STD1-316.18-2	1585	1585	1585	0	-
3-STD1-316.18-3	1585	1585	1585	0	-
2-STD2-316.18-1	1669	1669	1669	0	-
2-STD2-316.18-2	1669	1669	1669	0	-
2-STD2-316.18-3	1669	1669	1669	0	-
3-CCON-316.18-1	1585	1585	1585	0	-
3-CCON-316.18-2	1585	1585	1585	0	-
3-CCON-316.18-3	1585	1585	1585	0	-
2-WB-316.16-1	1669	172	172	0	-
2-WB-316.16-2	1669	172	172	0	-
2-WB-316.16-3	1669	172	172	0	-
3-CCON-316.16-1	1585	157	157	0	-
3-CCON-316.16-2	1585	157	157	0	-
3-CCON-316.16-3	1585	157	157	0	-
3-CREV-316.16-1	1585	157	157	0	-
3-CREV-316.16-2	1585	157	157	0	-
3-CREV-316.16-3	1585	157	157	0	-
3-CCRV-316.16-1	1585	157	157	0	-
3-CCRV-316.16-2	1585	157	157	0	-
3-CCRV-316.16-3	1585	157	157	0	-
2-BCAT-316.16-1	1669	172	144	28	0.4
2-BCAT-316.16-2	1669	172	124	48	0.2
2-BCAT-316.16-3	1196	159	147	12	0.2
2-CCNB-316.16-1	1669	172	101	71	0.3
2-CCNB-316.16-2	1669	172	124	48	0.3
2-CCNB-316.16-3	1669	172	86	86	0.3

the most part macro-cell current was zero. Specimen configurations for this reinforcement type were limited to those shown because of material stock limitations.

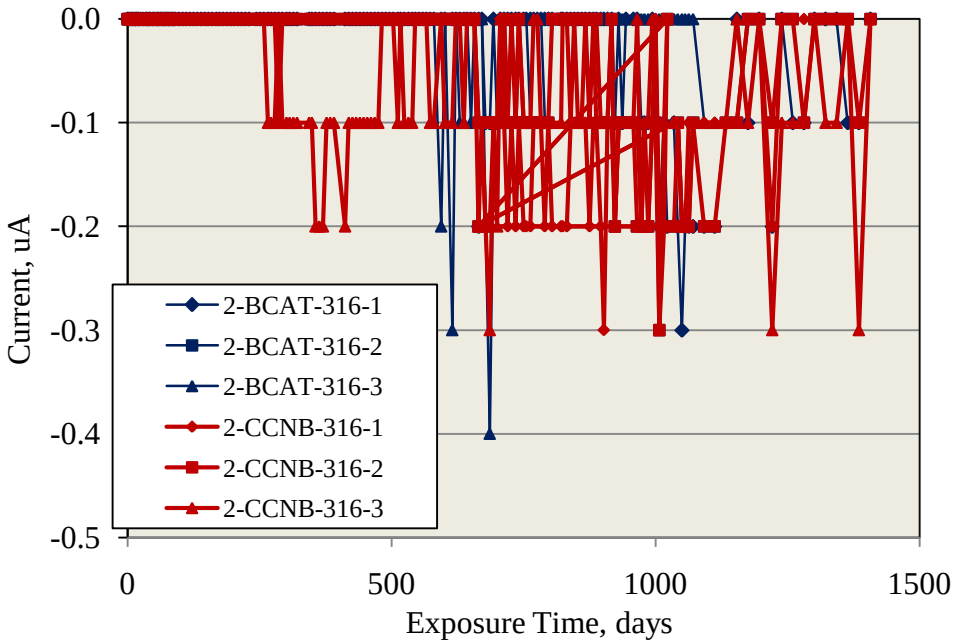

Figure 4-5: Macro-cell current history for 316 reinforced slabs with black bar lower steel.

Results for SMI reinforced SDS slabs, including those with a bar crevice, black bar lower layer, concrete crack, or clad defects (or combinations of these), are listed in Table 4-7. In general, the macro-cell current that did occur in some cases was small and infrequent. Table 4-8 lists results for the other SMI specimens which exhibited a distinct T_i. As indicated, T_i was zero for specimens of the CSDB condition (simulated concrete crack and 3 mm diameter holes through the cladding spaced at 25 mm intervals on the top of upper bars), 20-29 days for BCCD specimens (holes drilled through the cladding and black bar bottom layer), and 139-230 days for CVNC (top layer bars with a crevice and no caps on embedded bar ends). Figure 4-6 provides a plot of macro-cell current versus time for these latter two specimen sets.

Three Type 2304SS reinforced STD1 specimens have been under test for 929 days with no macro-cell current activity.

Table 4-9 lists all high performance alloy reinforcement/specimen types that did not initiate corrosion within the exposure time and the corresponding ratio of T_i for each to the mean T_i for STD1 black bar specimens (77 days, Figure 4-2). Because exposure times were different for different specimen sets, the ratios vary from one alloy to the next but are as high as >22.

Table 4-5: Listening of exposure times and macro-cell current data for Type 304SS reinforced slabs.

Specimen No.	Exposure Time, days	No. of Current Measurements	No. of Zero Current Readings	No. of Non-Zero Current Readings	Maximum Negative Current Recorded, μA
6-STD1-304-1	440	22	22	0	-
6-STD1-304-2	440	22	22	0	-
6-STD1-304-3	440	22	22	0	-
6-STD2-304-1	440	22	22	0	-
6-STD2-304-2	440	22	22	0	-
6-STD2-304-3	440	22	22	0	-
6-WB-304-1	440	22	22	0	-
6-WB-304-2	440	22	22	0	-
6-WB-304-3	440	22	22	0	-
6-CCON-304-1	440	22	22	0	-
6-CCON-304-2	440	22	22	0	-
6-CCON-304-3	440	22	22	0	-
6-CREV-304-1	440	22	22	0	-
6-CREV-304-2	440	22	22	0	-
6-CREV-304-3	440	22	22	0	-
6-CCRV-304-1	440	22	22	0	-
6-CCRV-304-2	440	22	22	0	-
6-CCRV-304-3	440	22	22	0	-
6-BCAT-304-1	440	22	22	1	0.2
6-BCAT-304-2	440	22	22	7	0.7
6-BCAT-304-3	440	22	22	5	0.6
6-CCNB-304-1	440	22	22	3	0.9
6-CCNB-304-2	440	22	22	3	0.8
6-CCNB-304-3	440	22	22	1	0.1

Table 4-6: Corrosion activity for Stelax reinforced SDS specimens.

Specimen No.	Exposure Time, days	No. of Current Measurements	No. of Zero Current Readings	No. of Non-Zero Current Readings	Current Recorded, μA
1-STD1-Stelax-1	1726	178	177	1	0.1
1-STD1-Stelax-2	1726	178	164	14	-0.2 to 0.3
1-STD1-Stelax-3	1726	178	171	7	0.1
1-STD2-Stelax-1	1726	178	178	0	0
1-STD2-Stelax-2	1726	178	178	0	0
1-STD2-Stelax-3	1726	178	178	0	0

Table 4-7: Listing of SMI reinforced SDS specimens along with macro-cell current results.

Specimen No.	Exposure Time, days	Total No. of Current Measurements	No. of Zero Current Readings	No. of Non-Zero Current Readings	Maximum Current Recorded, μA
4-STD1-SMI-1	944	112	112	0	-
4-STD1-SMI-2	944	112	112	0	-
4-STD1-SMI-3	944	112	112	0	-
4-STD2-SMI-1	944	112	112	0	-
4-STD2-SMI-2	944	112	112	0	-
4-STD2-SMI-3	944	112	112	0	-
4-CCON-SMI-1	944	112	111	1	0.1
4-CCON-SMI-2	944	112	112	0	-
4-CCON-SMI-3	944	112	112	6	0.1
4-CREV-SMI-1	944	112	112	0	-
4-CREV-SMI-2	994	112	111	1	0.6
4-CREV-SMI-3	994	112	112	0	-
4-CCRV-SMI-1	994	112	112	0	-
4-CCRV-SMI-2	994	112	103	9	0.6
4-CCRV-SMI-3	994	112	112	0	-
4-USDB-SMI-1	994	112	112	0	-
4-USDB-SMI-2	994	112	111	1	0.2
4-USDB-SMI-3	994	112	112	0	-

Table 4-8: Results for SMI reinforced SDS specimens that exhibited a defined T_i followed by measureable macro-cell corrosion.

Specimen Number	T_i, days	Exposure Duration, days
4-BCCD-SMI-1	29	944
4-BCCD-SMI-2	20	944
4-BCCD-SMI-3	20	944
4-CSDB-SMI-1	0	944
4-CSDB-SMI-2	0	944
4-CSDB-SMI-3	0	944
6-CVNC-SMI-1	139	440
6-CVNC-SMI-2	230	440
6-CVNC-SMI-3	139	440

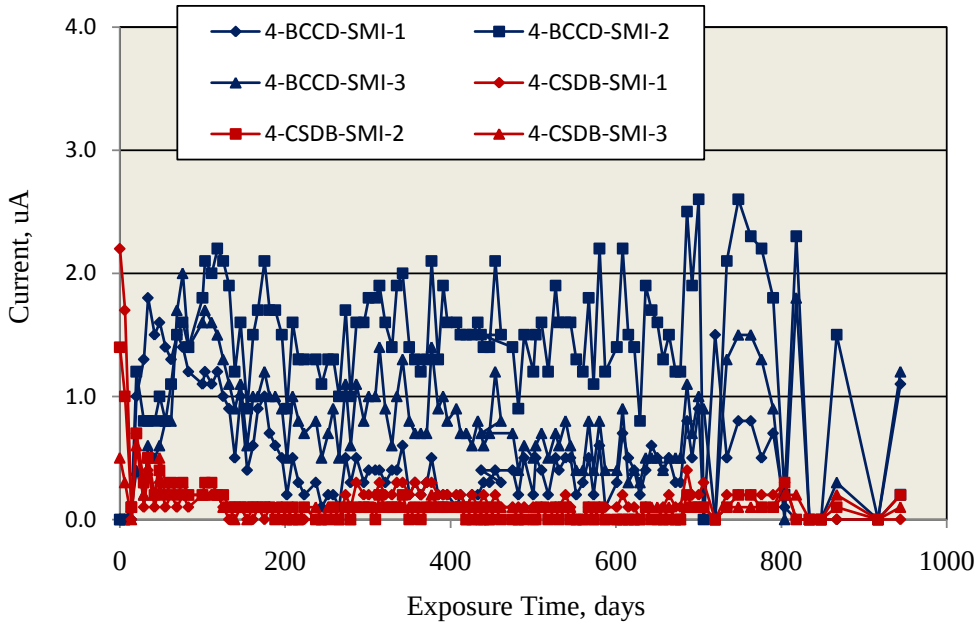

Figure 4-6: Current-time history for SDS-SMI specimens that initiated corrosion.

Table 4-9: Ratio of T_i for corrosion resistant reinforcements that did not initiate corrosion to the mean T_i for black bar specimens (77 days, Figure 4-2).

Alloy/Specimen Type	T_i(alloy)/T_i(BB)
STD1-316.16	>22
STD2-316.16	
STD1-316.18	>21
STD2-316.18	>22
CCON-316.16	>21
CCON-316.18	
WB-316.16	>22
CREV-316.16	>21
CCRV-316.16	
STD1-304	>6
STD2-304	
WB-304	
CCON-304	
CREV-304	
CCRV-304	
STD1-Stelax	>22
STD2-Stelax	
STD1-SMI	>12
STD2-SMI	
STD1-2304	>12

4.1.2. Macro-cell Slab (MS) Specimens

4.1.2.1. Improved Performance Reinforcements

Outdoor Exposures. The potential and macro-cell current versus time trends for STD1-MS specimens with improved performance reinforcements were generally similar to those indicated above for comparable SDS specimens (Figure 4-1), as shown by Figures 4-7 to 4-10. These plots show that macro-cell current was near zero initially but then abruptly increased in most, but not all, cases; and potential correspondingly became more negative. Time-to-corrosion was defined as for SDS specimens as initial occurrence of measureable, sustained macro-cell current. Because there was only a single top bar (anode) for this specimen type, no bar isolation procedure was performed as was done for SDS specimens. Table

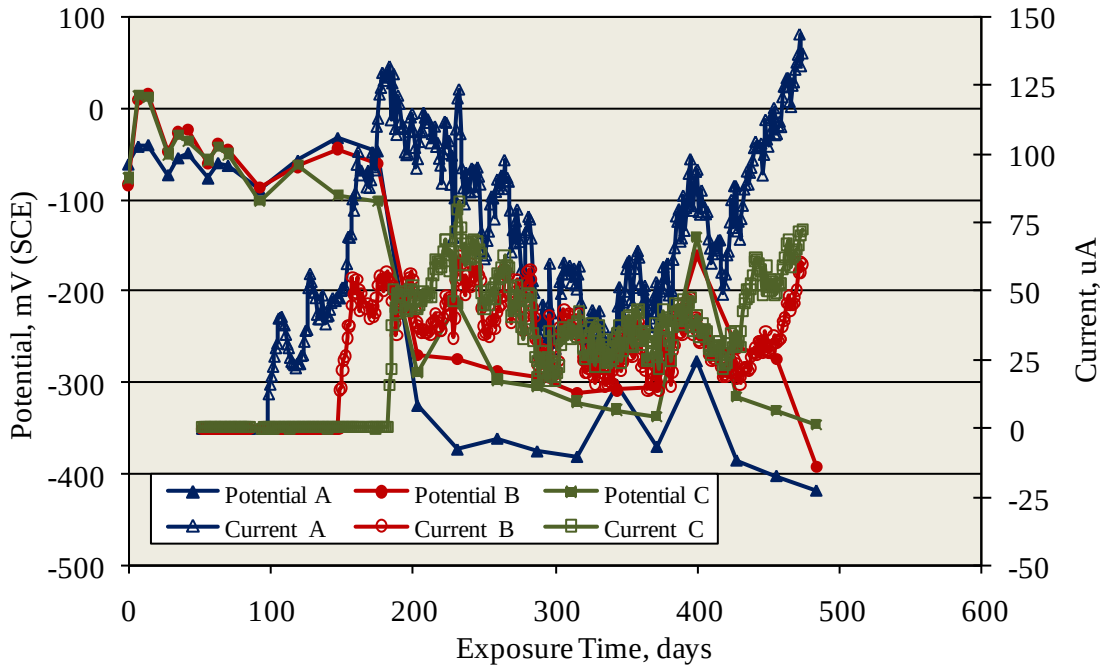

Figure 4-7: Potential and macro-cell current results for MS-STD1-BB specimens.

4-10 lists these T_i values for STD1-MS specimens reinforced with BB, 3Cr12, MMFX-2, and 2101, and Figure 4-11 shows a normal distribution CDF plot of T_i. In contrast to results for the SDS specimens (Figures 4-2 and 4-4), the extent to which T_i was enhanced for the improved performance reinforcements in STD1 concrete is modest, particularly at low percentages of corrosion initiation and if the single 3Cr12 datum at 488 days is neglected.

Table 4-11 shows T_i values for other STD1-MS specimen types reinforced with 3Cr12, MMFX-2, and 2101. Figure 4-12 shows a Weibull CDF plot of T_i that includes data for both the STD

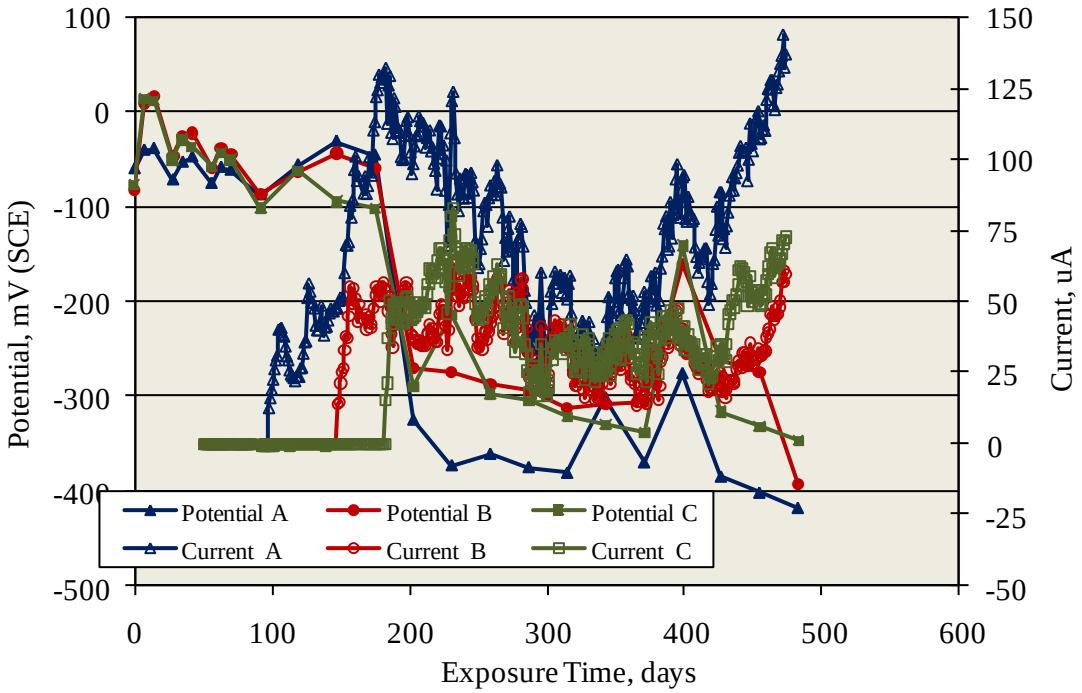

Figure 4-8: Potential and macro-cell current results for MS-STD1-3Cr12 specimens.

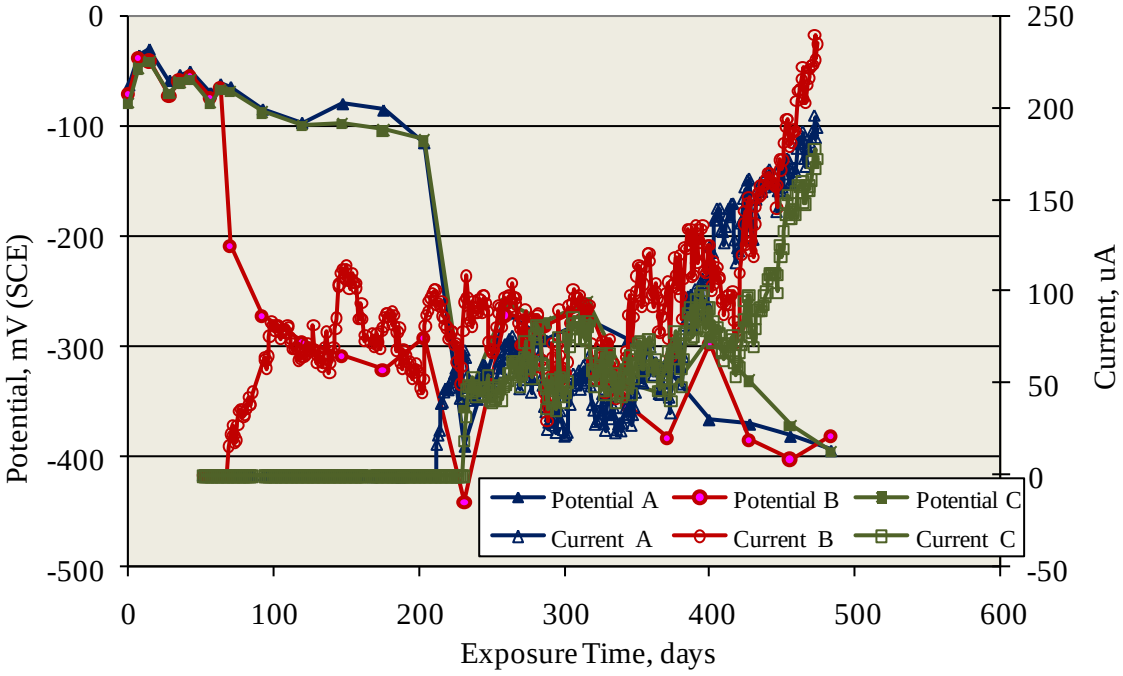

Figure 4-9: Potential and macro-cell current results for MS-STD1-MMFX-2 specimens.

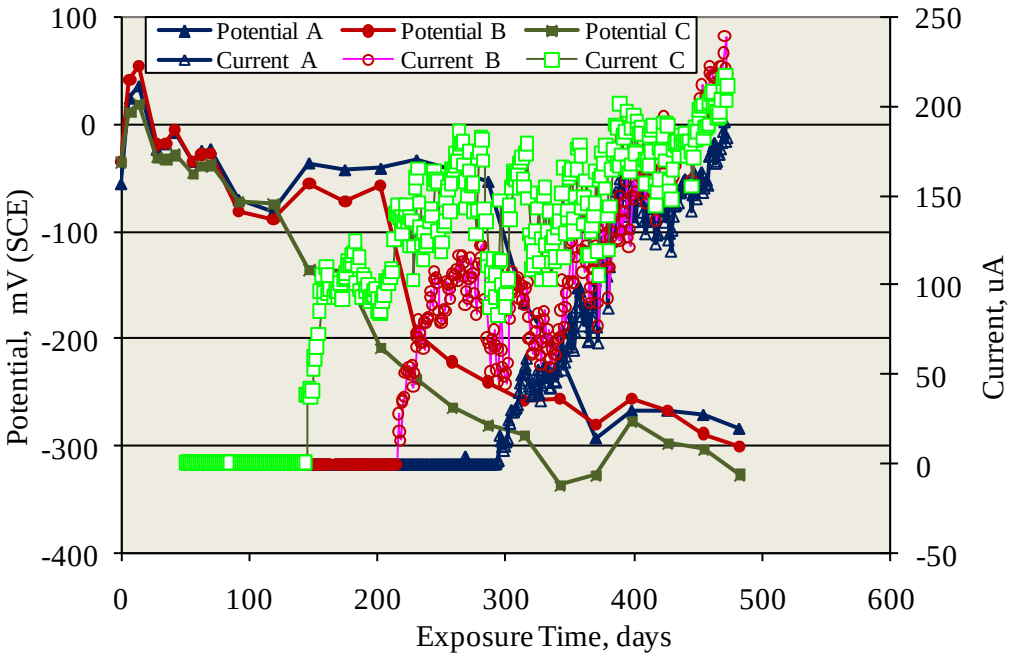

Figure 4-10: Potential and macro-cell current results for MS-STD1-2101 specimens.

Table 4-10: Listing of T_i values for MS STD1 specimens with improved performance reinforcements.

T_i, days			
BB	3Cr12	MMFX-2	2101
97	121	68	144
147	212	211	215
182	488	230	295

(Table 4-10 and Figure 4-12) and BENT, BNTB, BCAT, and USDB (Table 4-11) specimen types based on the assumption that data for each alloy conform to a common population. The results show that T_i is approximately the same for all reinforcements at a relatively low percentage activation but with T_i for 3Cr12, MMFX-2, and 2101 diverging to slightly higher values as the active percentage increases. For specimens with a simulated crack (CBDB, CBNB, CBNT, and CCNB, Table 4-11), corrosion initiated in less than 43 days for 3Cr12 and MMFX-2 but was greater for 2101.

Data for STD2-MS specimens were not always conduce for definitively identifying T_i. Thus, Figure 4-13 shows potential and macro-cell current data for the three black bar MS specimens and Figure 4-14 for the three 3Cr12 specimens. Here, positive macro-cell current corresponds to the top bar being

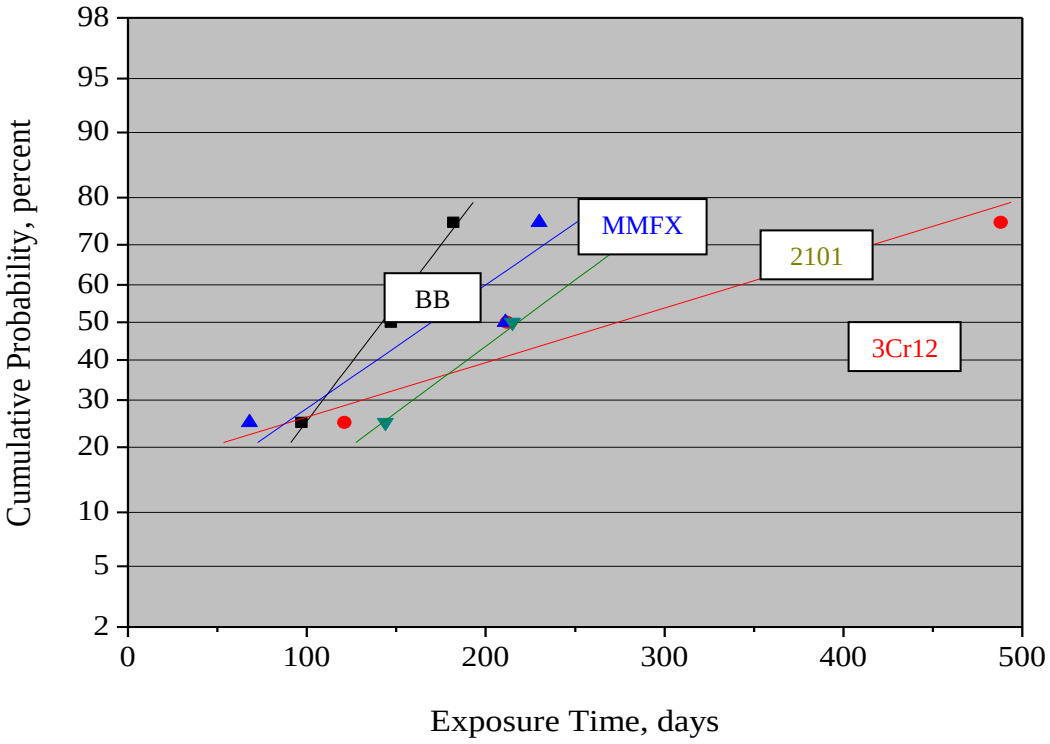

Figure 4-11: Cumulative probability plot of T_i for STD1.MS specimens with improved performance reinforcements.

anodic; and corrosion was assumed to have initiated at the time at which this current increased to above the background level, which was near zero. For MS-BB-1 in Figure 4-13, a negative current occurred after 168 days, indicating that a lower bar (or bars) had initiated corrosion with the top bar serving as a cathode. This situation continued to 405 days, at which time the top bar activated and was anodic to the four lower bars. In the intermediate period, the top bar was being cathodically polarized by one or more lower bars; and this is expected to have elevated the critical chloride concentration for corrosion initiation of the top bar. For MS-BB-2, corrosion initiated on the top bar after 180 days (positive macro-cell current); but this polarity reversed at 275 days, indicating that a lower bar had activated and its potential was now more negative than that for the top bar. Corrosion of the top bar reinitiated after 483 days. Specimen MS-BB-3 behaved in a more conventional manner in that macro-cell current was nil until the top bar activated after 488 days. In analysis of these data, a specimen was considered to have initiated corrosion upon initial occurrence of either a positive or negative current. For 3Cr12, current excursions were both positive and negative as for BB specimens but were smaller in magnitude and subsequently often reverted to near zero, indicating repassivation. Because of these complexities, data for 3Cr12 specimens was excluded in the T_i analysis. Specimens reinforced with MMFX-2 and 2101, on the other

hand, exhibited better defined corrosion initiation and for the top bar only. This is illustrated by Figure 4-15 for STD2-MMFX-2 MS specimens where specimen B initiated corrosion after 974 days, although the corresponding potential decrease was relatively modest (≤100 mV). Specimen C was removed after 1221 days, and dissection revealed no corrosion. Specimen A remains under test with no indications of corrosion initiation.

Table 4-11: Listing of T_i values (days) for MS specimens with improved performance reinforcements other than STD.

	3Cr12	MMFX-2	2101
ARWB	430	85	52
	433	223	137
	1229	244	195
BENT	57	152	178
	92	229	201
	228	284	345
BCAT	222*	149*	93
	505	1314	142
	980	1254*	163
BNTB	173	91	178
	185	93	254*
	346	222	466
CCON	<43	<43	69
	<43	208	85
	<43	458	158
CBNB	0	0	63
	0	0	159
	0	0	293*
CBNT	0	0	<43
	0	0	75
	0	0	498
CCNB	0	<43	110
	0	<43	142
	0	450	411
UBDB	-	232	-
	-	>358	-
	-	>358	-
USDB	-	179	-
	-	300	-
	-	324	-
CBDB	-	50	-
	-	138	-
	-	267	-

* Corrosion initiated on one or more of the lower black bars.

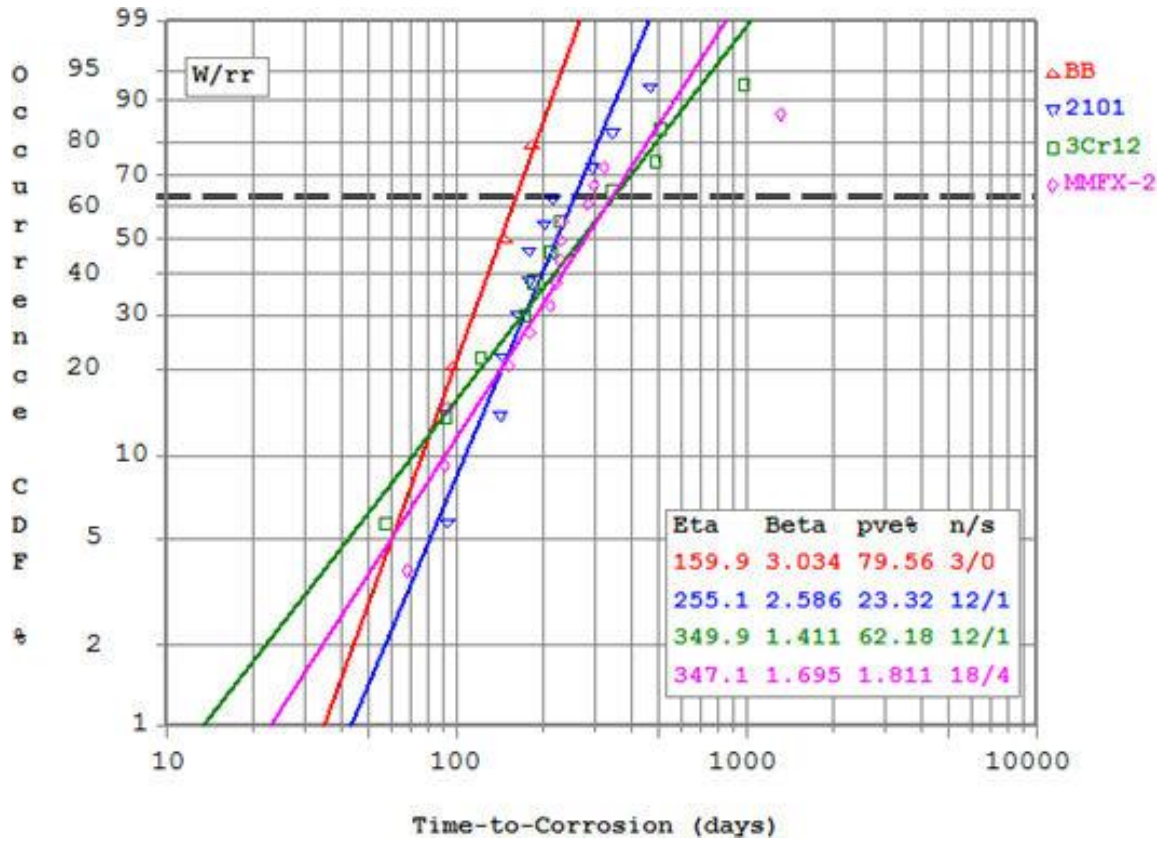

Figure 4-12: Weibull CDF plot of T_i for MS-STD1, -BCAT, -BENT, -BNTB, -UBDB, and -USDB specimens.

Based on the above stated protocol, Table 4-12 lists T_i values for the MS STD2 specimens. In the case of 3Cr12, one specimen was removed after 1233 days and dissected; however, no corrosion was apparent. A second specimen apparently initiated corrosion after 1181 days as an increase in macro-cell current from near zero to 4-7 μA occurred. The third specimen remains under test after 1399 days with macro-cell current in the range 0-2 μA. It is unclear if corrosion has initiated in this case. Figure 4-16 shows a CDF plot of T_i, where data for 3Cr12 have been omitted because of the uncertainties mentioned above; and corrosion initiation for BB specimens was considered to have occurred at the initial onset of macro-cell current, either positive or negative. Because of the limited data, it was necessary in generating this plot to treat runouts (two of the three MMFX-2 data and one of three for 2101) as having initiated corrosion at the time of termination, although either no corrosion was detected upon dissection of these specimens or the specimens remain under test. The data were insufficient for application of Weibull statistics. An attempt was made to project T_i(alloy)/T_i(BB), as was done above for SDS specimens; however, this was complicated by the fact that the best fit line through the three BB data points indicates

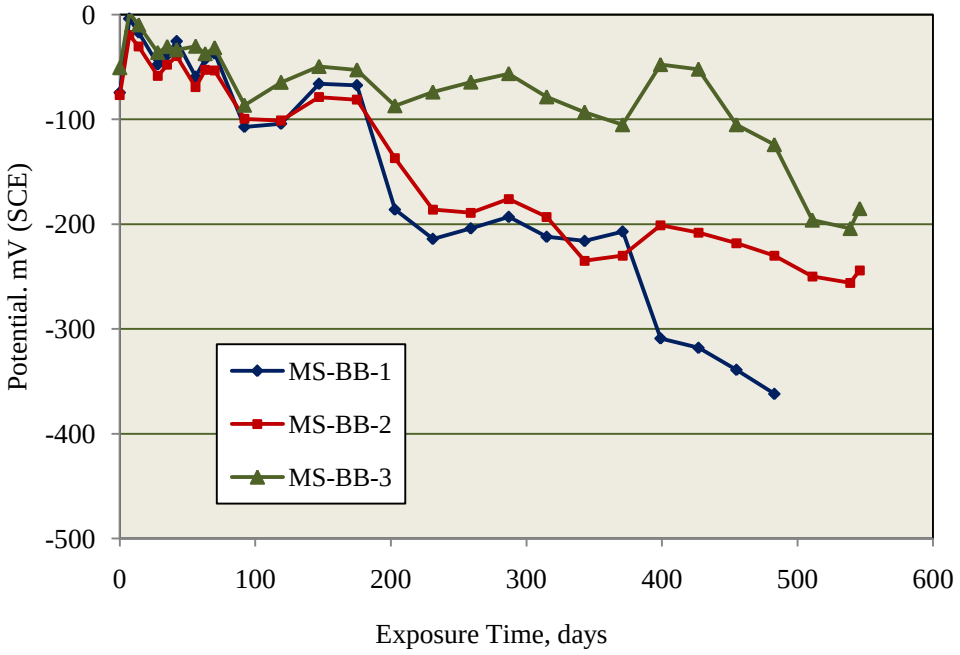

(a)

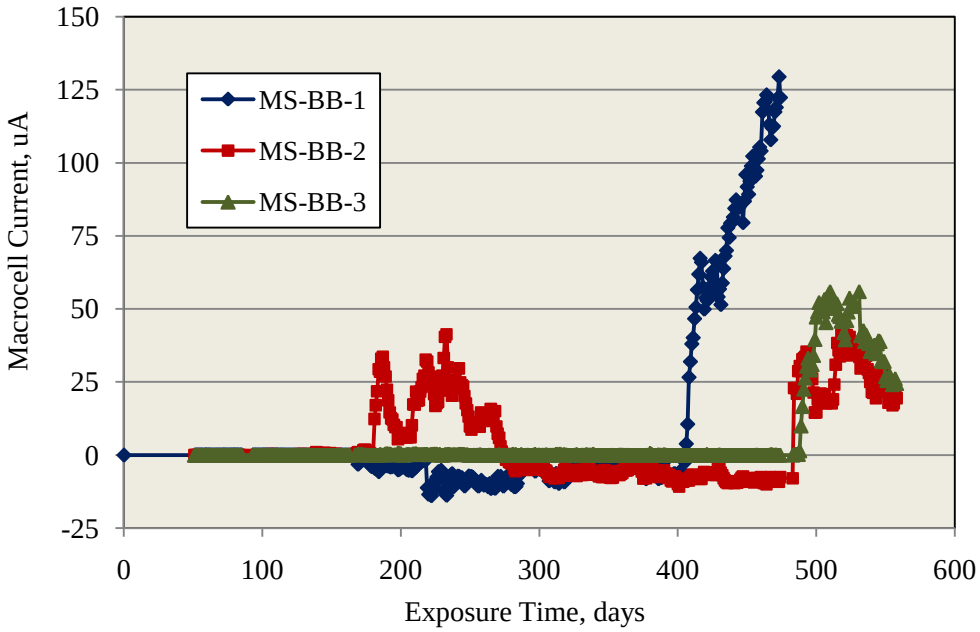

(b)

Figure 4-13: Potential (a) and macro-cell current (b) versus time for STD2 black bar MS specimens.

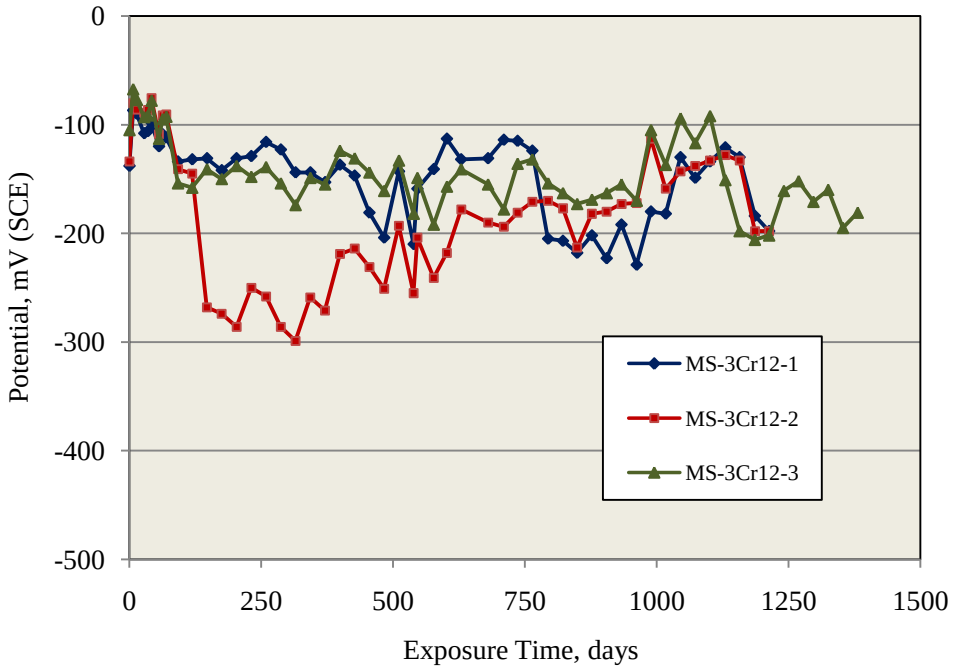

(a)

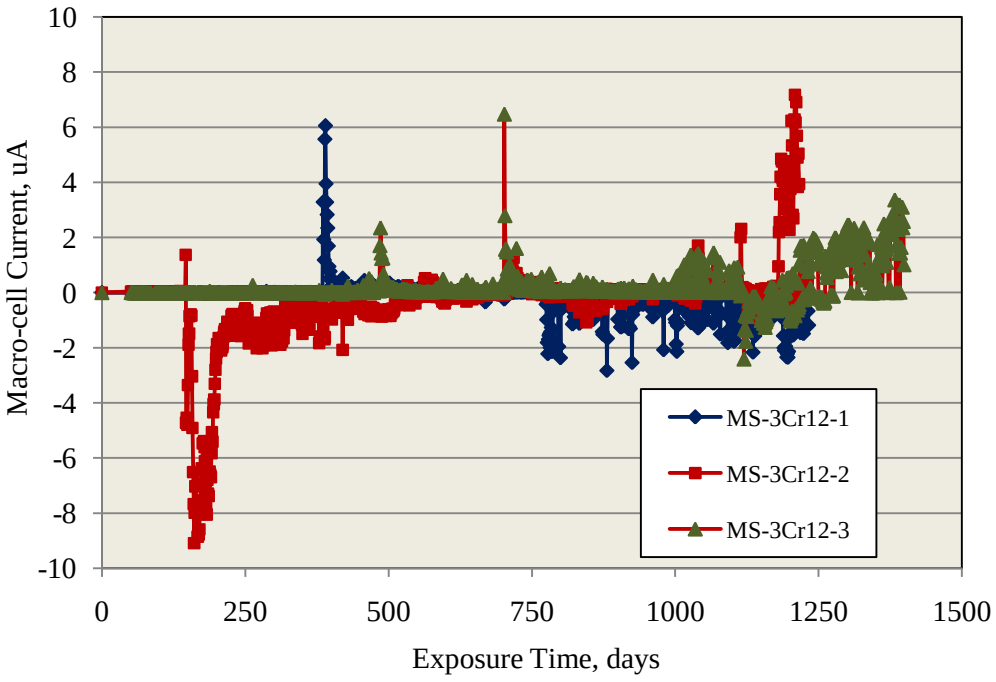

(b)

Figure 4-14: Potential (a) and macro-cell current (b) versus time for STD2 3Cr12 MS specimens (specimen MS-3Cr12-1 was terminated after 1233 days, and no corrosion was apparent upon dissection).

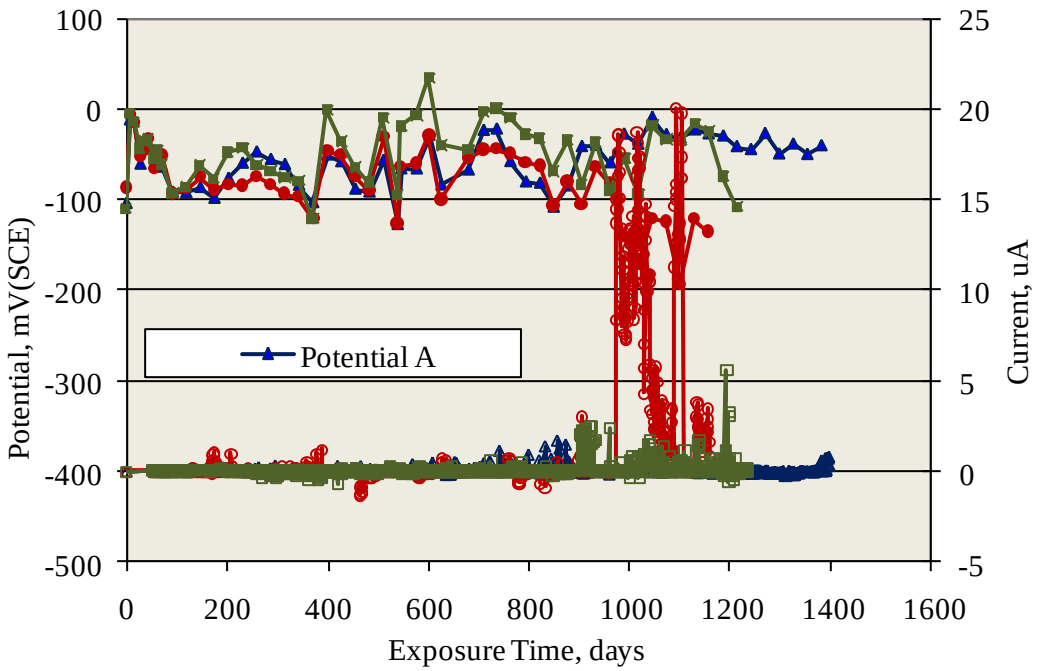

Figure 4-15: Potential and macro-cell current versus time for STD2 MMFX-2 MS specimens.

Table 4-12: Listing of T_i values for MS-STD2 specimens with improved performance reinforcements.

BB	3Cr12	MMFX-2	2101
168	1181	974	855
180	>1233	>1221	1017
488	>1399	>1387	>1224

negative T_i at small percentages active. For this reason, it was assumed that T_i at 2, 10, and 20 percent active was the value for the first BB specimen to become active (168 days). Doing this yields the T_i(alloy)/T_i(BB) results in Table 4-13. The higher values for these ratios compared to the STD1 results (Table 4-10 and Figures 4.11 and 4.12) suggest that better quality (lower permeability) concrete (STD2 compared to STD1) may be required if significantly greater T_i for these improved performance reinforcements compared to black bar is to be realized. Figure 4-17 shows a schematic plot of [Cl^-] at a particular depth into concrete versus exposure time assuming Fickian diffusional transport and illustrates that T_i(alloy)/T_i(BB) for relatively low permeability concrete exceeds this ratio in high permeability concrete.

Controlled Temperature and Relative Humidity Exposures. Table 4-14 lists T_i for individual specimens

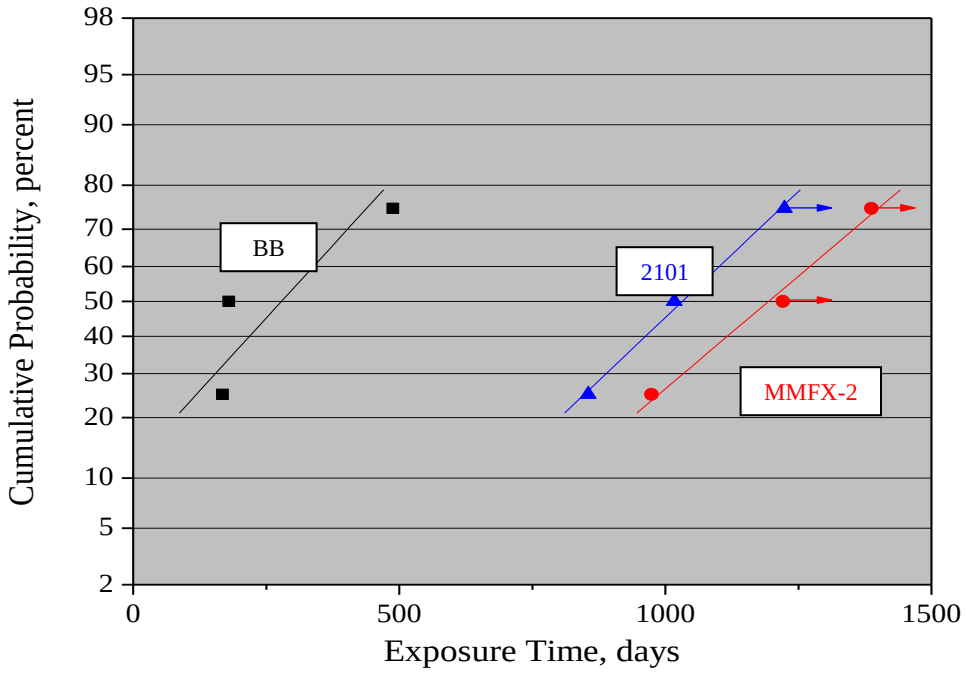

Figure 4-16: Normal CDF plot of T_i for MS-STD2 specimens that exhibited a well defined corrosion initiation. Runout data were treated as if corrosion had initiated at the indicated time.

Table 4-13: Listing of T_i(alloy)/T_i(BB) for STD2-MS-MMFX-2 and -2101 reinforced specimens.

Percent Active	T_i(alloy)/T_i(BB)	
	MMFX-2	2101
2	3.4	2.7
10	>4.8	3.9
20	>5.7	>4.8

that underwent this exposure, all of which were of the STD1 mix design (designated STD1G in this case) along with comparable STD1 data (Table 4-10) and the average for each specimen type. This shows that the average T_i for STD1G and STD1 is approximately the same for BB, but for the three more corrosion resistant reinforcements T_i for STD1G exceeded that for STD1. Variations in temperature and relative humidity, as occurred for the outdoor exposures, may have promoted sorptive transport of the ponding solution in the STD1 specimens such that C_T was reached at the bar depth in a shorter time than for the STD1G ones. Possibly, the relatively low C_T for BB specimens precluded this effect being apparent for this reinforcement.

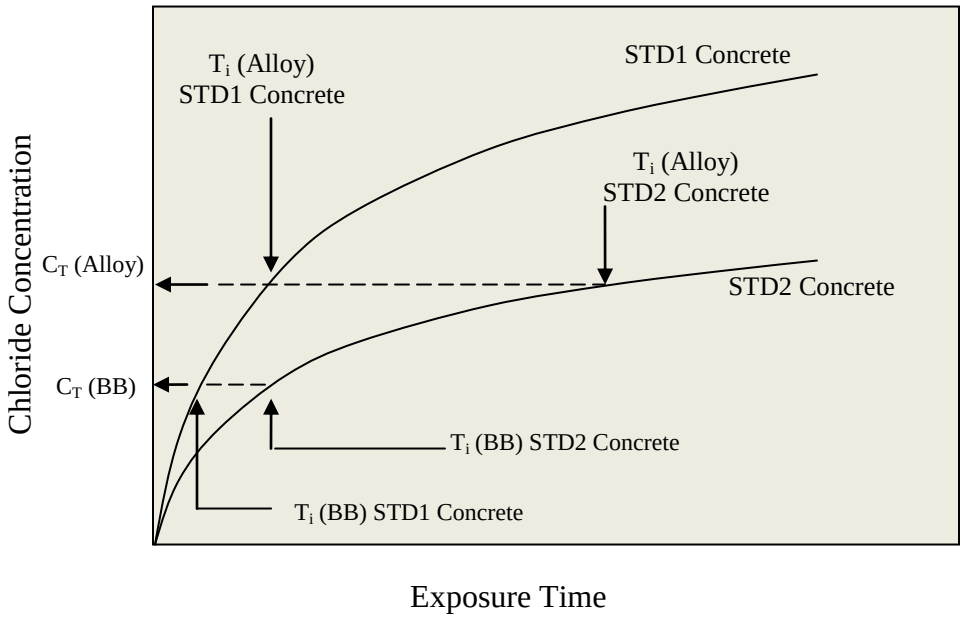

Figure 4-17: Schematic illustration of T_i for BB and an improved performance reinforcement in STD1 and STD2 concretes.

Table 4-14: Listing of T_i for STD1G and STD1 MS specimens along with the three specimen average for each of the two exposures.

STD1G				STD1			
BB	3Cr12	MMFX-2	2101	BB	3Cr12	MMFX-2	2101
64	320	201	348	97	121	68	144
201	433	201	433	147	212	211	215
201	516	376	680	182	488	230	295
Average							
155	423	259	487	142	274	170	218

4.1.2.2. High Performance Reinforcements.

Outdoor Exposures. Figures 4-18 to 4-22 show plots of potential and macro-cell current versus time, respectively, for 316.16SS, 316.18SS, 304SS, STAX, and SMI reinforced STD1-MS specimens. With the exception of the 316.16 data, for which macro-cell current excursions were relatively small, the plots consist of occasional current "bursts" to as high as 38 μA (Figure 4-21) followed by repassivation. For STD2-MS-304, -316.16, and -316.18 specimens, macro-cell current excursions were of lesser magnitude and more infrequent than for STD1. In the case of STD2-MS-SMI and -STAX, the excursions were about the same as for STD1. Table 4-15 lists the maximum and minimum currents that were recorded for

these STD1 and STD2 specimens, where the positive current corresponds to the top bar being cathodic to a lower bar (or bars) and negative to the top bar being anodic.

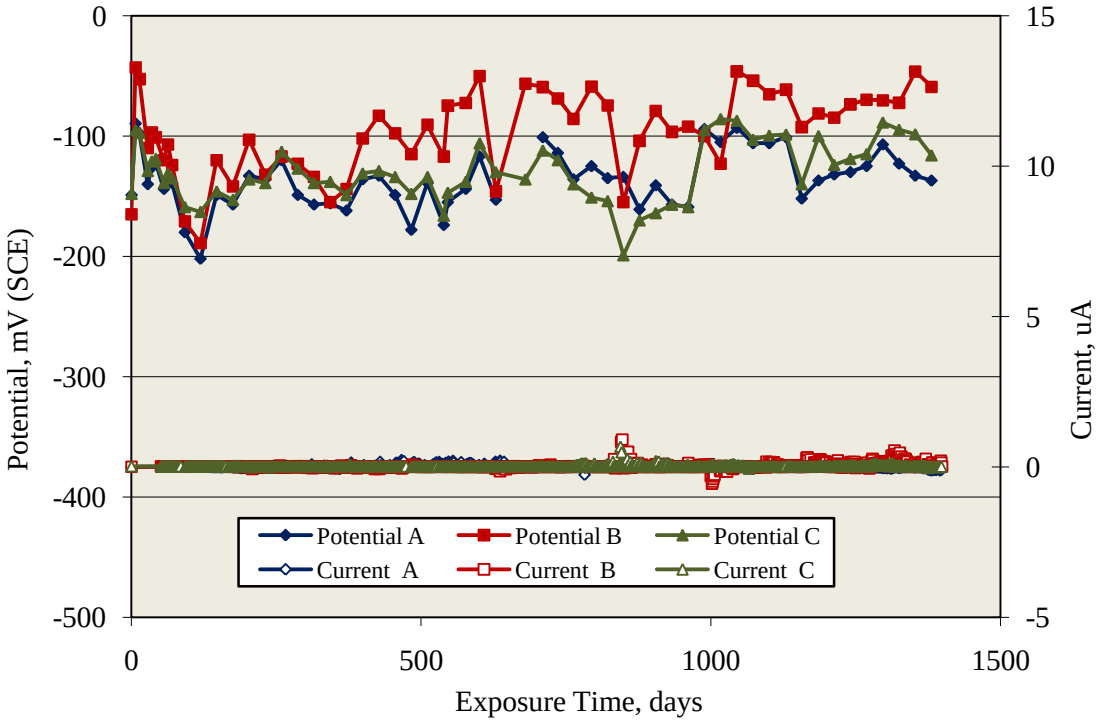

Figure 4-18: Potential and macro-cell current history for MS-STD1-316.16 specimens.

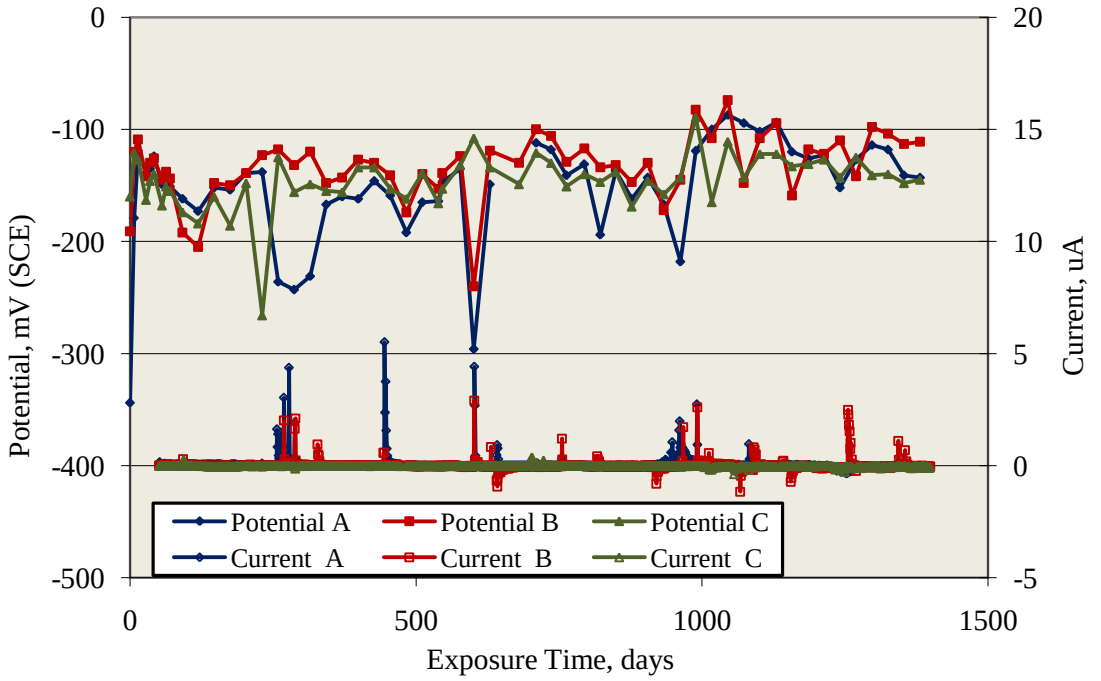

Figure 4-19: Potential and macro-cell current history for MS-STD1-316.18 specimens.

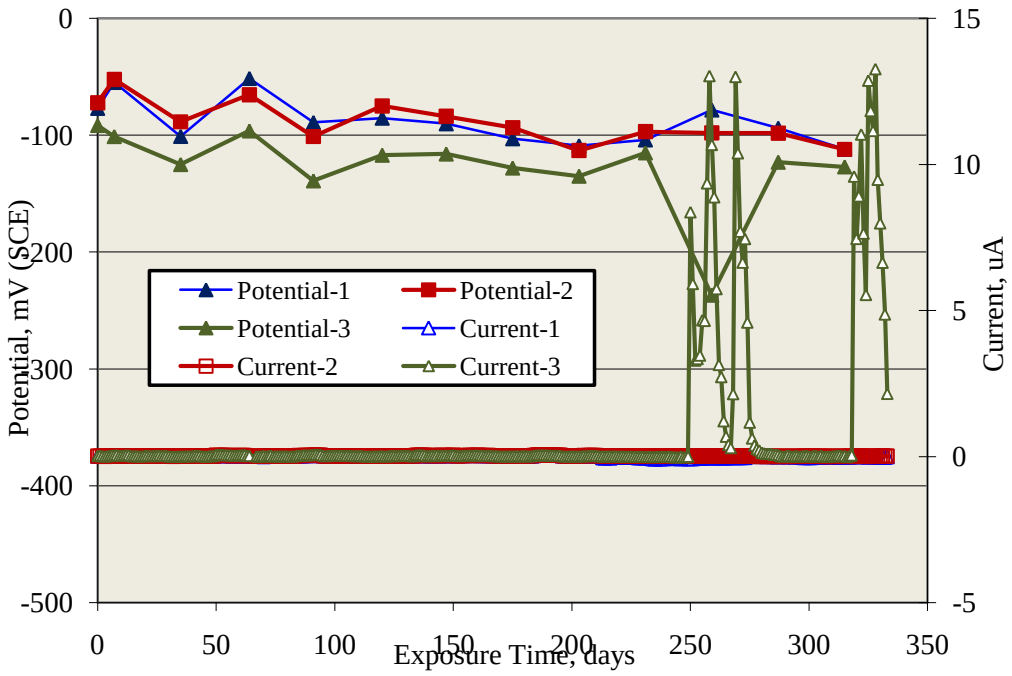

Figure 4-20: Potential and current history for MS-STD1-304 specimens.

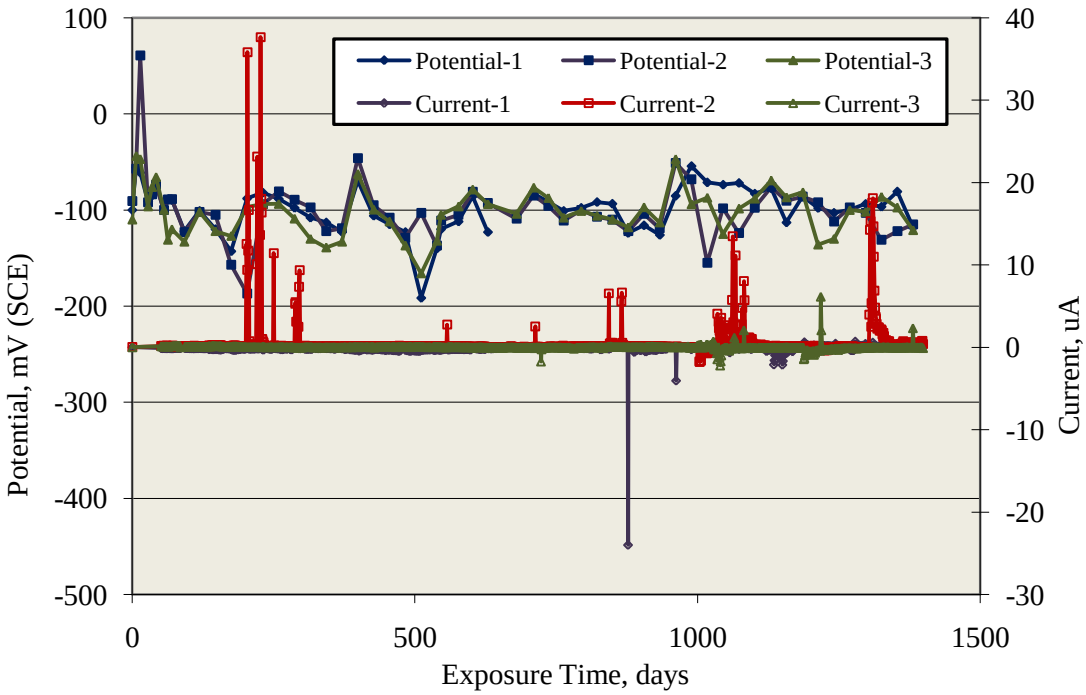

Figure 4-21: Potential and macro-cell current history for MS-STD1-STAX specimens.

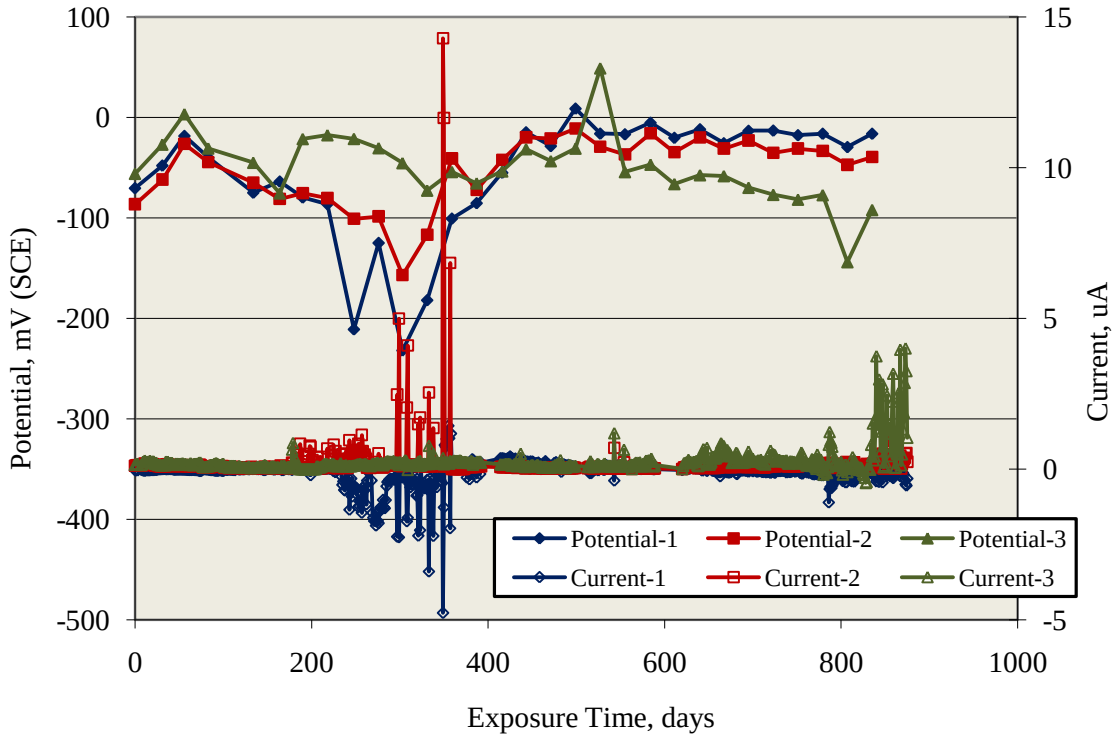

Figure 4-22: Potential and macro-cell current history for MS-SMI specimens.

Results for the other specimen types are presented according to type of reinforcement. Thus, Table 4-16 lists maximum and minimum macro-cell currents for 316.16 reinforced specimens; and Figure 4-23 shows potential and macro-cell current versus time for these CCNB specimens, which had the largest and most frequent current excursions. For 316.18, the only non-STD specimen type was CCON for which the maximum and minimum macro-cell currents were 7.0 and -14.2 μA, respectively. Table 4-17 lists results for non-STD 304 reinforced specimens, and Figure 4-24 plots potential and macro-cell current for the CCNB specimens with this reinforcement (same specimen type as for 316.16 (Figure 4-23)) which exhibited the largest current excursions. Table 4-18 shows the maximum and minimum macro-cell currents recorded for SMI reinforced specimens. For this alloy, the CSDB and USDB specimens exhibited relatively large current excursions; and Figures 4-25 and 4-26 show the time history for these. For each reinforcement, time of exposure is also shown, as this varied for the different cases. Exposure time for 316.18 specimens was 1,387 days.

Calculations were made to determine the corrosion rate associated with the above current excursions. To do this, charge transfer was computed as the area under the current-time plots; and this served as input to Faraday's law from which mass loss and, ultimately, wastage rate were determined.

Table 4-15: Listing of maximum and minimum macro-cell currents for high alloy STD1 MS specimen (positive current corresponds to the top bar layer being anodic to the lower layer and negative to the lower layer being anodic to the top).

Specimen Type	Macro-cell Current, μA									
	316.16		316.18		304		SMI		STAX	
	Max.	Min.	Max.	Min.	Max.	Min.	Max.	Min.	Max.	Min.
STD1	1.2	-5.5	0.4	-0.9	0	-13.3	4.8	-14.3	4.1	-37.7
STD2	2.8	-1.4	0.7	-6.2	0	-0.6	8	-3.7	1.3	-24.2

Table 4-16: Maximum and minimum macro-cell currents for Type 316.16 specimens other than STD1 and STD2.

Specimen Type	Macro-cell Current, μA		Exposure Time, days
	Max.	Min.	
ARWB	1.1	-0.7	1,370
BENT	1.3	-12.7	1,380
CCON	0.9	-1.9	1,383
BCAT	3.1	-42.7	1,388
BNTB	13.9	-20.4	1,378
CBNB	15.2	-32.9	1,376
CBNT	3.2	-12.0	1,376
CCNB	4.0	-46.1	1,380

1 mmpy = 39.4 mpy.

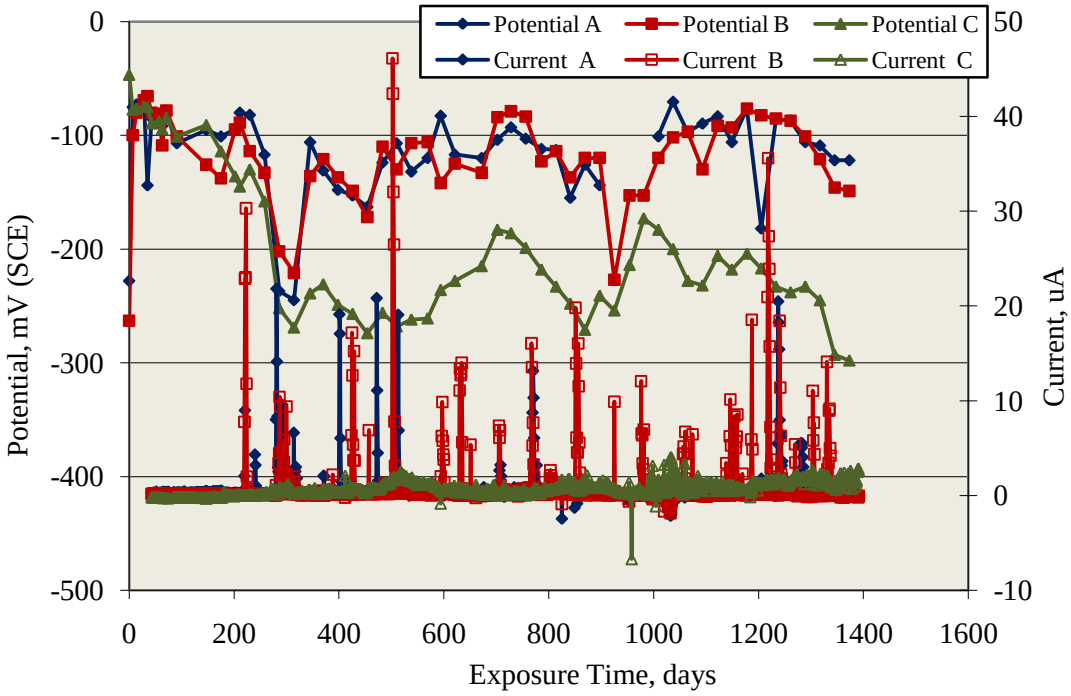

Figure 4-23: Potential and macro-cell current history for MS-CCNB-316.16 specimens.

Tables 4-19 to 4-29 show these results for specimens with relatively high charge transfer. In some cases, the calculations were made for cathodic current excursions as well as anodic, since these correspond to anodic activity on one or more of the lower bars. The columns labeled "Avg. Corr. Rate" list corrosion rates based upon the total exposure time assuming wastage occurred uniformly over the entire exposed surface. For "Avg. Corr. Rate During Current Spike," the calculations were based only the time during

Table 4-17: Maximum and minimum macro-cell currents for Type 304 specimens other than STD1 and STD2.

Specimen Type	Macro-cell Current, μA		Exposure Time, days
	Max.	Min.	
ARWB	0.2	-0.2	303
BENT	0.0	-0.1	302
CCON	0.9	-11.3	330
BCAT	0.1	-0.4	331
BNTB	0.9	-3.3	302
CBNB	0.0	-15.0	303
CBNT	0.0	-2.0	302
CCNB	0.2	-48.6	303

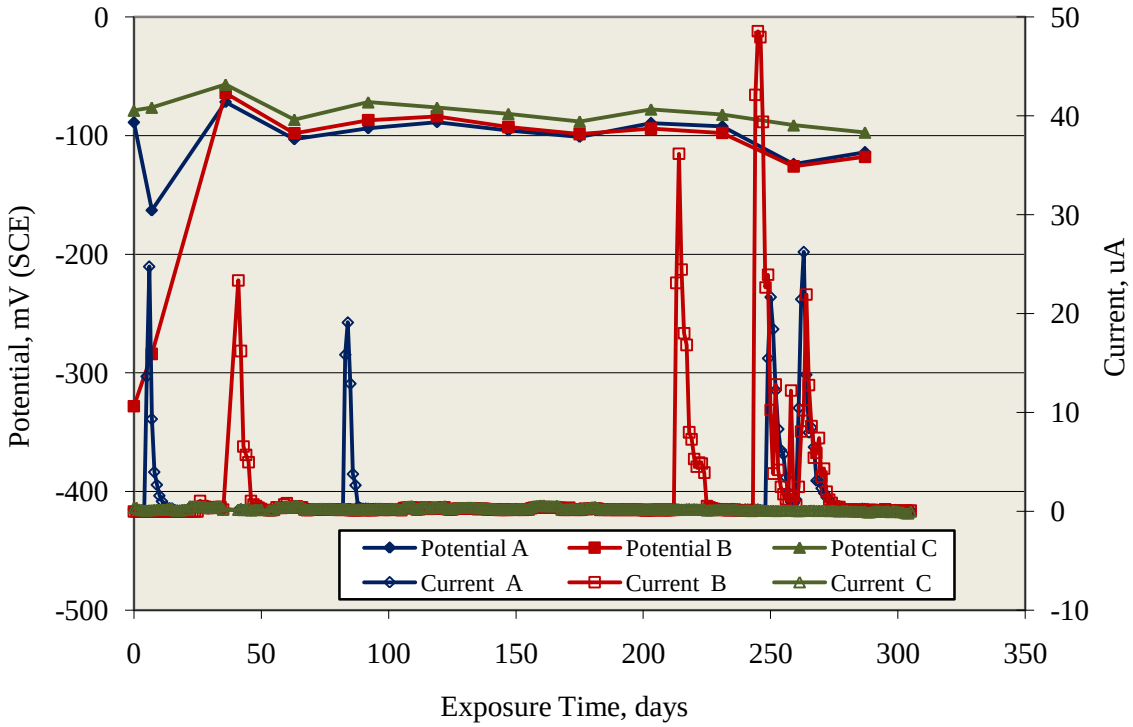

Figure 4-24: Potential and macro-cell current history for MS-CCNB-304 specimens.

which current excursions occurred. The column "Local Corr. Rate," on the other hand, assumes that wastage during the macro-cell current spikes occurred solely within a one mm square area such that the corrosion was localized and that all current activity occurred at the same location. While localization per se is likely, activation sites were probably random. Otherwise, successive activation and repassivation events would have occurred repeatedly at a single location. While this assumption is probably unrealistic, the calculation on which it is based does constitute a worst case situation. In most cases, this localized

attack was at a rate of several mmpy or less; however, for CSDB-MS-316.16-B corrosion rate exceeded 22 mmpy.

Table 4-18: Maximum and minimum macro-cell currents for SMI specimens other than STD1 and STD2.

Specimen Type	Macro-cell Current, μA		Exposure Time, days
	Max.	Min.	
ARWB	1.2	-2.7	302
BENT	16.1	-17.7	302
CCON	3.4	-3.6	330
CBNT	3.5	-13.7	302
BCCD	10.6	-6.4	877
CSDB	3.7	-32.2	917
UBDB	4.4	-28.7	903
USDB	2.8	-9.7	887

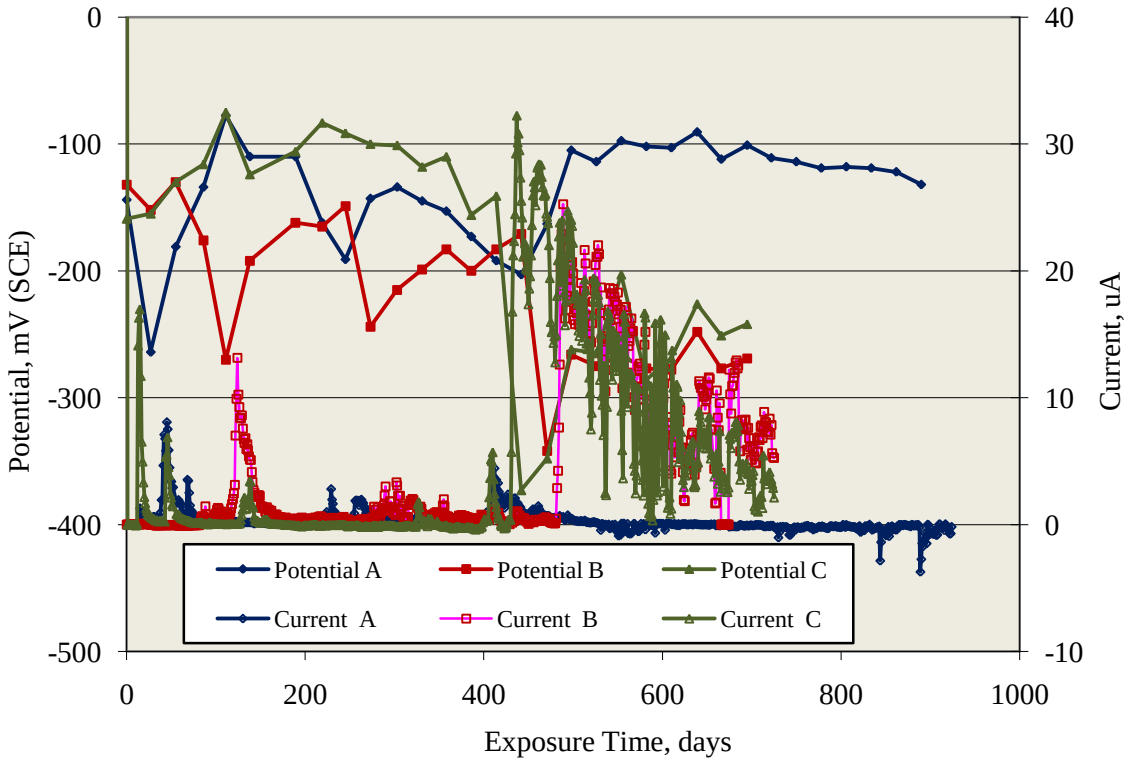

Figure 4-25: Potential and macro-cell current history for MS-CSDB-SMI specimens.

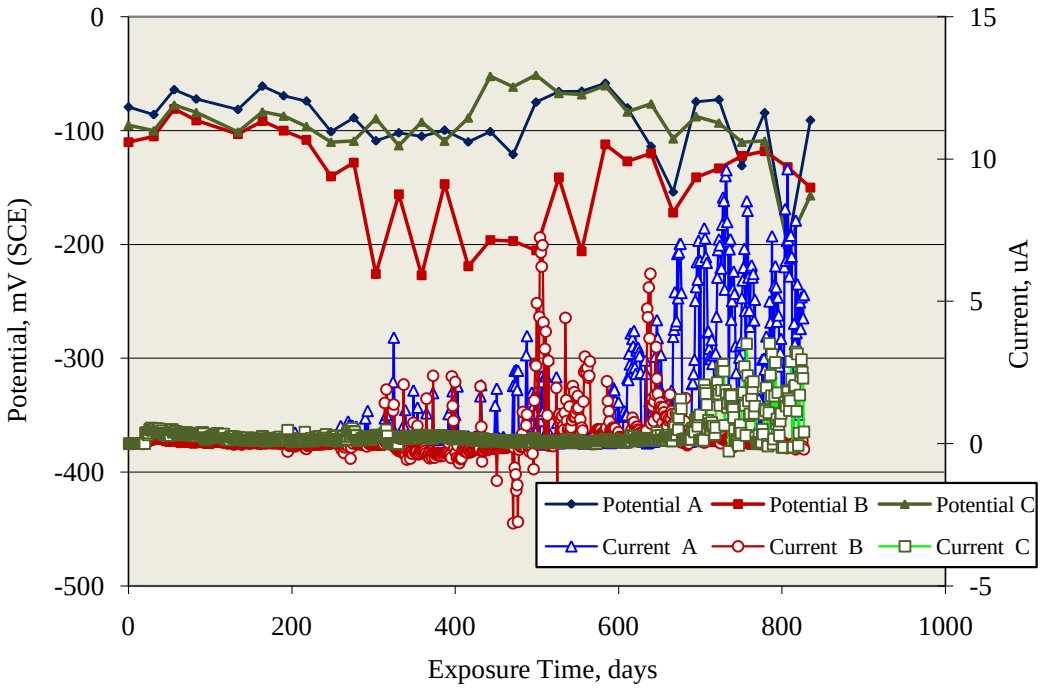

Figure 4-26: Potential and macro-cell current history for MS-USDB-SMI specimens.

Table 4-19: Corrosion rate calculations for STD1-MS specimens with relatively high current excursions.

Rebar Type	Avg. Corr. Rate, mmpy	Avg. Corr. Rate During Current Spike, mmpy	Local Corr. Rate, mmpy
316.16-A	1.01E-05	1.24E-04	0.78
316.16-B	5.16E-06	6.33E-05	0.40
304-C	1.52E-04	1.08E-03	6.82
SMI-C	2.34E-05	3.49E-05	0.22
SMI-B	3.90E-05	5.80E-05	0.37
STAX-B	8.54E-05	1.02E-05	0.06

Table 4-20: Corrosion rate calculations for the STD2-MS specimen with relatively high current excursions.

Rebar Type	Avg. Corr. Rate, mmpy	Avg. Corr. Rate During Current Spike, mmpy	Local Corr. Rate, mmpy
STAX-B	2.13E-04	6.20E-04	3.93

Table 4-21: Corrosion rate calculations for CCON-MS specimens with relatively high current excursions.

Rebar Type	Avg. Corr. Rate, mmpy	Avg. Corr. Rate During Current Spike, mmpy	Local Corr. Rate, mmpy
316.18-A	1.60E-05	6.51E-05	0.10
316.18-B	3.91E-05	2.80E-04	0.25

Table 4-22: Corrosion rate calculations for BENT-MS specimens with relatively high current excursions.

Rebar Type	Sense of Current	Avg. Corr. Rate, mmpy	Avg. Corr. Rate During Current Spike, mmpy	Local Corr. Rate, mmpy
316.16-A	Anodic	3.19E-05	1.49E-04	0.94
316.16-B	Anodic	2.24E-05	1.42E-04	0.90
316.16-C	Anodic	4.17E-05	1.13E-04	0.71
SMI-A	Anodic	1.42E-04	3.19E-04	2.02
	Cathodic	1.62E-04	5.74E-04	3.63
SMI-B	Anodic	1.72E-04	3.00E-04	1.90
	Cathodic	4.45E-05	4.05E-04	2.57
SMI-C	Anodic	2.47E-06	2.40E-04	1.52
	Cathodic	9.35E-05	1.58E-08	0.59

Table 4-23: Corrosion rate calculations for the BCAT-MS specimen with relatively high current excursions.

Rebar Type	Avg. Corr. Rate, mmpy	Avg. Corr. Rate During Current Spike, mmpy	Local Corr. Rate, mmpy
316.18-A	1.28E-04	2.32E-04	1.47

Table 4-24: Corrosion rate calculations for CBNT-MS specimens with relatively high current excursions.

Rebar Type	Avg. Corr. Rate, mmpy	Avg. Corr. Rate During Current Spike, mmpy	Local Corr. Rate, mmpy
316.18-A	2.96E-05	3.24E-04	0.19
SMI-A	8.34E-05	3.39E-04	2.14
SMI-B	1.27E-04	2.08E-04	0.80

Table 4-25: Corrosion rate calculations for CBNB-MS specimens with relatively high current excursions.

Rebar Type	Sense of Current	CBNB		
		Avg. Corr. Rate,	Avg. Corr. Rate During	Local Corr. Rate,
316.16-A	Anodic	3.25E-05	2.69E-04	1.70
	Cathodic	6.79E-04	3.49E-03	22.11
316.16-B	Anodic	1.62E-04	4.67E-04	2.96
	Cathodic	2.37E-04	4.10E-04	2.60
316.16-C	Anodic	3.74E-06	1.92E-04	1.21
	Cathodic	5.20E-04	6.81E-04	4.31

Table 4-26: Corrosion rate calculations for CSDB-MS specimens with relatively high current excursions.

Rebar Type	Avg. Corr. Rate, mmpy	Avg. Corr. Rate During Current Spike, mmpy	Local Corr. Rate, mmpy
SMI-A	6.82E-05	1.62E-04	1.02
SMI-B	6.82E-05	8.98E-05	0.57

Table 4-27: Corrosion rate calculations for CCNB-MS specimens with relatively high current excursions.

Rebar Type	Avg. Corr. Rate, mmpy	Avg. Corr. Rate During Current Spike, mmpy	Local Corr. Rate, mmpy
316.18-A	9.61E-05	1.38E-04	0.61
316.18-B	9.61E-05	1.63E-04	1.03

Table 4-28: Corrosion rate calculations for CCNB-MS specimens with relatively high current excursions.

Rebar Type	Avg. Corr. Rate, mmpy	Avg. Corr. Rate During Current Spike, mmpy	Local Corr. Rate, mmpy
SMI-A	1.84E-04	2.31E-04	1.46
SMI-B	5.36E-05	1.42E-04	0.90
SMI-C	5.72E-05	4.25E-01	0.00

Table 4-29: Corrosion rate calculations for the BCAT-MS specimen with relatively high current excursions.

Rebar Type	Avg. Corr. Rate, mmpy	Avg. Corr. Rate During Current Spike, mmpy	Local Corr. Rate, mmpy
SMI-A	4.73E-04	6.47E-04	4.10

Controlled Temperature and Relative Humidity Exposures. Table 4-30 lists maximum and minimum macro-cell currents for specimens in this category. Upon comparison to data in Table 4-15, it is apparent that the magnitude of these was less than for specimens exposed outdoors. In most cases, only a single excursion was recorded. Apparently, variable temperature or humidity (or both) enhanced macro-cell activity for the higher alloyed reinforcements to a greater extent than when temperature and relative humidity were controlled, although the magnitude of the effect was not of practical significance.

Table 4-31 lists the high performance reinforcement MS specimens that were tested and, assuming that the temporal current activity discussed above did not constitute corrosion initiation, shows also the T_i ratio for these to the average T_i for STD1-MS-BB specimens (142 days). Because exposure time varied

Table 4-30: Listing of maximum and minimum macro-cell currents for MS-STD1G specimens.

Specimen Type	Macro-cell Current, μA									
	316.16		316.18		304		SMI		STAX	
	Max.	Min.	Max.	Min.	Max.	Min.	Max.	Min.	Max.	Min.
STD1G	0	-3.9	0.3	-3.6	0	-0.1	0.3	-0.1	0.5	-0.1

Table 4-31: Listing of exposure times and T_i(alloy)/T_i(BB) for high performance reinforced MS specimens.

Exposure Time, days				
316.16	316.18	304	SMI	STAX
1,399	1,383-1,399	305-333	305-924	1,399
T_i(alloy)/T_i(BB)				
>9.8	>9.7 - >9.8	>2.1 - >2.3	>2.1 - >6.5	>9.8

depending on set number, the ratios also differ from one alloy to the next depending upon when testing commenced with the largest ratio being >9.8.

4.1.3. 3-Bar Tombstone Column (3BTC) Specimens

4.1.3.1. Reinforcements of Improved Performance

As noted in Section 3, either three or six standard 3BTC specimens of the STD2 and STD3 mix designs and selected reinforcement types were prepared; and potential of all bars connected as well as voltage drop across the resistor between each long bar (designated as bars 1 and 3) and the other (designation of the shorter bar was 2) were measured daily. Typical examples of the potential and macro-cell current versus time behavior that were observed are illustrated by Figures 4-27 to 4-30. In all cases, a relatively abrupt potential transition to more negative values occurred at a specific time; and this was considered as indicating corrosion initiation. Concurrently, a positive macro-cell current excursion for one of the two measurement pairs and a negative excursion for the other were noted; however, the relative polarity of individual bars sometimes changed subsequently such that the macro-cell current – time trends conformed to one of several types of behavior. Thus, in Figure 4-27 (3BCT-BB specimen A), the potential shift and corrosion current (bar 1) occurred at 89 days. However, after 102 days bar 3 became anodic also, indicating that bar 2 was serving as cathode to both of the longer bars. At 224 days, bar 3

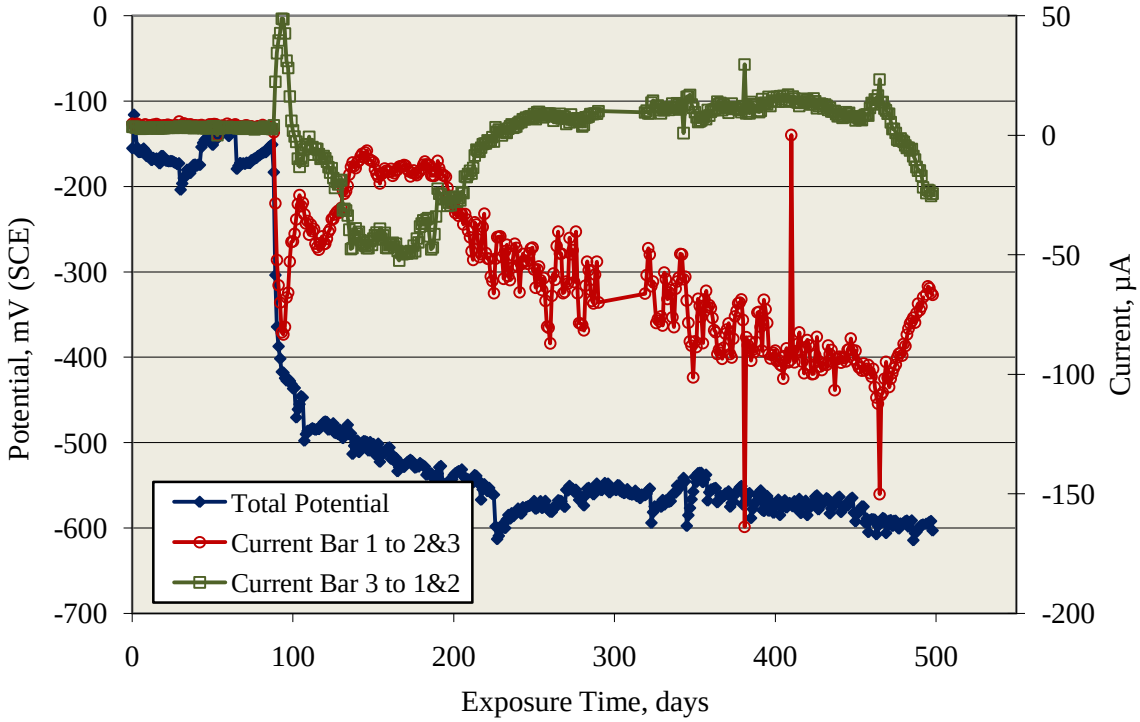

Figure 4-27: Potential and macro-cell current between indicated bars for 3BCT-BB specimen A.

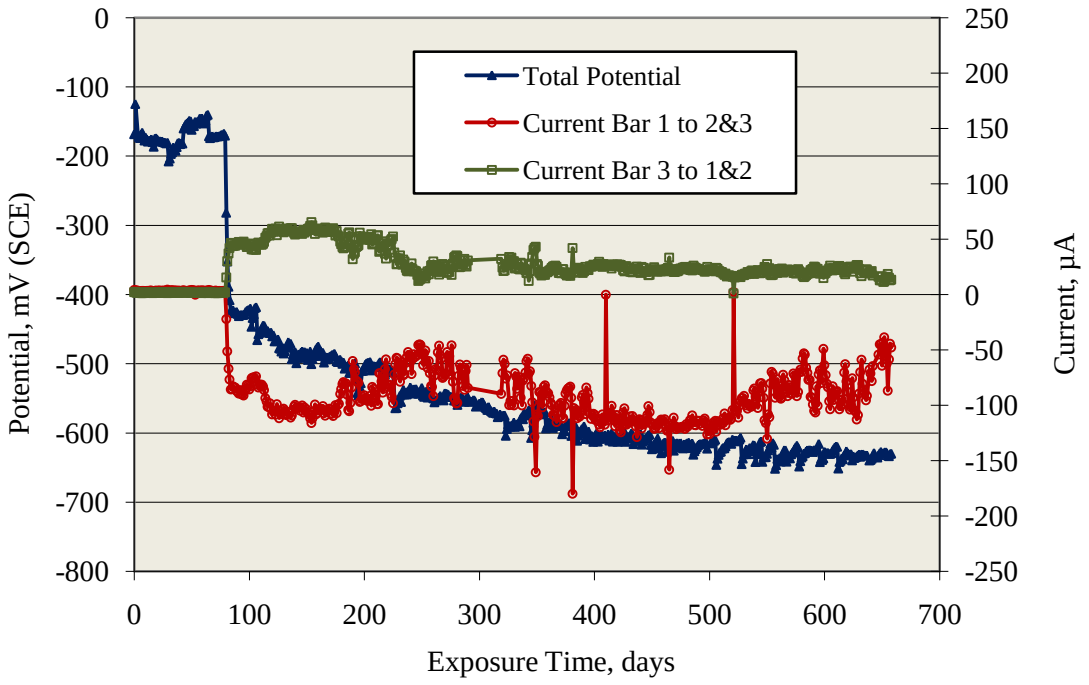

Figure 4-28: Potential and macro-cell current between indicated bars for 3BCT-BB specimen B.

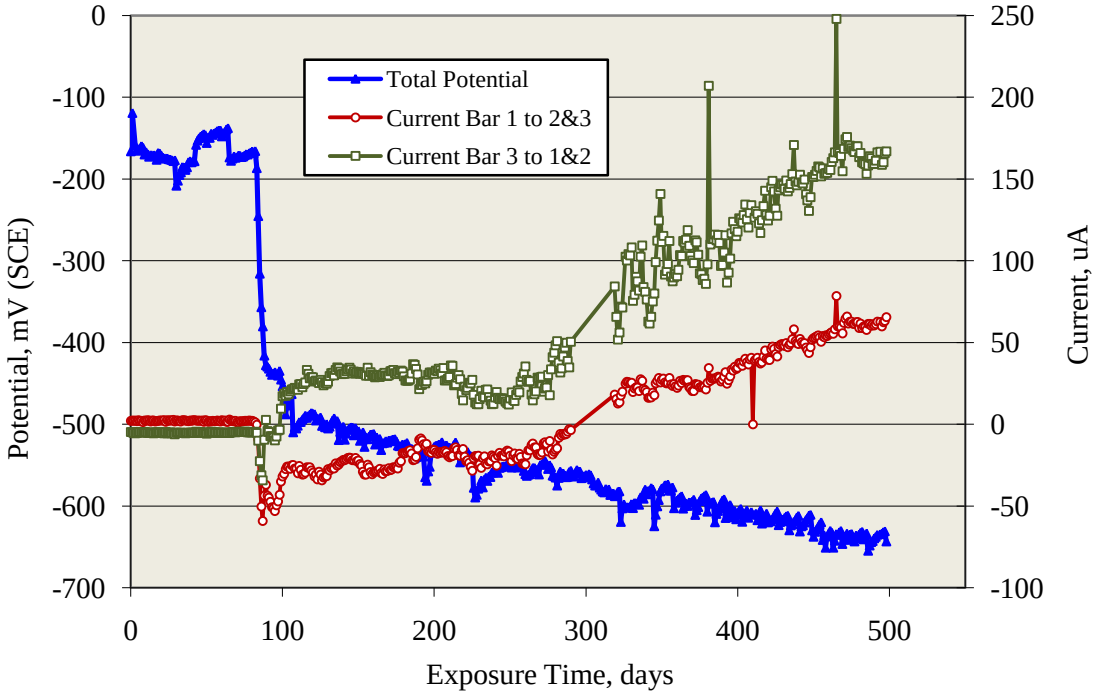

Figure 4-29: Potential and macro-cell current between indicated bars for 3BCT-BB specimen D.

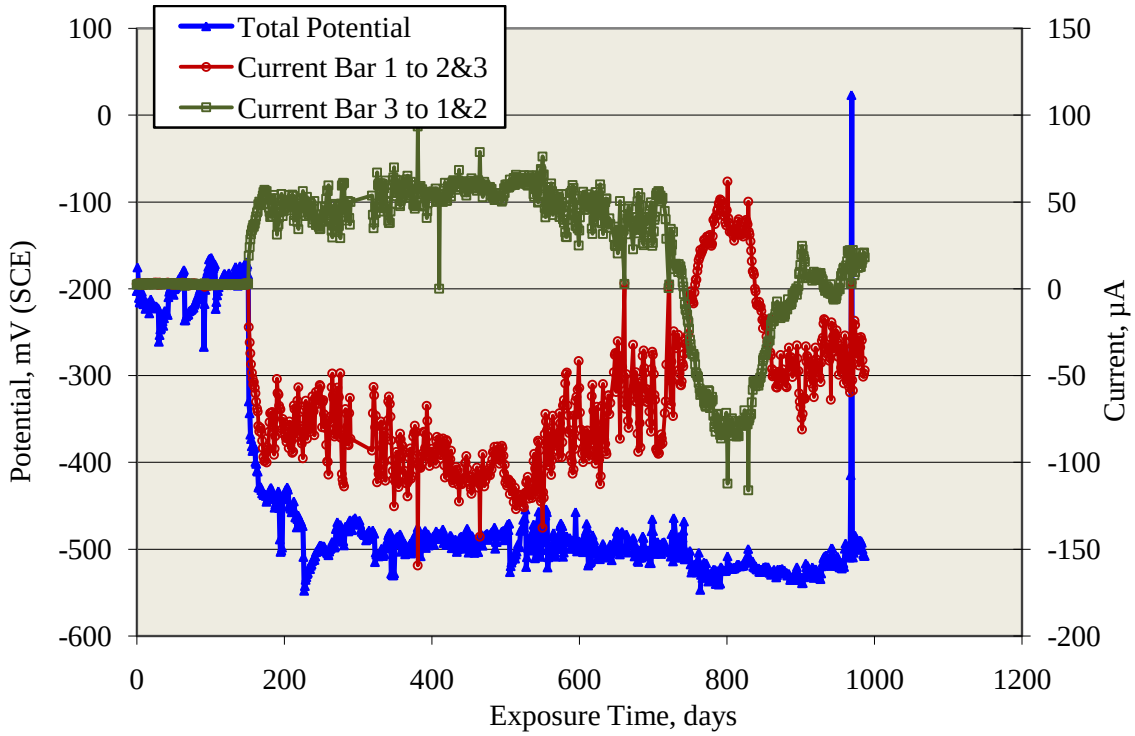

Figure 4-30: Potential and macro-cell current between indicated bars for 3BCT-BENT-3Cr12-C.

became cathodic again but reverted to anodic at 476 days. The second example is provided by Figure 4-28 (3BCT-BB specimen B), where corrosion initiated on bar 1 at 80 days with bar 3 serving as cathode. The fact that current for the former exceeded that of the latter indicates that bar 2 must also have been a cathode. These relative polarities remained throughout the test. In Figure 4-29 (3BTC-BB specimen D), corrosion initiated after 84 days with bar 1 being an anode and 3 the cathode. However, current from bar 3 to 1&2 reversed after 99 days such that it was now an anode as well and remained so thereafter, whereas current from bar 1 to 2&3 became cathodic at 290 days. Lastly, 3BTC-BENT-3Cr12 specimen C (Figure 4-30) initiated corrosion after 152 days with positive current from bar 1 to 2&3 indicating that bar 1 was an anode and negative current from bar 3 to 1&2 indicating that bar 3 was a cathode. Current remained positive for bar 1 to 742 days at which time it became a cathode (negative current), whereas current from bar 3 to 1&2 was anodic after 757 days. These polarities remained until 838 for bar 1 and 893 for bar 3 at which times both currents again reversed.

Table 4-32 lists the improved performance 3BTC specimens and provides the T_i for each. Normal cumulative distribution function plots of T_i for 3BTC-BB, -3Cr12, -MMFX-2, and -2101 reinforcements in both concretes (STD2 and STD3) are presented in Figures 4-31 to 4-35. The first of these (Figure 4-31) illustrates T_i distribution for the reinforcements in STD2 concrete and the second (Figure 4-32) in

Table 4-32: Listing of 3BTC specimens with improved performance reinforcements and the T_i for each.

Black Bar												
Concrete Mix	STD2						STD3					
Specimen No.	A	B	C	D	E	F	A	B	C	D	E	F
Ti	88	80	65	84	80	70	64	60	55	56	70	58
Average	78						61					

3Cr12															
Concrete Mix	STD2			STD3						BENT			ELEV		
Specimen No.	A	B	C	A	B	C	D	E	F	A	B	C	A	B	C
Ti	89	296	419	170	203	179	236	361	206	98	160	152	75	373	177
Average	268			226						137			208		

MMFX-2															
Concrete Mix	STD2			STD3						BENT			ELEV		
Specimen No.	A	B	C	A	B	C	D	E	F	A	B	C	A	B	C
Ti	520	406	366	279	349	165	154	248	316	239	351	248	172	304	336
Average	431			252						279			271		

2101															
Concrete Mix	STD2			STD3						BENT			ELEV		
Specimen No.	A	B	C	A	B	C	D	E	F	A	B	C	A	B	C
Ti	197	286	248	91	200	221	65	55	95	192	168	117	106	164	57
Average	244			121						159			109		

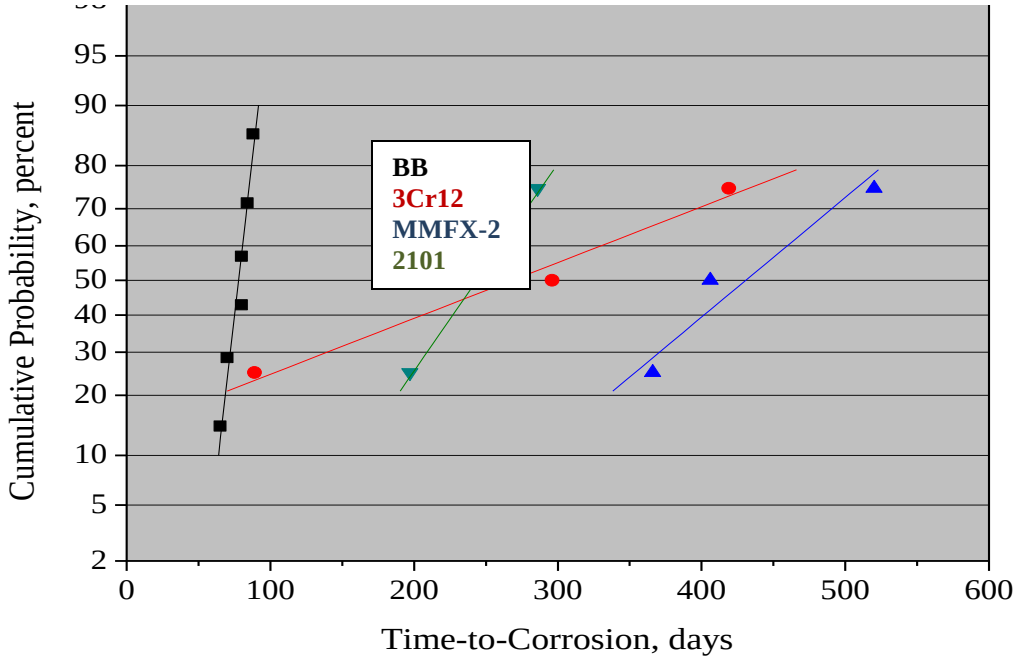

Figure 4-31: Cumulative probability plot of T_i for 3BTC-STD2 specimens for each reinforcement.

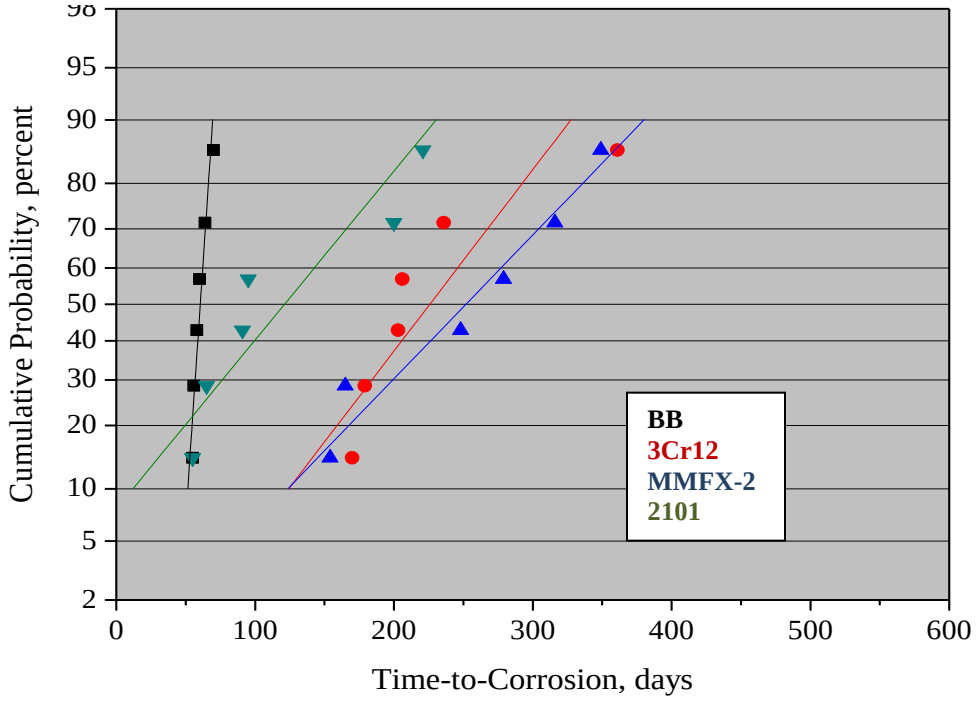

Figure 4-32: Cumulative probability plot of T_i for 3BTC-STD3 specimens with each reinforcement.

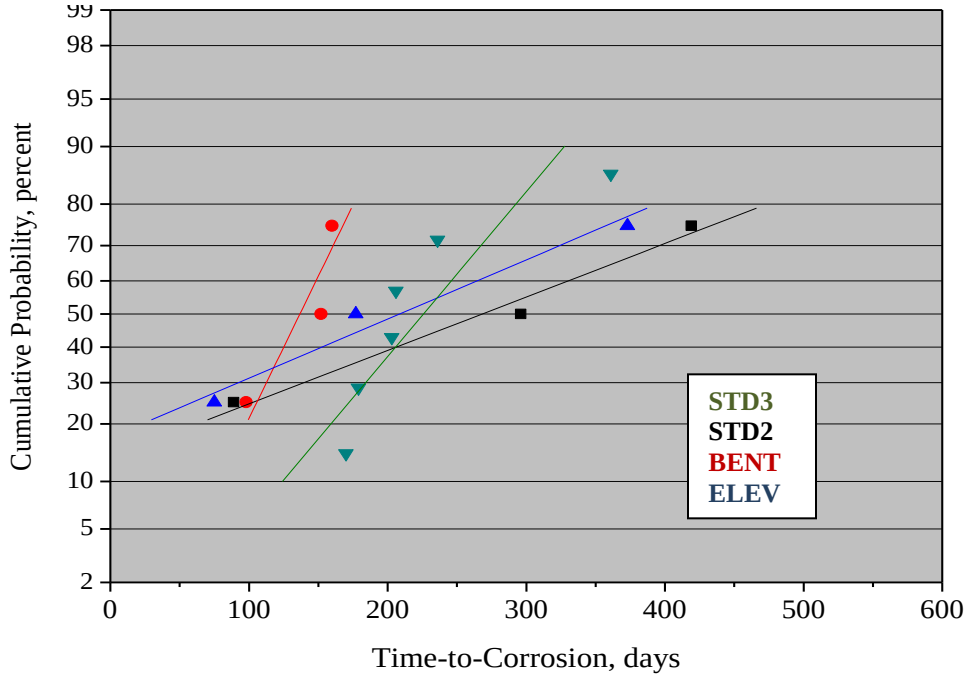

Figure 4-33: Cumulative probability plot of T_i for 3BTC-3Cr12 specimens.

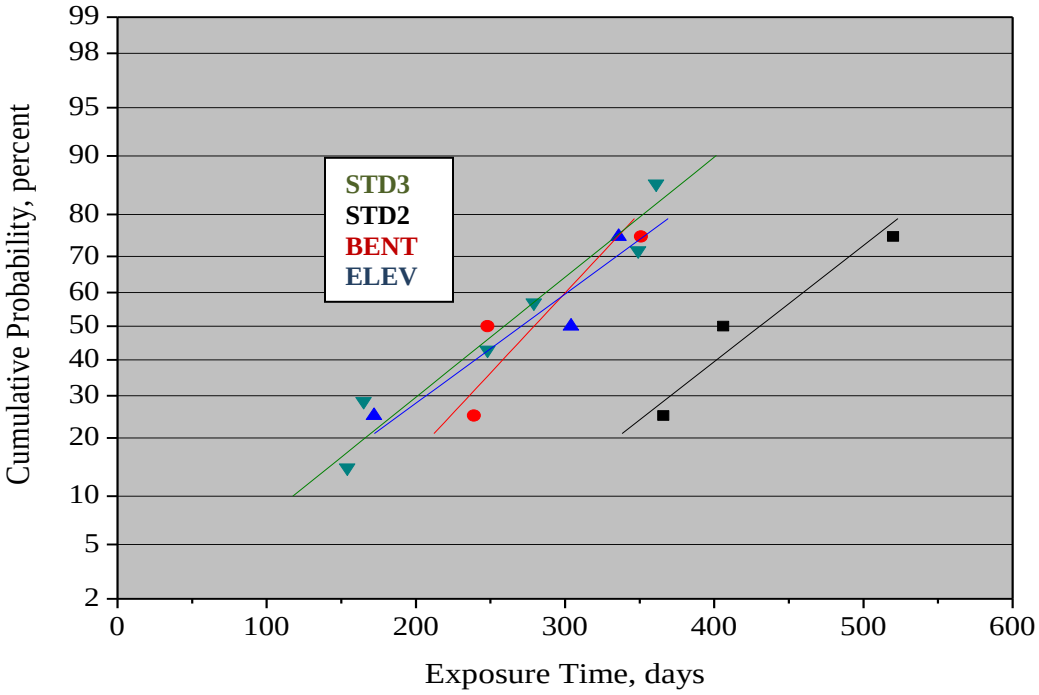

Figure 4-34: Cumulative probability plot of T_i for 3BTC-MMFX-2 specimens.

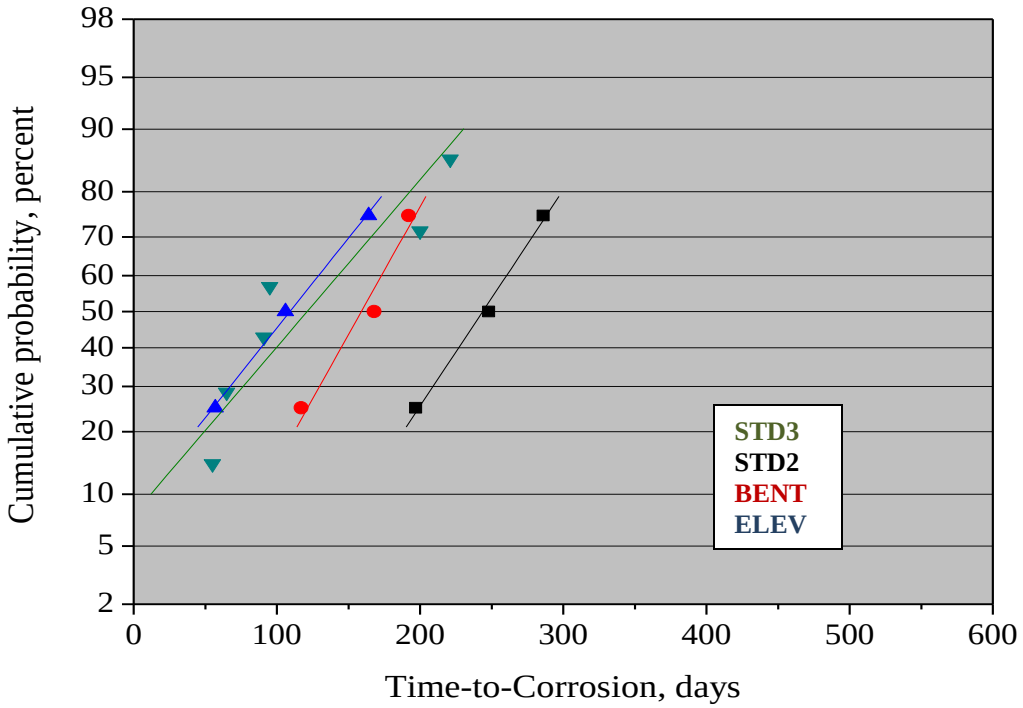

Figure 4-35: Cumulative probability plot of T_i for 3BTC-2101 specimens.

STD3. Tables 4-33 and 4-34 list T_i and T_i(alloy)/T_i(BB) values at 2, 10, and 20 percent corrosion activity for the STD2 and STD3 3BTC specimens, respectively, as determined by extrapolating the best for line for each specimen data set in Figures 4-31 and 4-32, respectively. This determination was not made in cases where the extrapolation yielded an unrealistically low or negative T_i. For all reinforcements, T_i is greater in STD2 than STD3 concrete, consistent with the former having lower water-to-cement ratio than the latter (0.41 compared to 0.50, see Table 3-3). Also, the T_i ratio of each corrosion resistant reinforcement to black bar at different percentages active was higher for the STD2 than STD3 concrete, which is consistent with results from the MS specimens, as mentioned above. Thus, T_i(alloy)/T_i(BB) for MMFX-2 in STD3 concrete was in the range 0.9 to 3.4, whereas in STD2 it was 3.7-6.4. The results indicate T_i ordering of these alloys relative to black bar (highest to lowest) as MMFX-2 ≈ 3Cr12 > 2101 > BB. Figures 4-33 to 4-35, on the other hand, plot normal CDF of T_i for the different bar configurations (straight, bent, and elevated) for 3Cr12, MMFX-2, and 2101, respectively, in STD3 concrete but with the STD2 data included for comparison. In the latter two cases (MMFX-2 and 2101, Figures 4-34 and 4-35), the difference in T_i distribution for the different bar configurations may be within the range of experimental scatter. The data are more distributed in the case of 3Cr12, however, with the ordering of T_i being (highest to lowest) STD2 > ELEV ≈ STD3 > BENT. Even here, it is unclear

Table 4-33: T_i data and T_i(alloy)/T_i(BB) at 2, 10, and 20 percent cumulative active for improved performance 3BTC specimens in STD2 concrete.

Cumulative Percentage Active	Reinforcement Type				T_i(alloy)/T_i(BB)	
	BB	3Cr12	MMFX-2	2101	MMFX-2	2101
2	53	-	198	112	3.7	2.1
10	61	-	282	160	5.3	3.0
20	65	-	337	190	6.4	3.6

Table 4-34: T_i data at 2, 10, and 20 percent cumulative active for 3BTC specimens with improved performance reinforcements in STD3 concrete.

Cumulative Percentage Active	Reinforcement Type				T_i(alloy)/T_i(BB)	
	BB	3Cr12	MMFX-2	2101	3Cr12	MMFX-2
2	48	56	45	-	1.2	0.9
10	49	127	128	-	2.6	2.7
20	51	156	162	-	3.3	3.4

Table 4-35: T_i data at 2, 10, and 20 percent cumulative active for 3BTC specimens reinforced with 3Cr12.

Cumulative Percentage Active	3Cr12			
	STD2	STD3	BENT	ELEV
2	-	56	45	-
10	-	127	78	-
20	-	156	100	-

Table 4-36: T_i data at 2, 10, and 20 percent cumulative active for 3BTC specimens reinforced with MMFX-2.

Cumulative Percentage Active	MMFX-2			
	STD2	STD3	BENT	ELEV
2	107	29	105	23
10	281	114	173	117
20	336	162	208	170

Table 4-37: T_i data at 2, 10, and 20 percent cumulative active for 3BTC specimens reinforced with 2101.

Cumulative Percentage Active	2101			
	STD2	STD3	BENT	ELEV
2	101	-	44	-
10	155	-	87	-
20	189	-	111	-

if the differences are real or simply reflect data scatter. Tables 4-35 to 4-37 list the T_i values at 2, 10, and 20 percent active according to extrapolation of the best fit line in Figures 4-33 to 4-35, respectively.

4.1.3.2. High Performance Reinforcements

For all high performance reinforcements that were included in 3BTC specimens (316.16, 304, and SMI), potential remained relatively positive for the duration of the exposures; and no sustained decreases (as seen in specimens with improved performance bars) occurred. Figures 4-36 and 4-37 illustrate the two general types of macro-cell current response that were observed. In both cases, macro-cell current, either from bar 1 to 2&3 or bar 3 to 1&2, was typically several μA starting from initial exposure. In the former case (Figure 4-36), the two sets of current measurements are of approximately the same magnitude but opposite sign, such that bar 3 was anode, bar 1 the cathode, and with little apparent contribution from bar 2. For Figure 4-37, however, both currents are negative, indicating that they served as cathodes to an anodic bar 2. Also, current spikes followed by repassivation

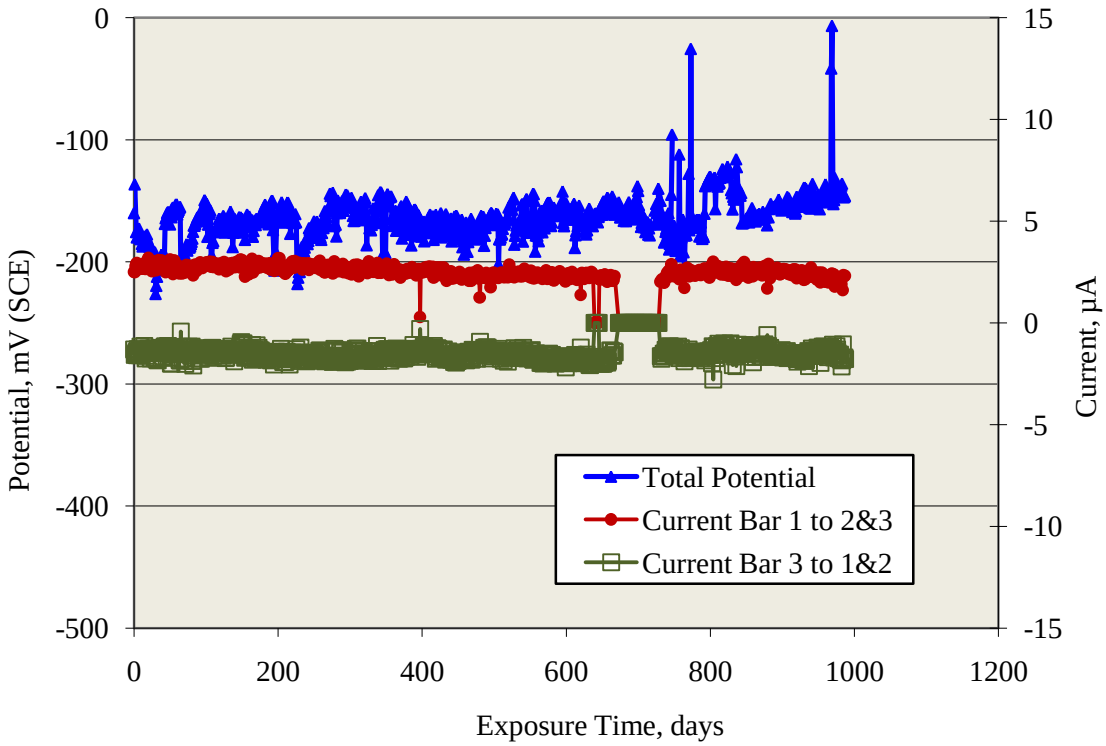

Figure 4-36: Potential and macro-cell current versus time for 3BTC-SMI-specimen B in STD 3 concrete.

are more apparent here than in Figure 4-36. The latter behavior (Figure 4-37) was more typical and reflects bar 2 having a more negative potential than bars 1 and 3, although all bars apparently remained passive. Table 4-38 lists the maximum and minimum currents recorded during exposure of each

specimen. As for the higher alloyed MS specimens, corrosion rate associated with these current excursions was minimal.

Table 4-38: Maximum and minimum macro-cell currents recorded for the high alloy reinforcement 3BTC specimens.

Specimen Type/Number	Macro-cell Current, μA					
	316.16		304		SMI	
	Max.	Min.	Max.	Min.	Max.	Min.
STD2-A	0.2	-4.1	-1.8	-4.9	-0.4	-4.7
STD2-B	0.3	-4.4	-1.8	-6.6	-0.3	-6.7
STD2-C	0.3	-4.7	-1.5	-4.4	-0.2	-7.5
STD3-A	-0.3	-5.0	2.1	-11.1	-0.7	-8.0
STD3-B	-0.3	-5.7	0.3	-6.9	-0.3	-3.2
STD3-C	0.0	-6.8	-0.3	-4.9	-0.5	-3.7
STD3-D	0.6	-4.2	1.1	-4.4	0.1	-9.1
STD3-E	1.6	-5.5	-0.3	-5.7	0.1	-6.3
STD3-F	-0.1	-3.8	-0.1	-7.0	0.2	-4.5
BENT-A	-0.2	-4.0	-0.3	-5.1	-0.4	-3.8
BENT-B	-0.3	-4.3	-0.4	-5.2	-0.1	-3.8
BENT-C	-0.3	-4.6	-0.3	-6.1	-0.2	-3.7
ELEV-A	1.2	-6.3	0.3	-5.7	-0.5	-4.2
ELEV-B	0.1	-6.7	-6.3	0.2	-0.3	-5.5
ELEV-C	-0.4	-4.9	0.1	-5.0	-0.6	-6.1

4.1.4. Field Column Specimens

Figures 4-38 to 4-44 show potential versus exposure time plots for field column specimens with each type of reinforcement (BB, 3Cr12, MMFX-2, 2101, 316.16, 304, and SMI). The letters W, G, R, and Y in the specimen designation identify each of the four reinforcing bars in each column specimen. Data for the improved performance (3Cr12, MMFX-2, and 2101) and black bar specimens (Figures 4-38 to 4-41) exhibit a potential shift to relatively negative values. This often occurred within the first few days of exposure. Apparently, the high permeability concrete (STD1 mix design), facilitated by rapid sorptive Cl^- transport and possibly defects in the concrete or cracks, caused the threshold concentration for this species to be achieved relatively early in the exposures. The potential – time behavior for one of the three 316.16SS reinforced specimens (-C, Figure 4-38) was similar to that of the improved performance reinforced specimens. However, this particular specimen was damaged upon installation; and the negative potentials compared to the other two 316.16 reinforced specimens probably resulted from this.

Results of the R_p determinations are presented in Figure 4-45 for improved performance

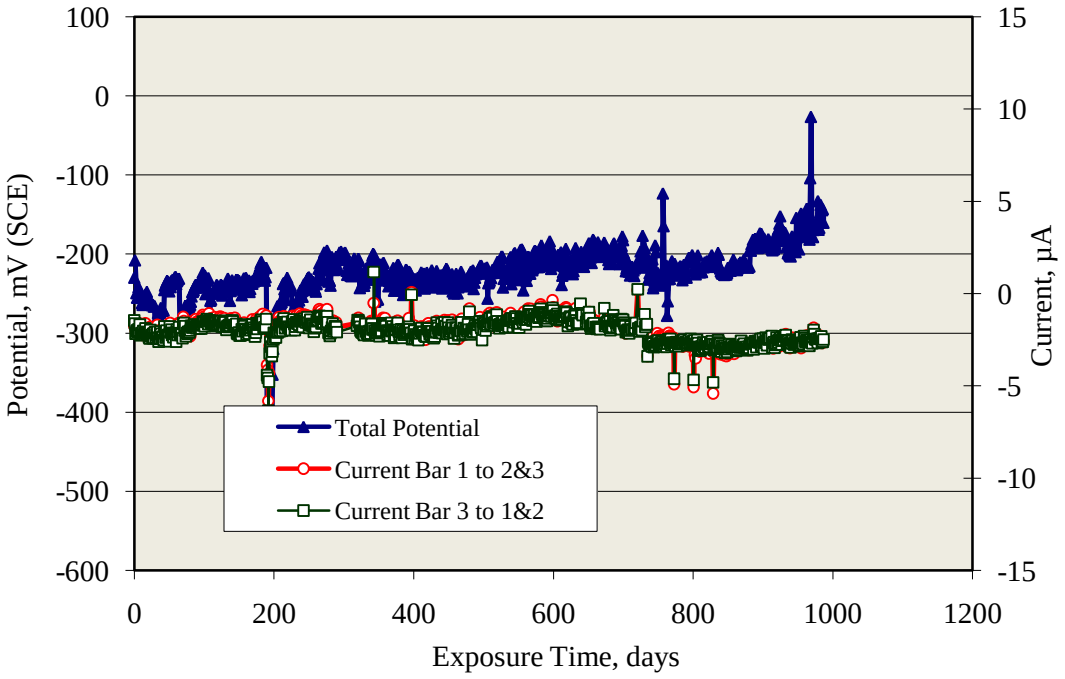

Figure 4-37: Potential and macro-cell current versus time for 3BTC-316.16-ELEV specimen A.

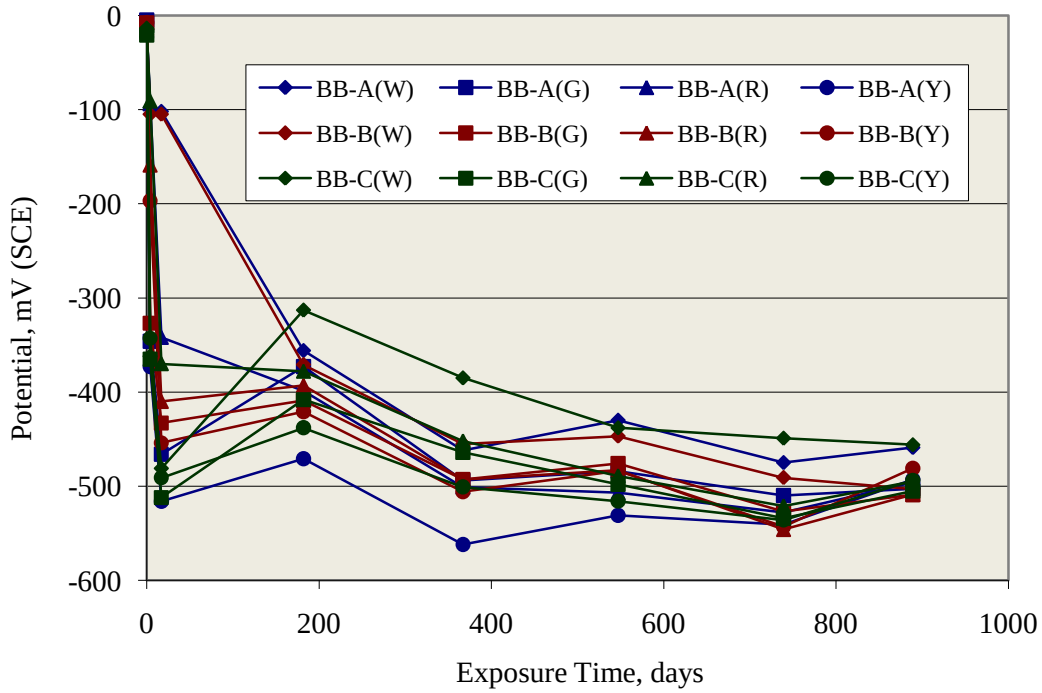

Figure 4-38: Potential versus exposure time plot for field columns with BB reinforcement.

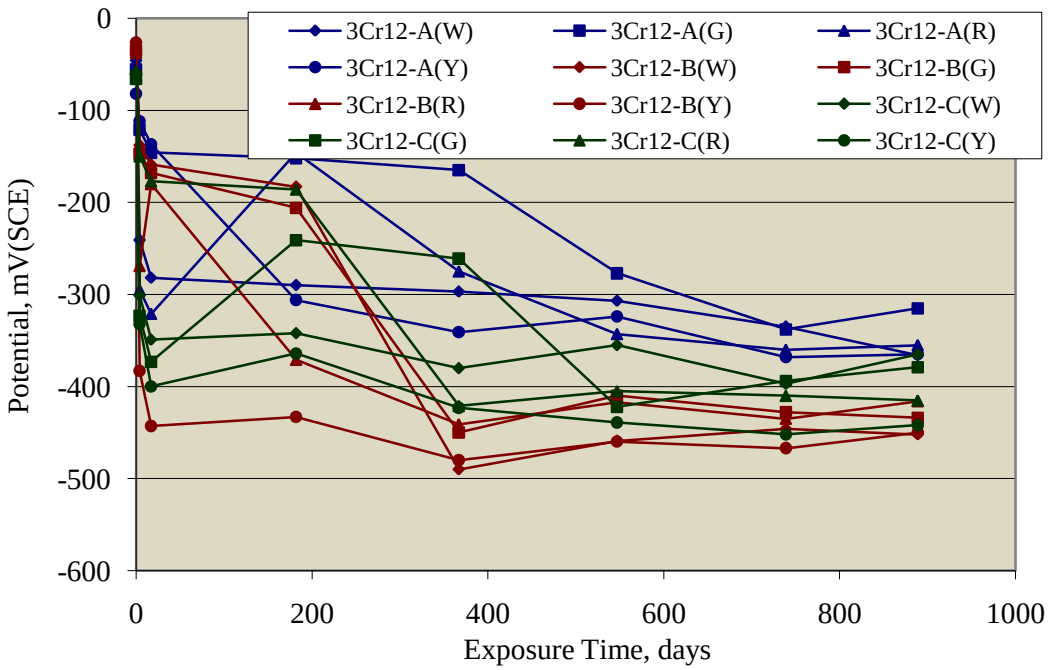

Figure 4-39: Potential versus exposure time plot for field columns with 3Cr12 reinforcement.

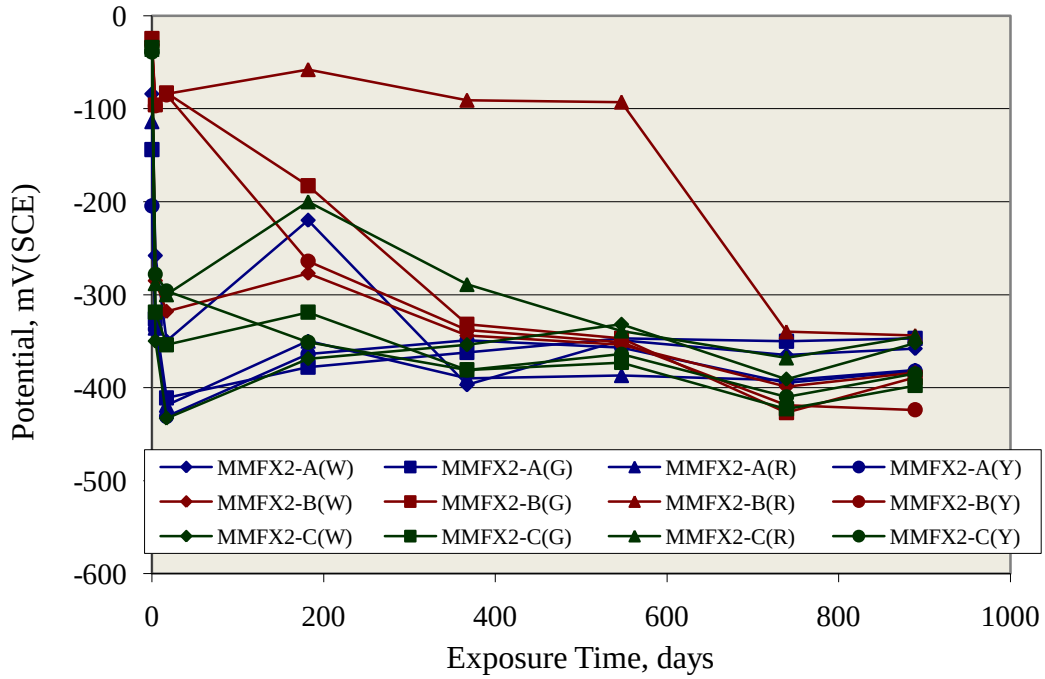

Figure 4-40: Potential versus exposure time plot for field columns with MMFX-2 reinforcement.

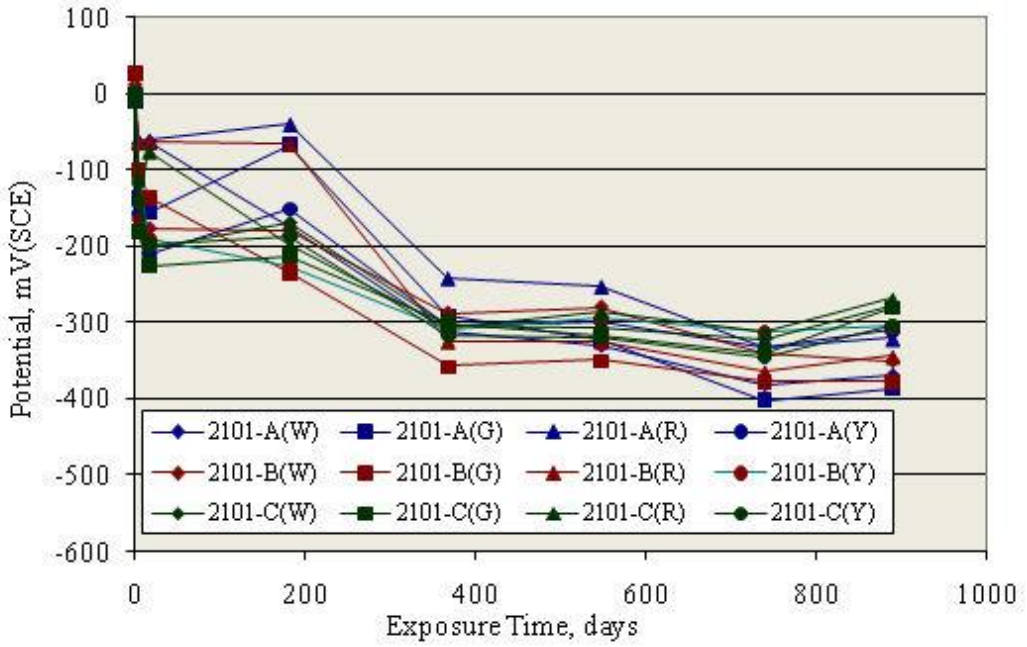

Figure 4-41: Potential versus exposure time plot for field column with 2101 reinforcement.

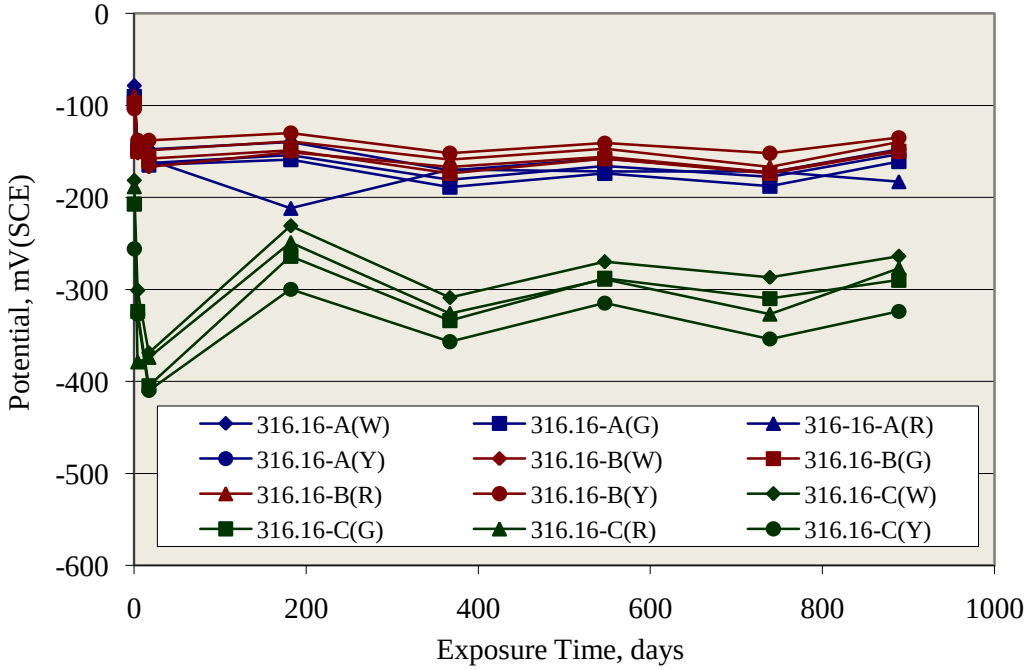

Figure 4-42: Potential versus exposure time plot for field columns with 316.16 reinforcement.

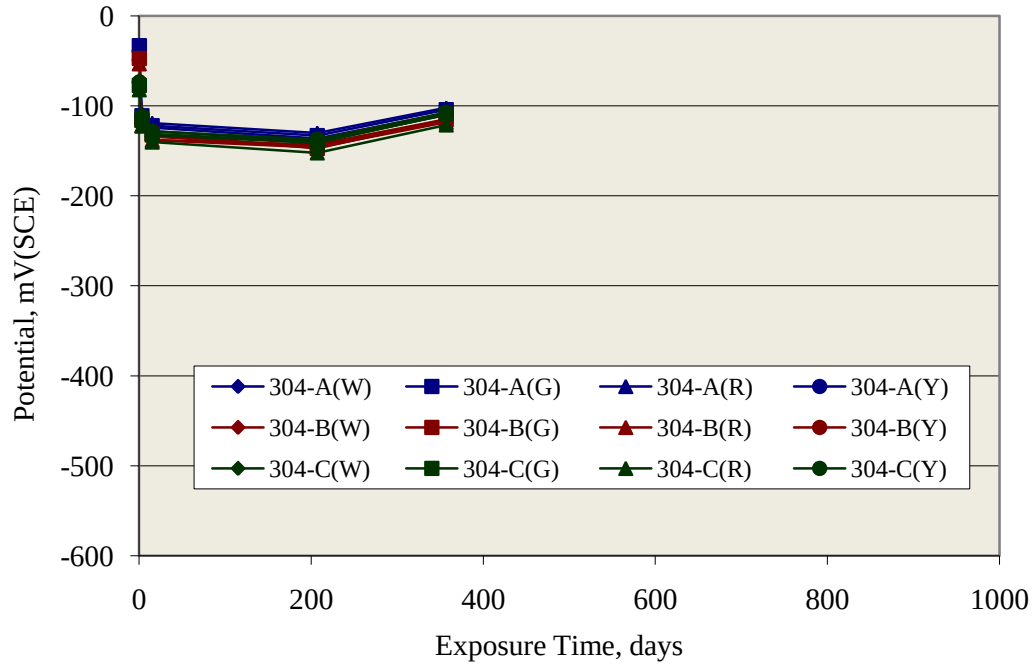

Figure 4-43: Potential versus exposure time plot for field columns with 304 reinforcement.

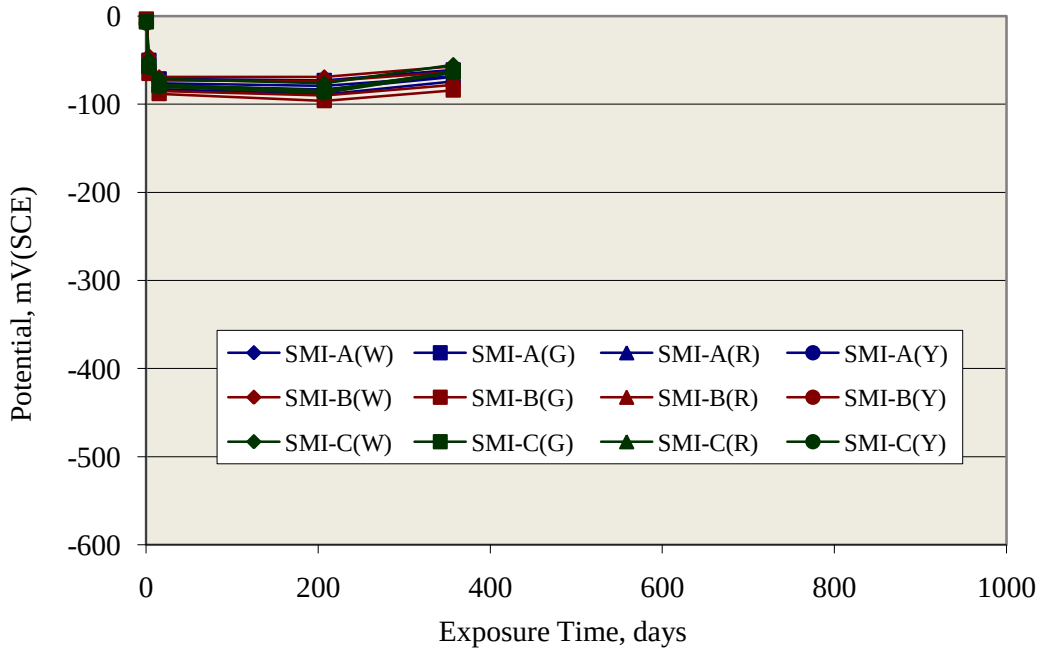

Figure 4-44: Potential versus exposure time plot for field column with SMI reinforcement.

reinforcements and in Figure 4-46 for the high alloy ones. For the former, R_p decreased with exposure time according to a generally common trend; and since corrosion rate is inversely proportional to R_p, the relatively low values are consistent with the corresponding potential data (Figures 4-38 to 4-41) and

support the likelihood that corrosion had initiated. Polarization resistances for the high performance bar specimens (Figure 4-46) were generally more than an order of magnitude or more greater than for the improved performance bars. Also, these values remained relatively constant with time and ordered (high to low) as 316.16, 304, and SMI. Specimen 316.16-C, which was discussed above, is an exception to this. Because surface area of the working electrode for the R_p measurements was unknown, the units are in Ohms rather than the more conventional Ohm·cm^2.

Figures 4-47 and 4-48 show plots of R_p versus potential for the improved and high performance bar specimens, respectively. In the former plot, the data generally track from high R_p and potential to low according to the decrease in both parameters as the exposures progressed. This trend is displaced somewhat to lower R_p at a given potential for 2101 and to higher for MMFX-2. For the high performance specimens (Figure 4-48), 316.16-C and 304-C exhibited potentials near -300 mV(SCE), whereas for other specimens potentials were positive to -200 mV(SCE). The SMI bars have the most positive potentials compared to the other reinforcements in this category despite R_p being relatively low. Because of the limited data, no attempt was made to estimate T_i for the different bar types.

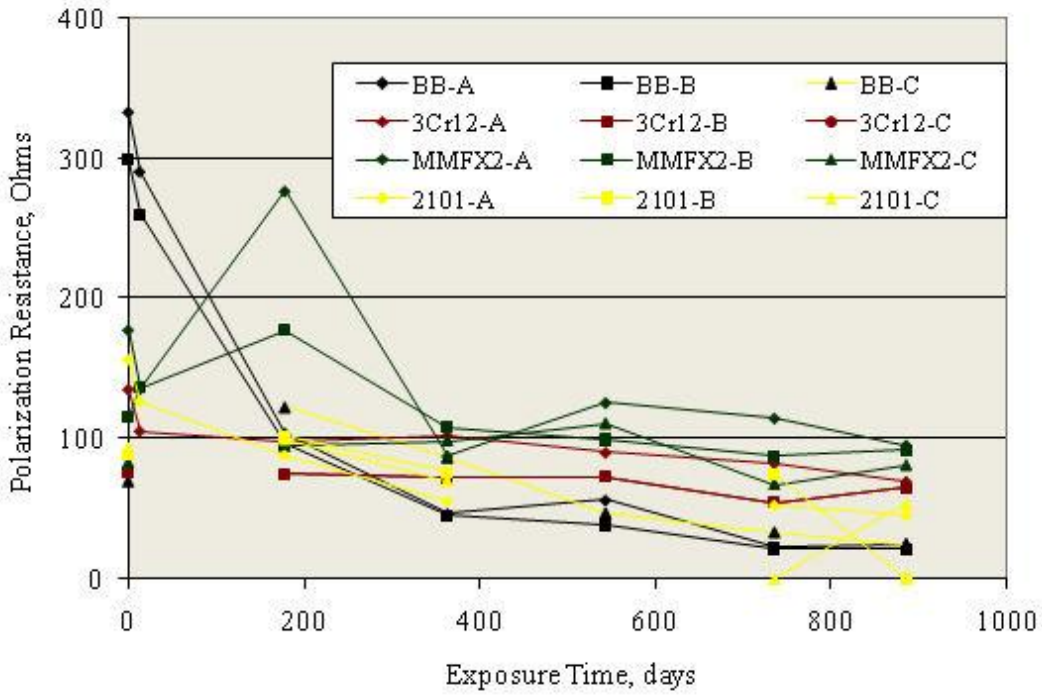

Figure 4-45: Polarization resistance versus exposure time plot for field columns with improved performance reinforcements.

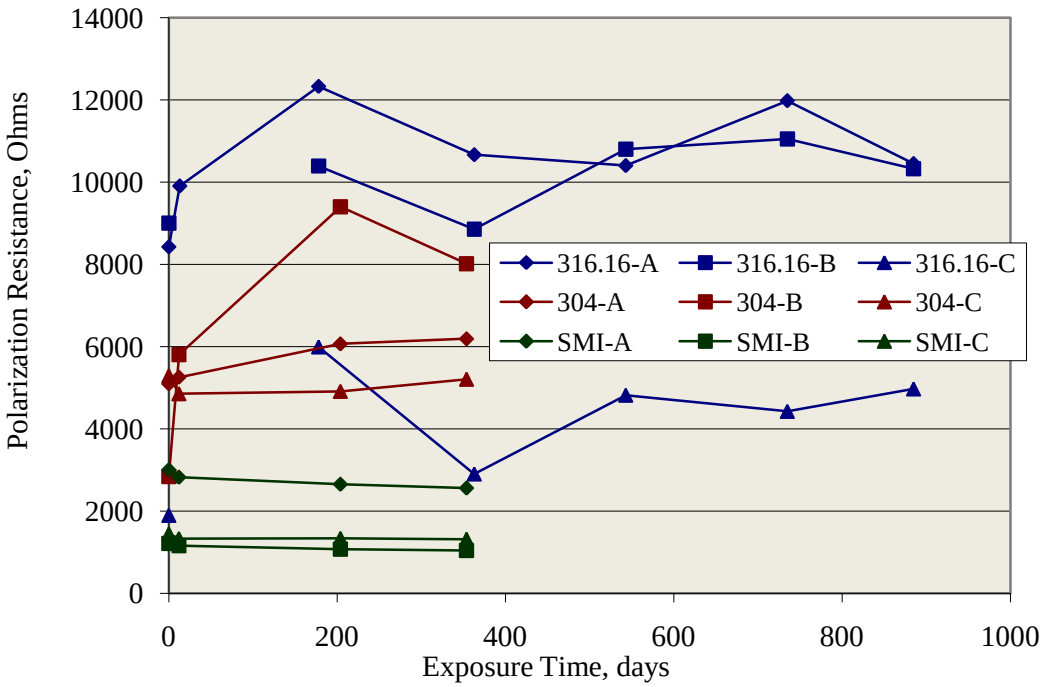

Figure 4-46: Polarization resistance versus exposure time plot for field columns with high alloy reinforcements.

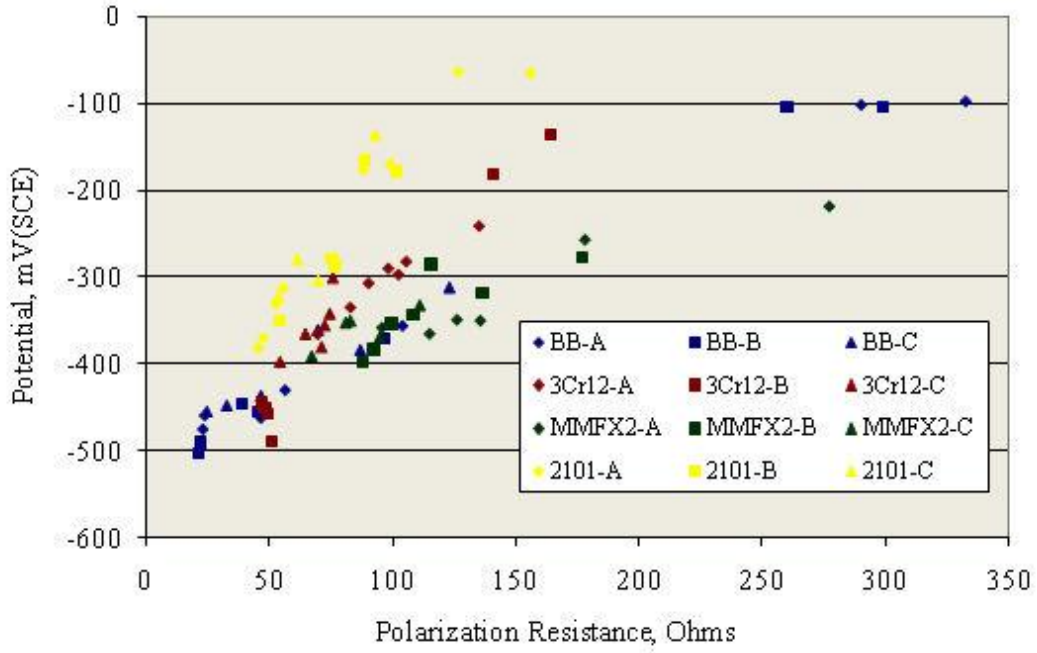

Figure 4-47: Plot of polarization resistance versus potential for field columns with improved performance reinforcements.

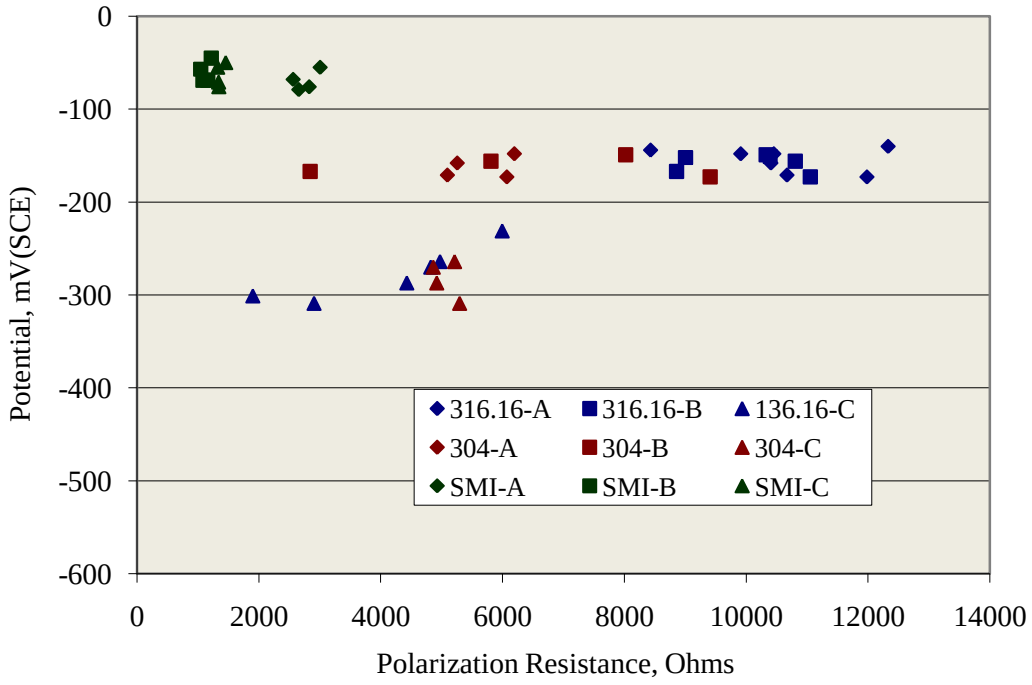

Figure 4-48: Plot of polarization resistance versus potential for field columns with high alloy reinforcements.

During each visit to the exposure site, specimens were inspected for visible indications of corrosion damage and cracking. It was determined that each of the three black bar field columns exhibited a crack in line with one of the four reinforcing bars after approximately one year exposure. At the end of two years, each of these cracks had grown, and the three 2101 field columns also exhibited cracks. Table 4-39 summarizes observations at these two times, and Figures 4-49 and 4-50 show photographs of cracking on a BB and 2101 reinforced field column specimen, respectively, after 735 days exposure.

4.2. Critical Chloride Threshold Concentration for Corrosion Initiation, C_T

4.2.1. Chloride Analyses

Tables 4-40 to 4-43 list [Cl^-] analysis results for samples acquired both by coring and milling of SDS specimens. In all cases, [Cl^-] determined from milled samples was from locations along the bar trace where the reinforcement remained passive. Figure 4-51 plots [Cl^-] versus depth for all cores, and Figures 4-52 to 4-54 show individual [Cl^-] versus depth data for both cores and millings for 3Cr12, MMFX-2, and 2101 specimens, respectively, for which these determinations were made. The core data generally indicate decreasing [Cl^-] with depth into concrete as expected with differences in individual profiles presumably a consequence of spatial concrete inhomogeneity. No trends are apparent from these data that suggest differences in concrete age at the time of coring was a factor. Scatter of milling [Cl^-] data for

Table 4-39: Summary of field observations for cracks that developed on field column specimens.

Exposure Time, days	Bar Type	Specimen Number	Description
363	BB	A	One crack (0.46 m long) extending from 0.71 to 1.17 m from the pile top.
		B	One crack (0.20 m long) extending from 0.63 to 0.83 m above mud line
		C	One crack (0.42 m long) with corrosion bleed-out extending from 0.43 to 0.85 m above mud line
735	BB	A	Crack had grown from 0.46 to 0.63 m in length.
		B	Crack had grown from 0.20 to 0.64 m in length.
		C	Crack had grown from 0.42 to 0.71 m in length.
	2101	A	One crack (0.13 m long) extending from 0.61 to 0.74 m from the pile top.
		B	Three cracks (0.20, 0.25, and 0.33 m long), each opposite a separate bar.
		C	Two cracks (0.11 and 0.13 m long), each opposite a separate bar.

Figure 4-49: Photograph of cracking on a BB reinforced field column after 735 days exposure.

Figure 4-50: Photograph of cracking on a 2101 reinforced field column after 735 days exposure.

Table 40: Listing of [Cl^-] results for black bar reinforced specimens, as acquired from coring.

Depth, m	Chloride Concentration					
	5-STD1-BB-1		5-STD1-BB-2		5-STD1-BB-3	
	kg/m^3	wt/o cem.	kg/m^3	wt/o cem.	kg/m^3	wt/o cem.
3.20E-03	11.31	4.08	13.20	4.77	11.47	4.14
9.60E-03	10.82	3.91	12.64	4.56	9.64	3.48
1.60E-02	9.42	3.40	9.22	3.33	7.28	2.63
2.24E-02	8.48	3.06	7.00	2.53	4.24	1.53
2.88E-02	6.00	2.17	0.10	0.03	2.13	0.77
3.52E-02	4.71	1.70	0.09	0.03	0.05	0.02
4.16E-02	3.05	1.10	0.09	0.03	0.00	0.00
4.80E-02	1.92	0.69	0.13	0.05	0.08	0.03
5.44E-02	0.12	0.04	0.07	0.02	0.03	0.01
6.08E-02	0.85	0.31	-0.02	-0.01	-0.06	-0.02

individual specimens is by a factor of 1.25 for 3Cr12 and 2101 specimens but 2.4 for MMFX-2; however, for individual MMFX-2 specimens the range is 1.1 to 1.4. Differences in coarse aggregate volume percentage (CAVP) in the powder samples acquired by milling and the relatively small sample size (1.0-1.5 g) were probably responsible. Invariable, [Cl^-] for milled samples exceeded that for cores. This is attributed to a combination of the bar obstruction[21] and CAVP[22,23] effects.

Table 41: Listing of [Cl^-] results for 3Cr12 reinforced specimens as acquired from (a) cores and (b) millings.

(a)

Depth, m	Chloride Concentration	
	5-STD1-3Cr12-2	
	kg/m^3	wt/o cem.
3.20E-03	8.98	3.24
9.60E-03	8.60	3.11
1.60E-02	7.22	2.61
2.24E-02	5.53	2.00
2.88E-02	3.44	1.24
3.52E-02	1.76	0.63
4.16E-02	0.49	0.18
4.80E-02	0.38	0.14
5.44E-02	0.10	0.03
6.08E-02	0.09	0.03

(b)

Bar Designation	Depth, m	Chloride Concentration	
		5-STD1-3Cr12-2	
		kg/m^3	wt/o cem.
L	2.49E-02	7.87	2.84
C	2.49E-02	9.80	3.54
R	2.49E-02	8.60	3.10

Table 4-42: Listing of [Cl^-] results for MMFX-2 reinforced specimens, as acquired from coring (a) and milling (b).

(a)

Depth, m	Chloride Concentration							
	5-STD1-MMFX-2-1		5-STD1-MMFX-2-2		5-STD1-MMFX-2-3		5-USDB-MMFX-2-1	
	kg/m^3	wt% cem.	kg/m^3	wt% cem.	kg/m^3	wt% cem.	kg/m^3	wt% cem.
3.20E-03	8.03	2.90	7.88	2.85	16.42	5.93	7.88	2.85
9.60E-03	10.27	3.71	8.62	3.11	17.17	6.20	8.45	3.05
1.60E-02	8.39	3.03	8.09	2.92	12.72	4.59	7.99	2.88
2.24E-02	6.64	2.40	6.49	2.34	9.58	3.46	5.66	2.04
2.88E-02	5.22	1.88	4.89	1.77	5.86	2.11	4.80	1.73
3.52E-02	3.84	1.39	3.82	1.38	2.78	1.00	3.44	1.24
4.16E-02	2.49	0.90	2.63	0.95	0.51	0.19	1.93	0.70
4.80E-02	1.35	0.49	2.02	0.73	0.13	0.05	0.62	0.22
5.44E-02	0.52	0.19	0.75	0.27	0.16	0.06	0.38	0.14
6.08E-02	0.11	0.04	0.11	0.04	1.30	0.47	0.29	0.10

(b)

Bar Designation	Depth, m	Chloride Concentration							
		5-STD1-MMFX-2-1		5-STD1-MMFX-2-2		5-STD1-MMFX-2-3		5-USDB-MMFX-2-1	
		kg/m^3	wt% cem.	kg/m^3	wt% cem.	kg/m^3	wt% cem.	kg/m^3	wt% cem.
L	2.49E-02	7.52	2.71	11.31	4.08	13.29	4.80	12.01	4.34
C	2.49E-02	6.94	2.50	16.33	5.90	11.83	4.27	8.46	3.06
R	2.49E-02	8.96	3.23	11.31	4.08	12.70	4.59	8.41	3.04

Table 4-43: Listing of [Cl^-] results for 2101 reinforced specimens, as acquired from coring (a) and milling (b).

(a)

Depth, m	Chloride Concentration			
	5-STD1-2101-1		5-STD1-2101-2	
	kg/m^3	wt% cem.	kg/m^3	wt% cem.
3.20E-03	12.28	4.43	8.37	3.02
9.60E-03	11.96	4.32	6.72	2.43
1.60E-02	9.84	3.55	5.54	2.00
2.24E-02	7.69	2.78	3.87	1.40
2.88E-02	5.71	2.06	1.73	0.63
3.52E-02	4.83	1.75	0.68	0.25
4.16E-02	2.74	0.99	0.02	0.01
4.80E-02	1.08	0.39	-0.01	-0.01
5.44E-02	-0.31	-0.11	0.02	0.01
6.08E-02	-0.27	-0.10	-0.05	-0.02

(b)

Bar Designation	Depth, m	Chloride Concentration			
		5-STD1-2101-1		5-STD1-2101-2	
		kg/m^3	wt% cem.	kg/m^3	wt% cem.
L	2.49E-02	12.74	4.60	10.77	3.89
C	2.49E-02	11.66	4.21	10.60	3.83
R	2.49E-02	10.23	3.69	11.60	4.19

4.2.2. Diffusion Coefficient and Chloride Threshold

Based upon the [Cl^-] data from individual cores (Tables 4-39 to 4-42), values for the effective diffusion coefficient, D_e, were calculated using a least squares fit to the one dimensional solution to Fick's second law (Equation 1-3) and are listed in Table 4-44. Using the average D_e ($2.59 \cdot 10^{-11}$ m^2/s), C_T was calculated for each top bar of all improved performance specimens using Equation 1-3, based upon T_i for each individual top bar and assuming C_s = 18 kg/m^3 (7.22 cement wt% basis). Figures 4-55 and 4-56 show Weibull CDF plots of C_T, where for the former C_T is in units of kg Cl^- per m^3 of concrete and in the latter wt% Cl^- referenced to cement. Similar to what was done for the T_i data, Table 4-45 lists C_T for each of the four steels at 2, 10, and 20 percent active and C_T(alloy)/C_T(BB) for 3Cr12, MMFX-2, and 2101. Values for the C_T ratio range from a low of 3.3 for 2101 at 20 percent active to a high of 4.8 for MMFX-2 at two percent active. These results are in general agreement with those of Clemeña and Virmani[24] who reported values for C_T(alloy)/C_T(BB) as 4.7-6.0 for MMFX-2 and 2.6-3.4 for 2101, also based upon slab experiments in 0.50 w/c concrete.

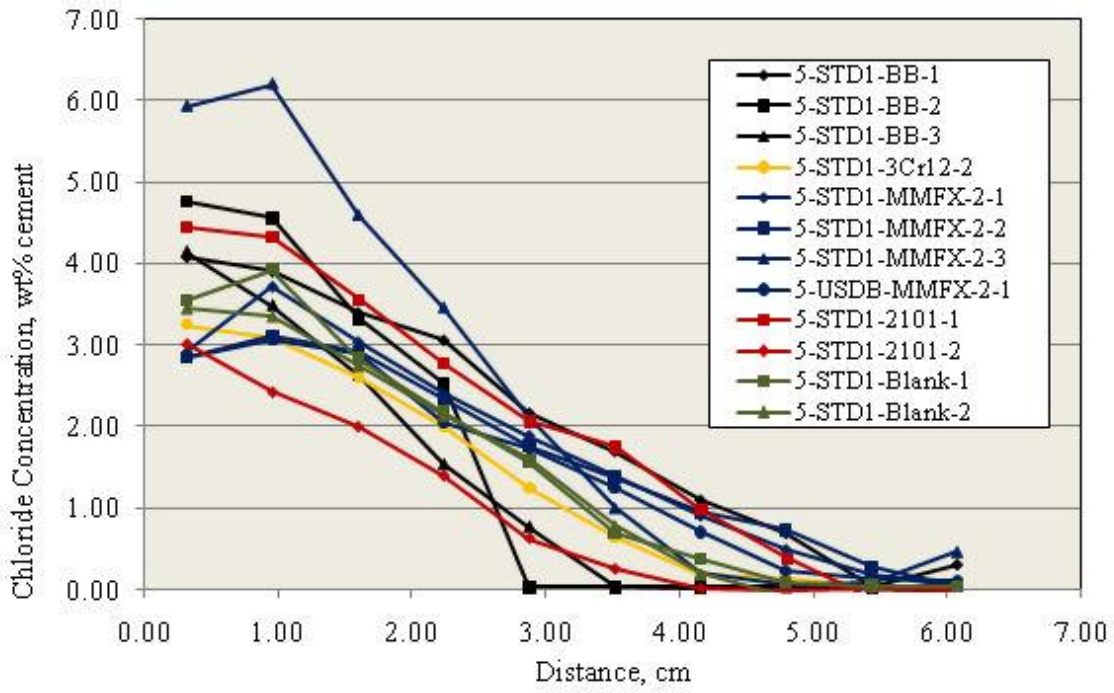

Figure 4-51: Chloride concentrations as a function of depth into concrete as determined from cores taken from the indicated specimens.

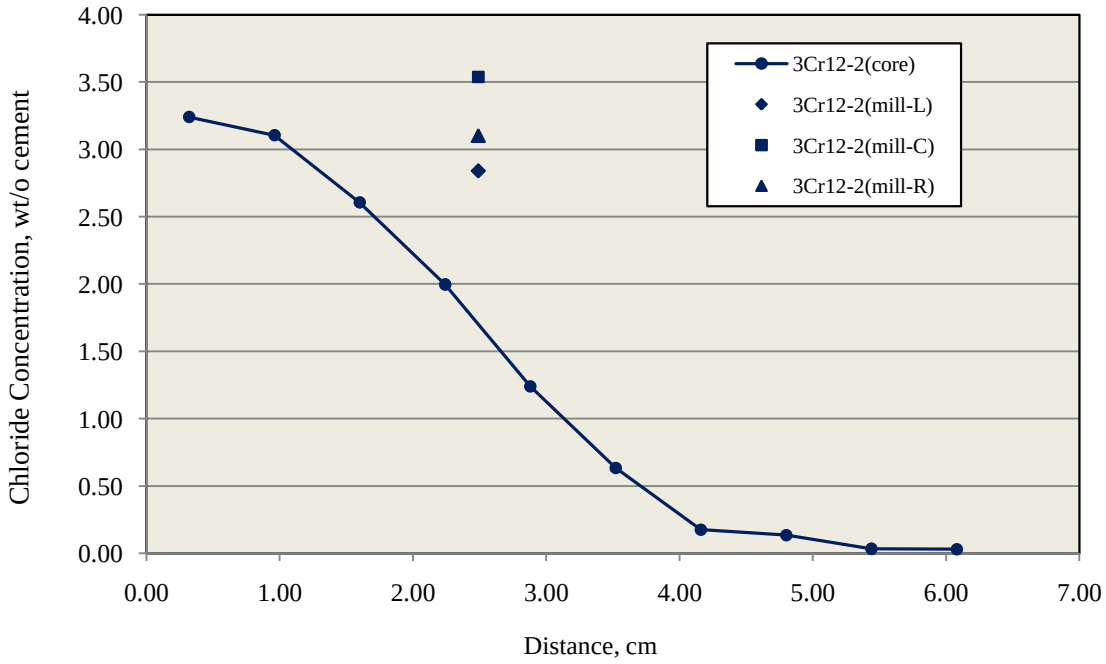

Figure 4-52: Chloride concentrations determined from a core and millings for specimen 5-STD1-3Cr12-2.

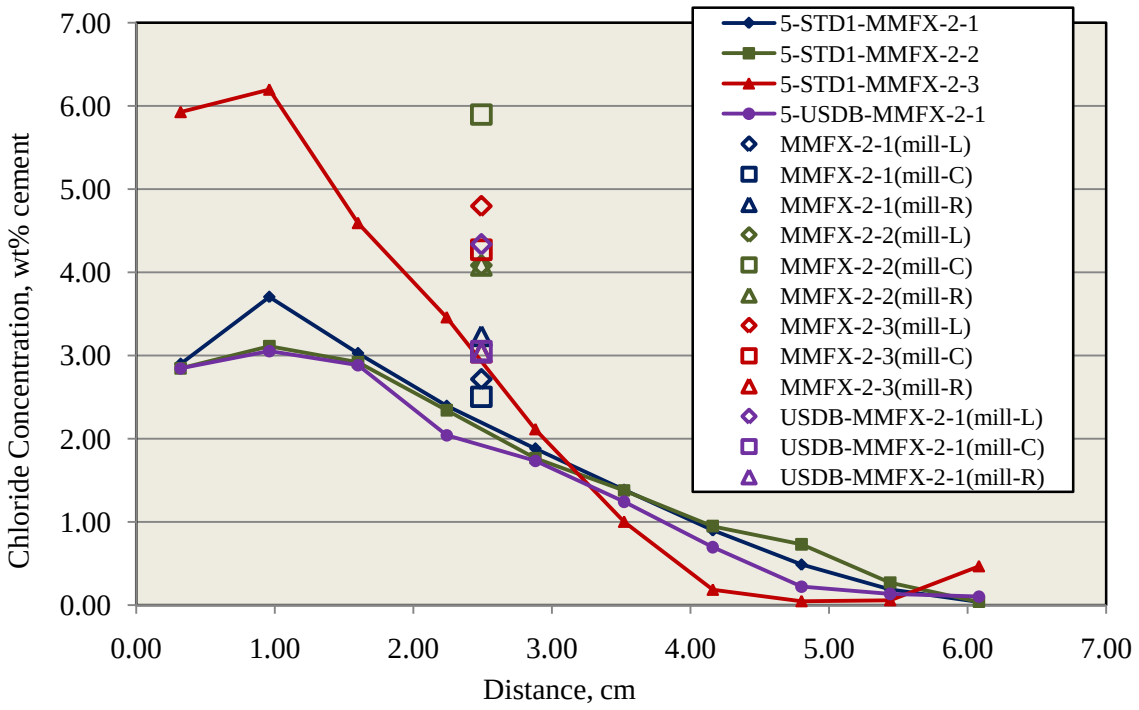

Figure 4-53: Chloride concentrations determined from a core and millings for MMFX-2 reinforced specimens.

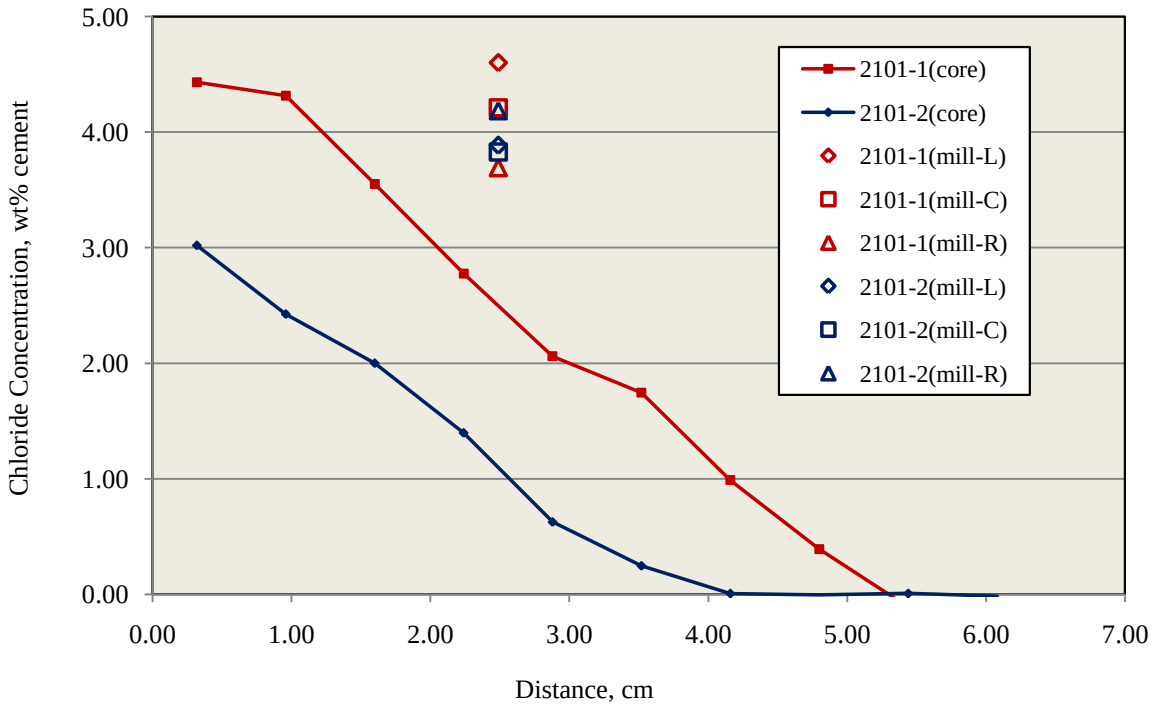

Figure 4-54: Chloride concentrations determined from a core and millings for 2101 reinforced specimens.

Table 4-44: D_e values calculated from core [Cl^-] data.

Specimen Number	D_e, m^2/s
BB-1	7.41E-11
BB-2	2.72E-11
BB-3	2.36E-11
3Cr12-1	2.60E-11
MMFX-2-1	1.56E-11
MMFX-2-2	1.93E-11
MMFX-2-3	1.78E-11
USDB-MMFX-2-1	1.60E-11
2101-1	1.95E-11
2101-2	2.03E-11
Average	2.59E-11

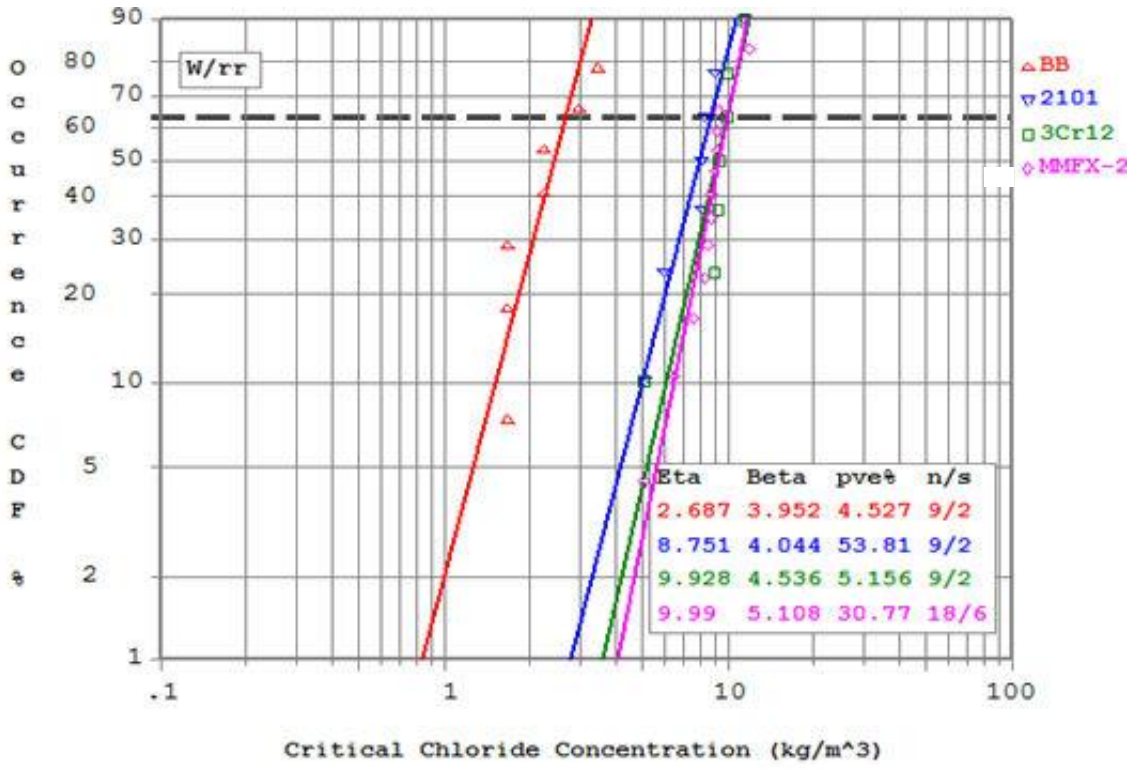

Figure 4-55: Weibull cumulative distribution of C_T in units of kg Cl^- per m^3 of concrete.

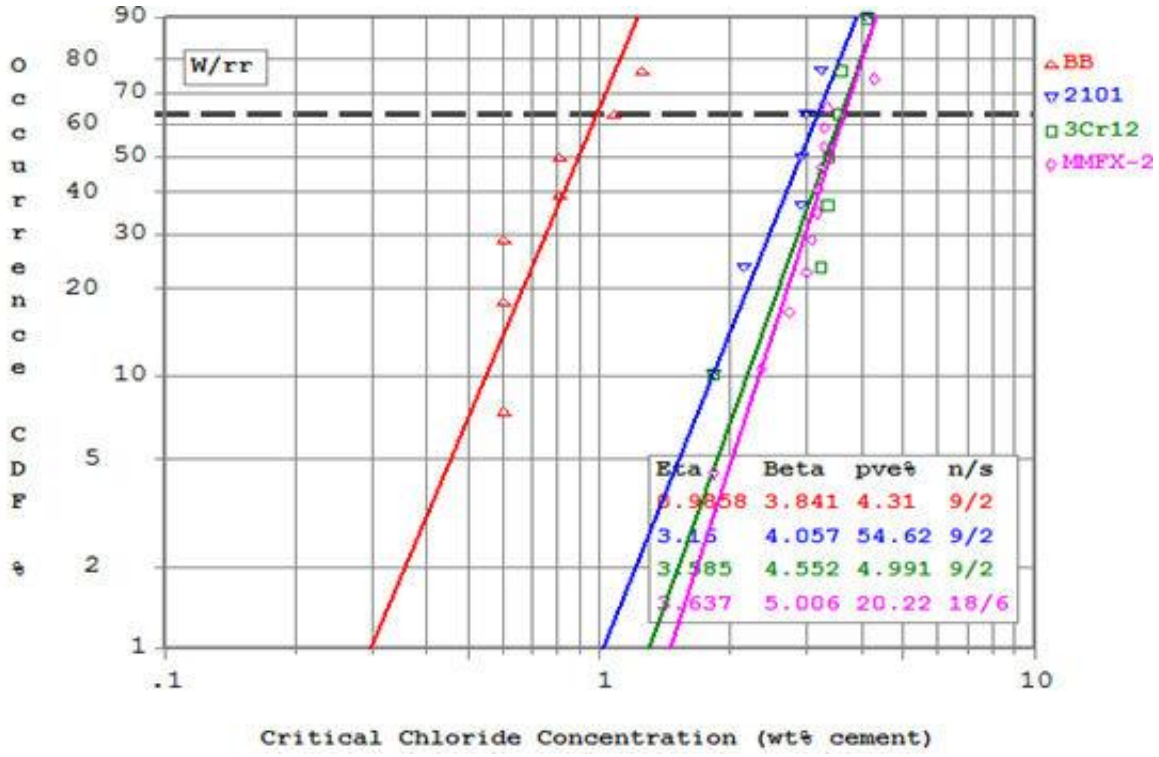

Figure 4-56: Weibull cumulative distribution of C_T in units of wt% Cl^- referenced to cement.

Table 4-45: Listing of C_T (kg/m^3) for the improved performance reinforcements and black bar and C_T(alloy)/C_T(BB).

Percent Active	Alloy				C_T(alloy)/C_T(BB)		
	BB	3Cr12	MMFX-2	2101	3Cr12	MMFX-2	2101
2	1.0	4.4	4.8	3.6	4.4	4.8	3.6
10	1.4	6.3	6.5	5.2	4.5	4.6	3.7
20	1.9	7.2	7.2	6.2	3.9	3.9	3.3

As noted above, minimal or no corrosion activity occurred for high alloy reinforcements except in conjunction with clad defects and perhaps crevices. Table 4-46 lists the five stainless steels in this category along with the time each was exposed and the corresponding [Cl^-] that is projected to be present at the bar depth based upon the diffusion analysis explained above (C_s = 18 kg/m^3 and $D_e = 2.59 \cdot 10^{-11}$ m^2/s). It is concluded that C_T for the individual bar types is greater than the indicated concentration.

4.3. Comparison of C_T from Concrete Exposures and Accelerated Aqueous Solution Experiments

In the initial Interim Report for this project,[19] an attempt was made to correlate C_T results from an accelerated aqueous solution test method with T_i data from Lot 1-3 reinforced concrete exposures. The

Table 4-46: Projected [Cl^-] at the bar depth for the different reinforcement types after the indicated times.

Table 4-46: Projected [Cl^-] at the bar depth for the different reinforcement types after the indicated times

Reinforcement Type	Exposure Time, days	[Cl^-], kg/m^3
316	1,726	13.9
304	440	10.2
2304	929	12.5
Stelax	1726	13.9
SMI	944	12.5

former method involved potentiostatic polarization at +100 mV (SCE) of ten identical specimens of each reinforcement in synthetic pore solution (0.05N NaOH and 0.30N KOH of pH ≈ 13.2-13.25) to which Cl^- was incrementally added. The results indicated a general correlation in the two data sets but with large scatter which may have resulted from absence of heat shrink on the reinforcement ends, as explained earlier. The possibility of such a correlation was revisited based upon results from the Set 5 SDS and MS specimen data reported above.

Figure 4-57 reproduces the aqueous solution accelerated C_T results reported previously, and Table 4-47 lists the mean and standard deviation of these data for each alloy. Figure 4-58 plots these data versus those from the SDS-STD1 slabs for 10 and 20 percent active and the mean. The accelerated test data indicate 2101 to have a highest C_T of the four reinforcements. The SDS data, on the other hand, indicate MMFX-2 and 3Cr12 to have the highest C_T, although the difference between these and 2101 is small and may be within experimental variability. However, the average accelerated test C_T data for 3Cr12 are about 60 percent below that for 2101 and MMFX-2. Figure 4-59 provides a similar plot for STD-MS specimens where accelerated test C_T data at 20 percent and mean active are plotted versus T_i for the concrete specimens. Arrows on the MMFX-2 and 2101 data connecting lines indicate that one or both of the two respective points are runouts. These results are similar to those for the SDS-STD1 specimens in Figure 4-58 in that the accelerated, aqueous solution results indicate CT for 3Cr12 specimens to be only slightly greater than for black bar and well below that for MMFX-2 and 2101, whereas Ti for 3Cr12 concrete specimens was among the highest vales recorded. It is concluded that the accelerated test method did not adequately project performance of 3CR12 reinforcement in concrete.

4.4. Specimen Dissections

4.4.1. SDS Specimens

Figures 4-60 is a photograph of a typical rebar trace upon dissection of specimen 5-STD1-BB-1 two

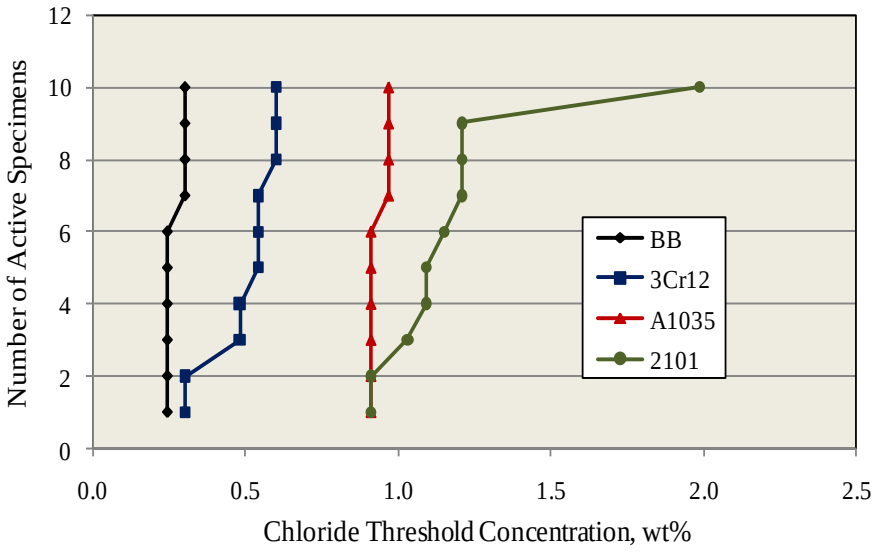

Figure 4-57: Previously reported chloride threshold concentrations as determined from aqueous solution potentiostatic tests.

Table 4-47: Listing of C_T data (wt%) from accelerated aqueous solution testing.

Alloy	Mean	St.Dev.
BB	0.26	0.03
3Cr12	0.50	0.11
MMFX-2	0.94	0.03
2101	1.18	0.31

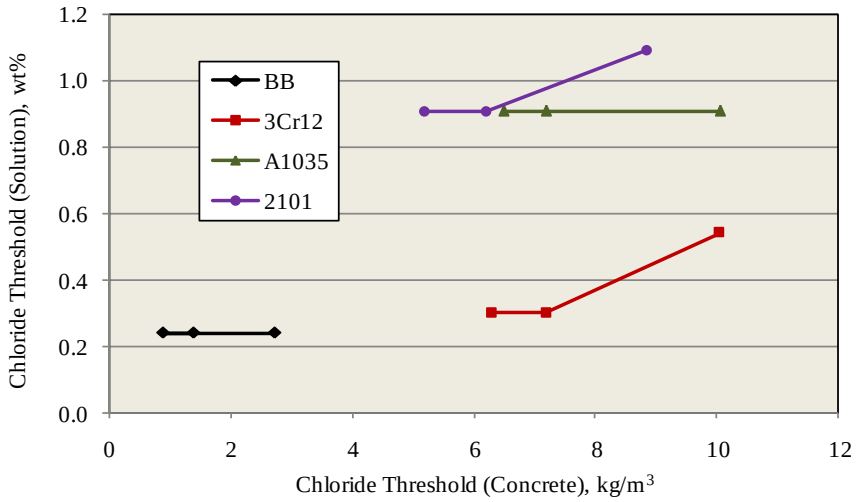

Figure 4-58: Plot of C_T determined from accelerated aqueous solution testing versus C_T from SDS concrete specimens (the three successive data points with increasing threshold of each alloy correspond to 10, 20, and mean percent activation).

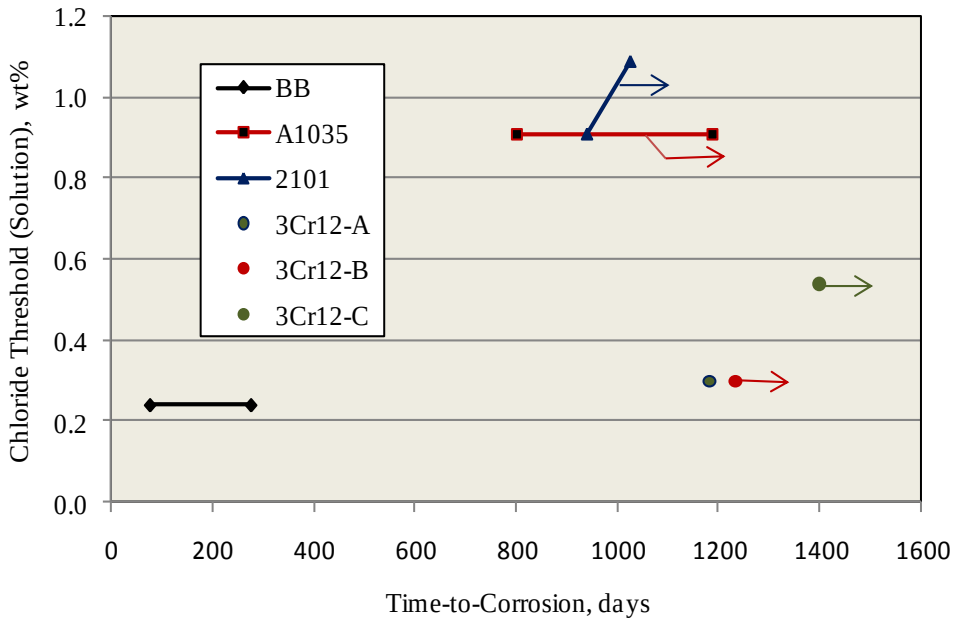

Figure 4-59: Plot of C_T determined from accelerated aqueous solution testing versus T_i for STD2-MS concrete specimens (the two successive data points with increasing T_i for BB, MMFX-2, and 2101 correspond to 20 percent active and mean C_T whereas the three 3Cr12 are the actual T_i values). Arrows indicate runouts.

Figure 4-60: Photograph of upper R bar trace of dissected specimen 5-STD1-BB-1 showing localized corrosion products (circled).

weeks after detection of macro-cell current, showing a relatively small area of corrosion product is apparent. Figure 4-61 shows an exceptional case where corrosion was more advanced prior to test termination. These observations are taken as confirmation of the experimental approach for defining T_i and C_T, as explained above.

Figure 4-61: Photograph of upper L bar trace of dissected specimen 5-STD1-BB-1 showing corrosion products.

In addition, dissections were performed on selected high performance reinforced specimens that either exhibited corrosion damage or were considered to potentially have corrosion. These are listed in Table 4-48 along with the exposure time at termination for each. Figures 4-62 shows a side view photograph of specimen 2-BCAT-316-1 prior to dissection. Corrosion products are apparent extending from the BB on the lower left, and a thin concrete crack emanates from this and extends to the lower center bar. No corrosion was apparent upon dissection on any of the three top bars (Figure 4-63); however, corrosion was extensive on the bottom black bars (Figure 4-64). The fact that corrosion appears most advanced at the bar ends indicates that absence of end sleeves was a contributing factor.

Figure 4-65 shows a photograph of specimen 2-CCNB-316-2 prior to dissection. Although corrosion products are minimal, the concrete was delaminated along the plane of the bottom bars because of corrosion induced cracking. Minor staining was apparent on top bars at locations beneath the simulated crack, as illustrated by the photograph in Figure 4-66. Concrete cracks that occurred during

Table 4-48: Listing of high alloyed specimens that were autopsied.

Specimen Number	Exposure Time, days
2-BCAT-316-1	1,669
2-CCNB-316-2	1,669
4-BCCD-SMI-1	944
6-BCAT-304-2	440
6-CCNB-304-1	440
6-CVNC-SMI-1	440

Figure 4-62: Photograph of specimen 2-BCAT-316-1 prior to dissection (red markings identify specimen for removal).

dissection are seen here extending from the simulated crack. Figure 4-67 shows typical condition of the bottom bars, which were heavily corroded.

Figures 4-68 and 4-69 show typical appearance of top and bottom bars, respectively, from specimen 4-BCCD-SMI-1. In the former case, corrosion has occurred locally at several of the 3 mm diameter holes drilled through the cladding. Corrosion on the bottom black bars was extensive, as seen in Figure 4-69.

Figure 4-63: Photograph of top R bar and bar trace of specimen 2-BCAT-316-1 subsequent to dissection.

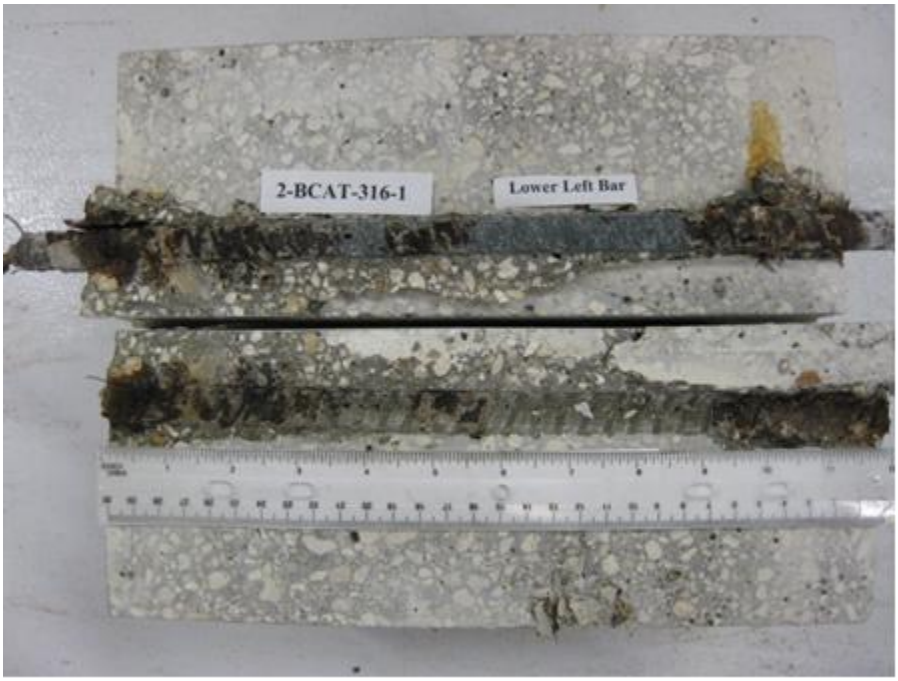

Figure 4-64: Photograph of lower L BB and bar trace of specimen 2-BCAT-316-1 subsequent to dissection.

Figure 4-65: Photograph of specimen 2-CCNB-316-2 prior to dissection (red markings identify specimen for removal).

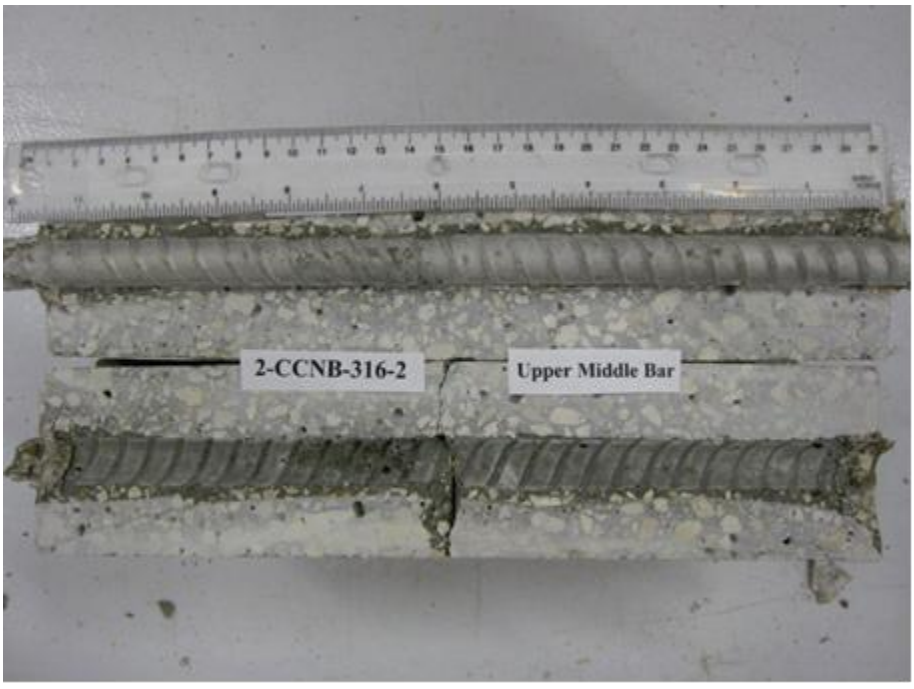

Figure 4-66: Photograph of top C bar and bar trace of specimen 2-CCNB-316-2 subsequent to dissection.

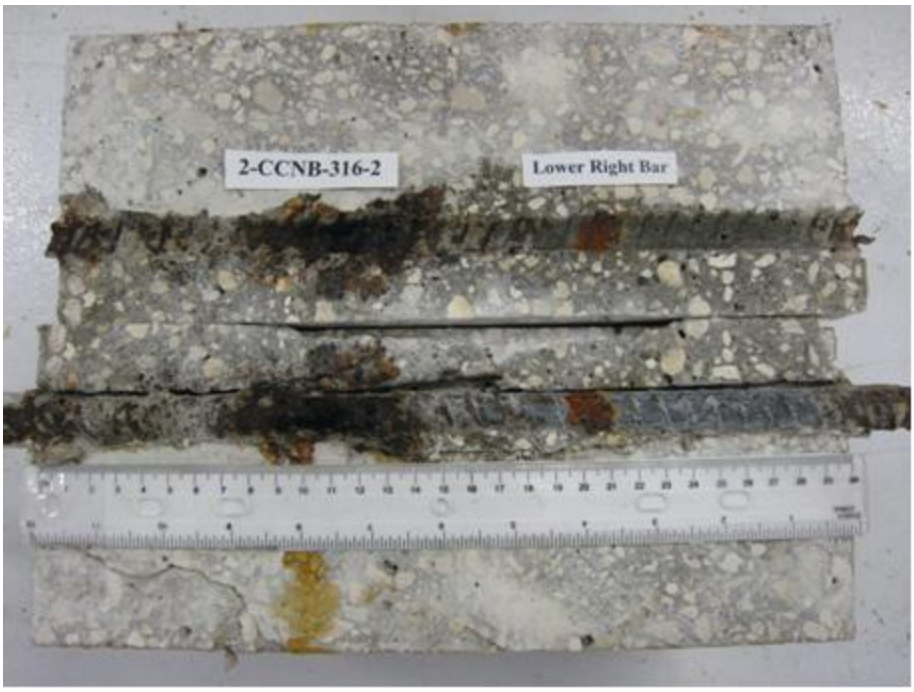

Figure 4-67: Photograph of lower R bar and bar trace of specimen 2-CCNB-316-2 subsequent to dissection.

Figure 4-68: Photograph of top L bar and bar trace of specimen 4-BCCD-SMI-1 subsequent to dissection.

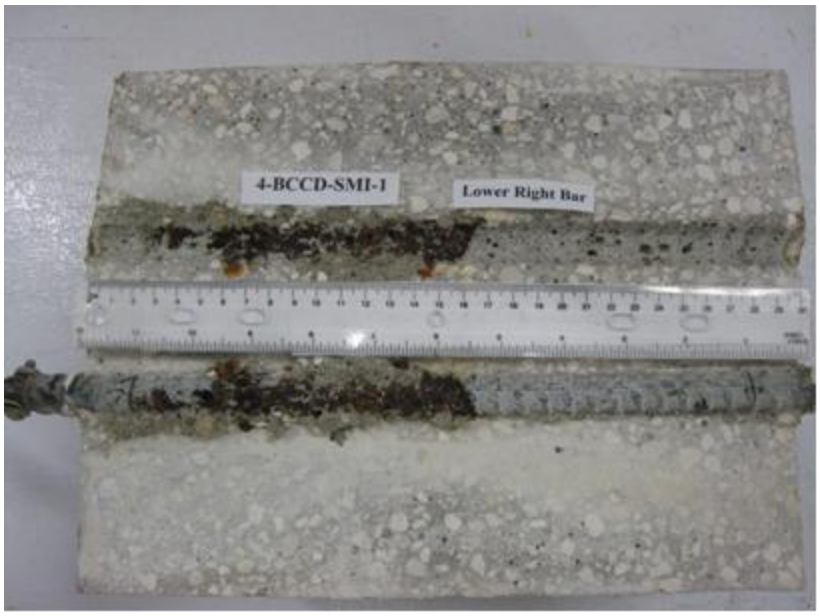

Figure 4-69: Photograph of lower R bar and bar trace of specimen 4-BCCD-SMI-1 subsequent to dissection.

Figures 4-70 to 4-72 show appearance of the three top bars of specimen 4-CSDB-SMI-1 subsequent to dissection. Here, corrosion ranges from slight product staining (Figure 4-72) to extensive at the crack base (Figure 4-71). Corrosion at several of the 3 mm diameter holes drilled through the cladding is also apparent away from the crack in Figures 4-70 and 4-71.

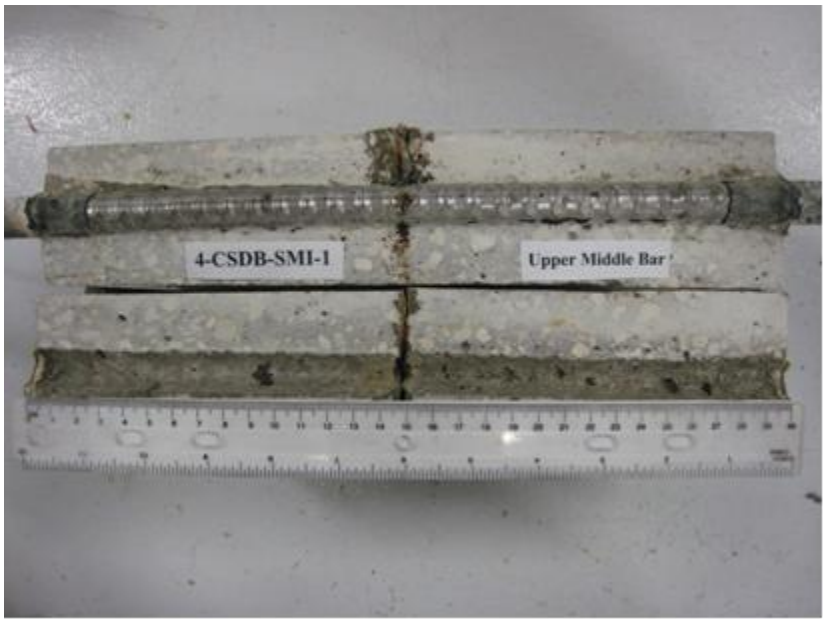

Figure 4-70: Photograph of top C bar and bar trace of specimen 4-CSDB-SMI-1 subsequent to dissection.

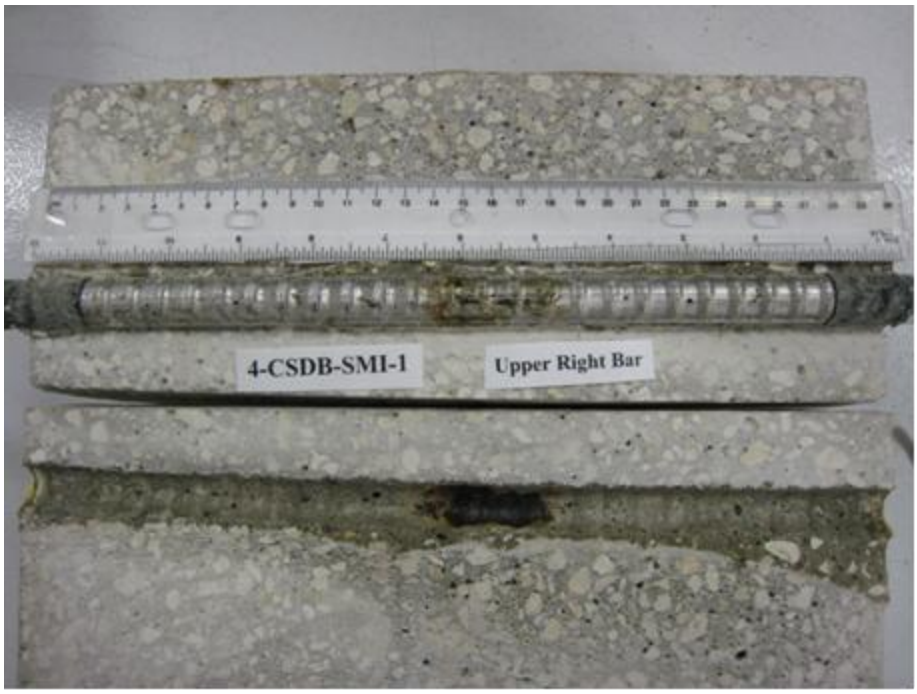

Figure 4-71: Photograph of top R bar and bar trace of specimen 4-CSDB-SMI-1 subsequent to dissection.

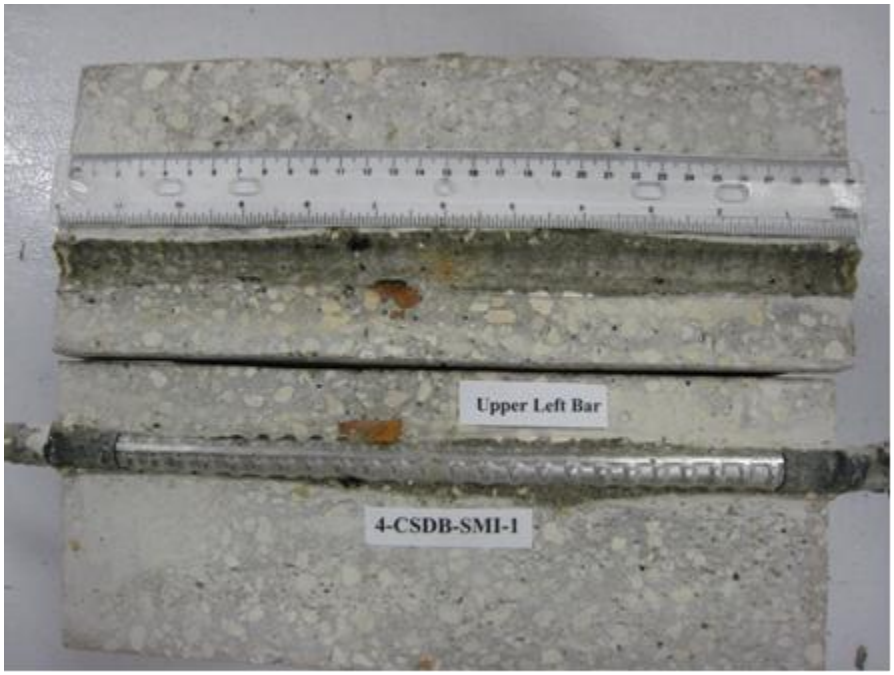

Figure 4-72: Photograph of top L bar and bar trace of specimen 4-CSDB-SMI-1 subsequent to dissection.

External appearance of specimen 6-BCAT-304-2 prior to dissection was characterized by corrosion product staining from each of the three bottom bars as shown in Figure 4-73. No corrosion was apparent on any of the top bars (Figure 4-74) and ranged from nil to extensive on the bottom BB (Figure 4-75). Likewise, no top bar corrosion was apparent on any of the three top bars of specimen 6-CCNB-304-1 (Figure 4-76), and only minor corrosion was evident on the bottom BB (Figure 4-77).

Figure 4-78 shows a photograph of specimen 6-CVNC-SMI-1 after dissection where corrosion of the exposed carbon steel core is apparent (circled areas).

4.4.2. MS Specimens

All but one of the improved performance MS specimens have been terminated and dissected; and as indicated by Figures 4-7 to 4-10, this was done well after corrosion had initiated. Table 4-49 reproduces T_i for these specimens from Table 4-10 and also lists time at termination and time under test subsequent to T_i (propagation time, T_p). In general, observations regarding corrosion of bars from dissected MS specimens were in accord with those for SDS specimens, as discussed above. This is illustrated by Figures 4-79 to 4-81, which show photographs of the three STD1-MMFX-2 specimens. For these and other specimens, the extent of corrosion tended to correspond to the length of T_p. Exceptions to this and examples of interest are discussed below.

Figure 4-73: Photograph of specimen 6-BCAT-304-2 prior to dissection (red markings identify specimen for removal).

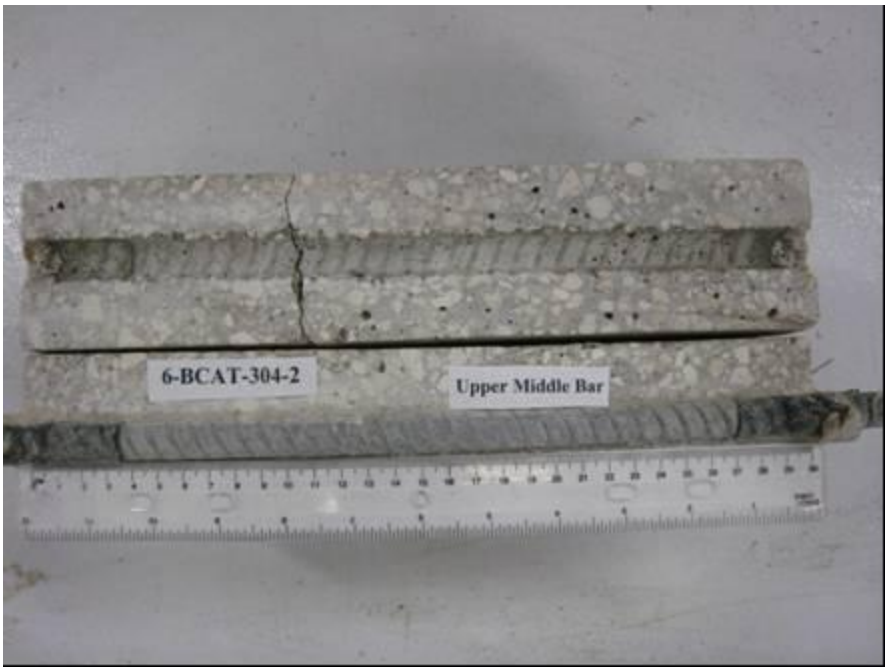

Figure 4-74: Photograph of top C bar and bar trace of specimen 6-BCAT-304-2 subsequent to dissection.

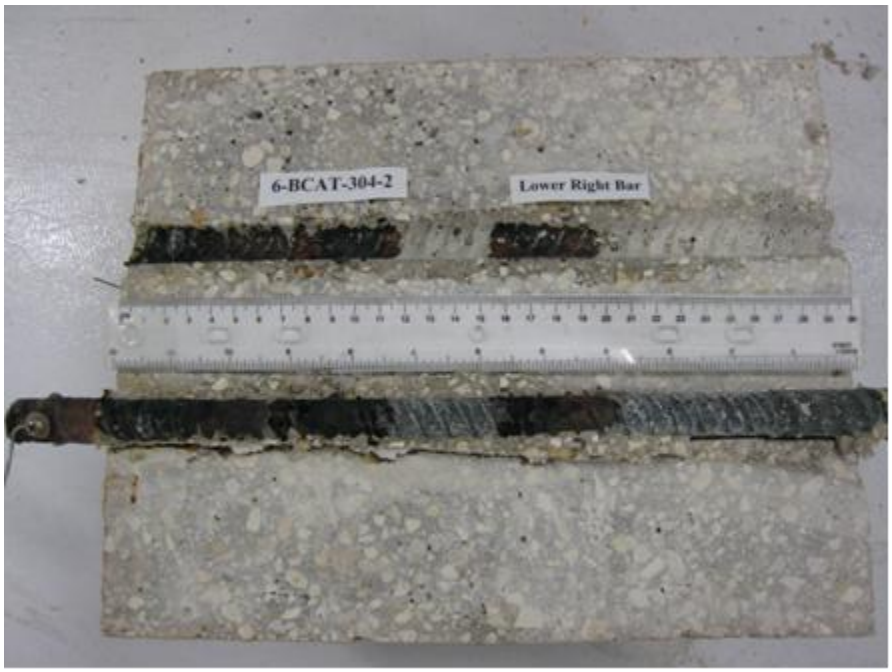

Figure 4-75: Photograph of lower right BB and bar trace of specimen 6-BCAT-304-2 subsequent to dissection.

Figure 4-76: Photograph of top C bar and bar trace of specimen 6-CCNB-304-1 subsequent to dissection.

Figure 4-77: Photograph of lower left BB and bar trace of specimen 6-CCNB-304-1 subsequent to dissection.

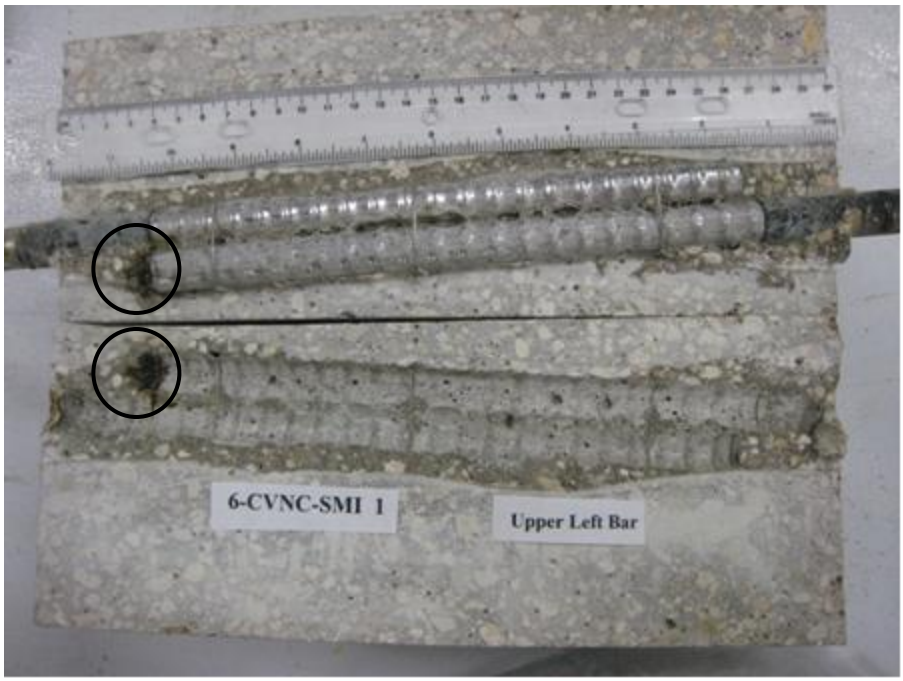

Figure 4-78: Photograph of top L bar pair and bar pair trace of specimen 6-CVNC-SMI-1 subsequent to dissection.

Table 4-49: Listing of T_i, propagation time (T_p), and total time of testing for BB and improved performance bars in MS specimens.

Reinforcement Type	Time-to-Corrosion, days			Time-at-Termination, days			Propagation Time, days		
	A	B	C	A	B	C	A	B	C
BB	97	147	182	474	474	474	377	327	292
3Cr12	121	212	488	474	474	505	353	262	17
MMFX-2	211	68	230	474	474	474	263	406	244
2101	295	215	144	474	474	474	179	259	330

Figure 4-82 shows a photograph of specimen MS-CBDB-MMFX-2-A after sectioning above the top bent bar. A small amount of corrosion products is apparent at what was the crack base and also near the bar ends. Figure 4-83 shows the top bar from this specimen after removal from the concrete.

Corrosion was also disclosed on several of the high performance bars in MS specimens. Figure 4-84 provides one example where a small amount of corrosion products is apparent on the bar trace of specimen MS-CTNB-316-C (circled region) subsequent to dissection. The attack was beyond the footprint of the ponding bath and appeared to have resulted from crevice corrosion beneath the heat shrink

Figure 4-79: Photograph of top bar and bar trace for specimen MS-MMFX-2-A.

Figure 4-80: Photograph of top bar and bar trace for specimen MS-MMFX-2-B.

Figure 4-81: Photograph of top bar and bar trace for specimen MS-MMFX-2-C.

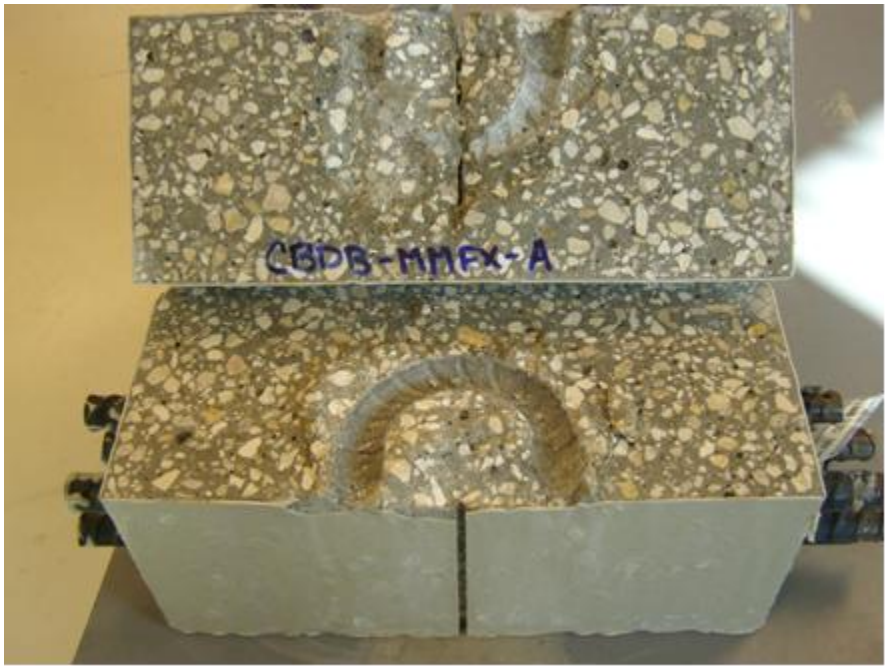

Figure 4-82: Photograph of top bent bar trace in concrete for specimen MS-CBDB-MMFX-2-A.

Figure 4-83: Photograph of top bent bar from specimen MS-CBDB-MMFX-2-A after removal.

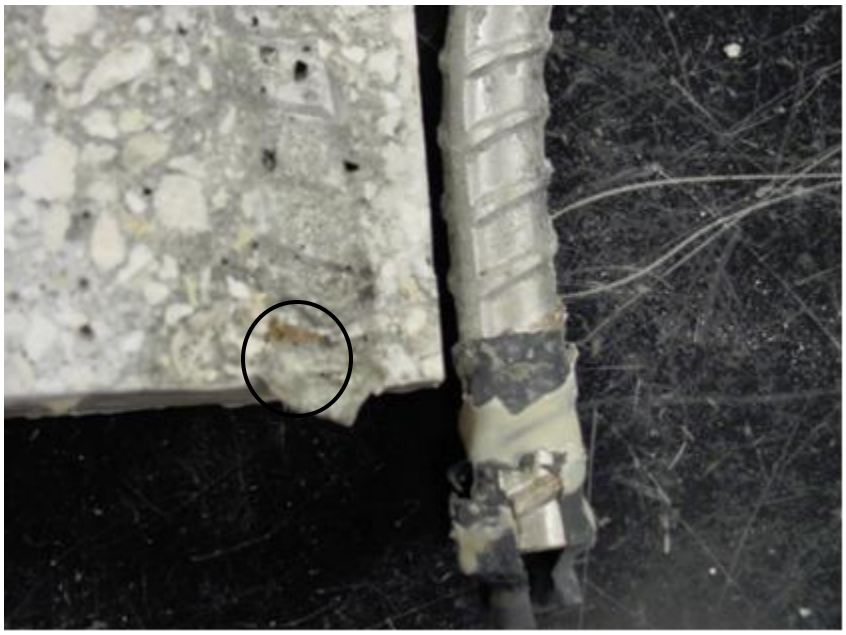

Figure 4-84: Photograph of top bent bar from specimen MS-BTNB-316-C after removal.

sleeve. Figure 4-85 shows similar corrosion that occurred on the top bent bar of specimen MS-CBNB-316-B. Lastly, Figures 4-86 and 4-87 show corrosion at intentional 3mm diameter cladding defects on

Figure 4-85: Photograph of localized corrosion on the top bent bar from specimen MS-CBNB-316-B.

Figure 4-86: Photograph of corrosion at an intentional clad defect on the top bent bar from specimen MS-CBDB-SMI-B.

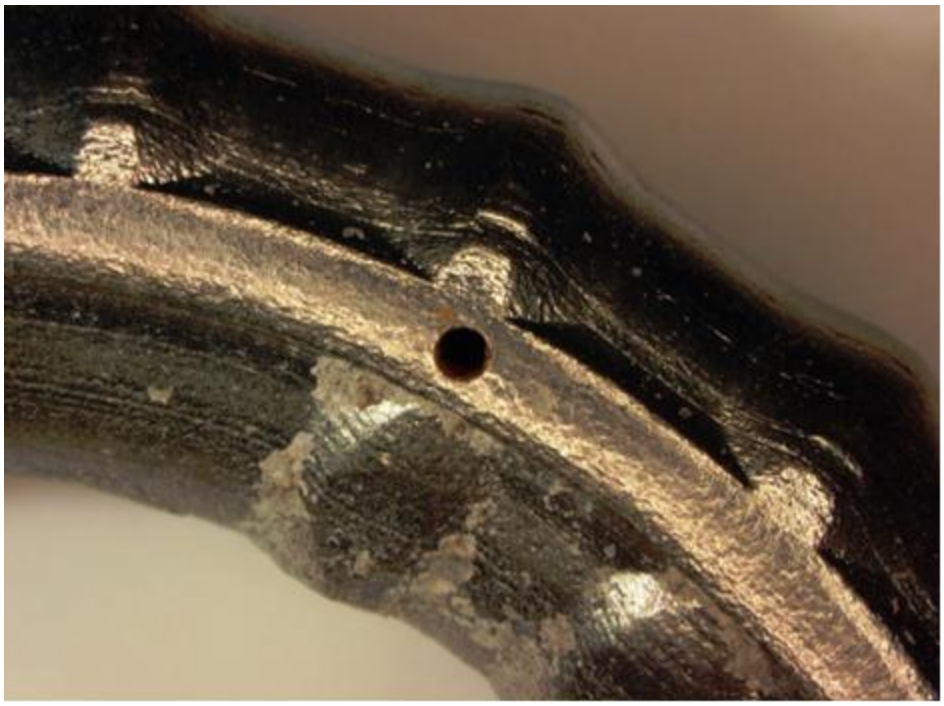

Figure 4-87: Photograph of corrosion at a second intentional clad defect on the top bent bar from specimen MS-CBDB-SMI-B.

the top bent bar of specimen MS-CBDB-SMI-B. The defect in the first case was directly beneath the simulated crack, whereas the one in the second was away from the crack in sound concrete.

4.4.3. 3BTC Specimens

Only two 3BTC specimens (3BTC-STD2-BB-B and 3BTC-STD2-2101-C) were dissected. Photographs of these are shown in Figures 4-88 and 4-89, respectively. In both cases, concrete surface cracks were present in line with the longer bars. Corrosion is apparent upon the exposed bars and corrosion products along the rebar trace beginning about 200 mm above the specimen base.

4.5. Comparison of Results from Different Specimen Types

Table 4-50 lists the mean T_i for BB, 3Cr12, MMFX-2, and 2101 reinforced STD1-SDS and -MS specimens and the percent difference. Although caution must be exercised in placing too much emphasis on the differences because results for the MS specimens are based on data for only three bars of each type, still T_i was shorter for MS specimens than for SDS in the case of three of the four rebar types. This is in spite of the fact that the former were ponded with three wt% NaCl and the latter with 15 wt%. Apparently, the rate controlling step(s) for corrosion initiation were more rapid with the MS specimen

Figure 4-88: Photograph of specimen 3BTC-STD2-BB-B after sectioning and opening along the two longer bars.

Figure 4-89: Photograph of specimen 3BTC-STD2-2101-C after sectioning and opening along the two longer bars.

design. Further, comparison of the T_i results shows that for the SDS specimens, T_i(alloy)/T_i(BB) was in the approximate range 2-4 for 3Cr12, MMFX-2, and 2101 (Figure 4-4 and Table 4-2) at 2-20 percent active, whereas for the MS (Figures 4-11 and 4-12) this ratio was near unity (within the range of expected experimental scatter). Thus, there was a lack of agreement between the two specimen types for ranking these reinforcements.

Table 4-50: Comparison of T_i values for STD1-SDS and –MS specimens.

	Mean Time-to-Corrosion, days			
	BB	3Cr12	MMFX-2	2101
SDS	77	459	435	296
MS	142	274	170	218
Percent Difference, MS to SDS	46	-68	-156	-36

The STD2 mix design was common to both MS and 3BTC specimens, for which T_i(alloy)/T_i(BB) for MS MMFX-2 specimens was 3.4 to >5.7 and for 2101 2.7 to >4.8 (Table 4-12). For 3BTC specimens, these same ratios were 3.7-6.4 and 2.1-3.6, respectively (Table 4-33), indicating general mutual agreement. Data scatter precluded including results for 3Cr12 in this analysis. For 3BTC STD3 specimens, the ratios were 1.2 to 3.3 for 3Cr12 and 0.9 to 3.4 for MMFX-2 (Table 4-34) at 2, 10, and 20 percent active. For this class of specimens, experimental scatter for 2101 rebar specimens was sufficiently large that an analysis could not be performed. These results indicate that the T_i enhancement realized by these improved performance reinforcements was greater the higher the concrete quality, since greatest T_i(alloy)/T_i(BB) occurred for the STD2 mix design and least for STD1. The STD1-MS specimens apparently provided too severe an exposure to reveal differences between these reinforcements.

As noted in the preceding section, macro-cell current subsequent to T_i was greater for MS than SDS specimens, suggesting that the relative severity of the MS type specimen applies to the propagation as well as initiation phases.

4.6. Example Analysis

An example projection was made of T_i for a concrete member reinforced with 1) black steel and 2) an improved performance CRR with properties within the range reported above. In doing this, the C_T data in Table 4-45 at 2, 10, and 20 percent active for BB and the average for 3Cr12 and MMFX-2 were employed (see also, Figure 4-55). These data are based upon exposures in STD1 concrete; however, for high quality

concrete greater enhancement of C_T for CRR relative to that for BB should result as noted above, in which case an analysis based upon the above choices should be conservative.

An effective Cl^- diffusion coefficient of 10^{-12} m^2/s, concrete cover of 63 mm, and a surface [Cl^-] of 18 kg/m^3 were assumed. The solution to Fick's second law (Equation 1-3) was then employed to calculate T_i for each C_T. This yielded times-to-corrosion of 17 and 43 years for BB and the CRR, respectively, at two percent active and 24 and 86 years, respectively, at 20 percent. Figure 4-90 provides a plot of these results.

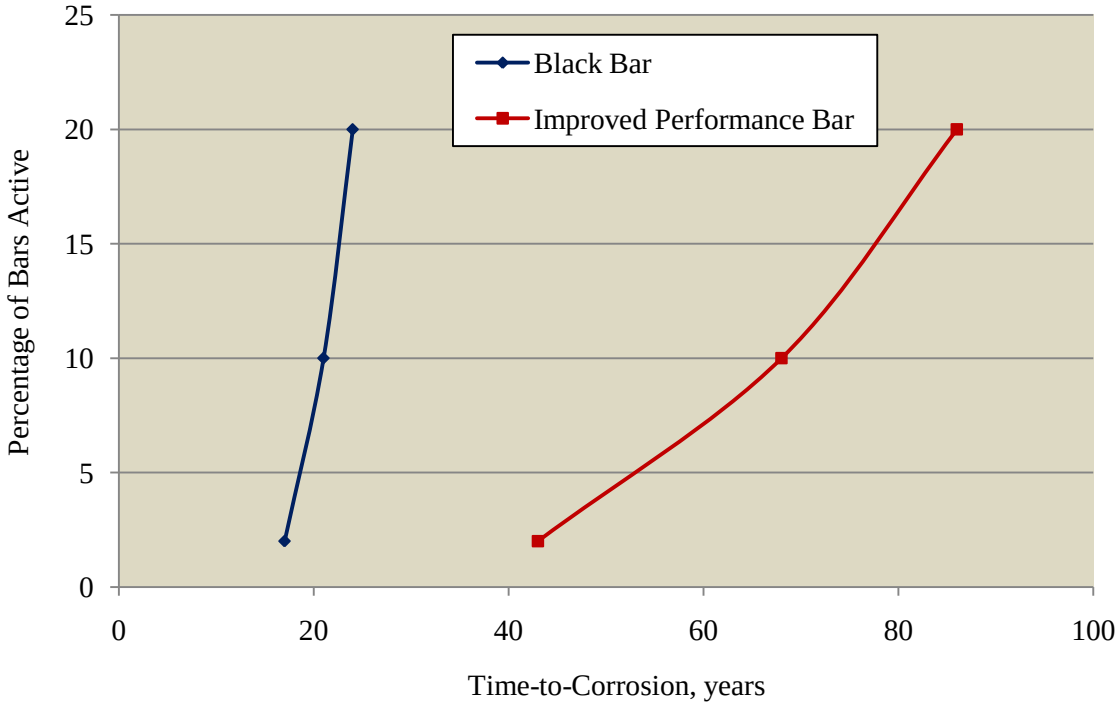

Figure 4-90: Comparison of Ti at 2-20 percent activation for BB and improved performance bar under conditions relevant to actual structures.

A limitation of this analysis is that it is based on mean values for D_e, x, and C_s, whereas, if fact, each of these parameters conforms to a distribution. Consequently, corrosion initiation at locations where D_e or x (or both) are less than the mean values and/or C_s is greater must be anticipated at lesser times than projected by Figure 4-90. Also, the calculation is based on one-dimensional diffusion; however, a lesser T_i should occur for bars at concrete corners where diffusion is in two dimensions.[25] Also assumed is that enhanced Cl^- transport along concrete cracks is not significant. This shorter T_i compared to what is projected in Figure 4-90 should be offset to some extent by the conservative choice for C_T for high performance concrete, as noted above.

Time-to-corrosion calculations were not possible for the high performance reinforcements since T_i and C_T for these exceeded the exposure times and chloride concentrations, respectively, that occurred. Certainly, C_T for these was greater than for the improved performance reinforcements such that maintenance free service life should extend well beyond the values in Figure 4-90. In addition, the high performance bars provide greater confidence and margin for error.

5.0. CONCLUSIONS

Two specimen types, termed simulated deck slab (SDS) and macro-cell slab (MS), that were intended to represent a reinforced concrete bridge deck exposed to deicing salts and two, termed 3-bar tombstone column (3BTC) and field column (FC), that represented a marine substructure element, were exposed to chlorides. Reinforcements included stainless steels 316 (UNS-S31603), 304 (UNS-S30400), 2304 (UNS-S32304), 2101 (ASTM A955-98), 3Cr12 (UNS-S41003), two types of 316 clad black bar (AASHTO MP 13M/MP 13-04), and MMFX-2 (ASTM A1035), and black bar (ASTM A615), the last being for baseline comparison purposes. Bars were cast into concrete specimens in the as-received condition, which was either as-rolled or pickled depending upon the source, after solvent cleaning. Specimen configurations included a) bent bars, b) bars wire brushed, c) presence of a simulated concrete crack or crevice between adjacent bars (or both), d) corrosion resistant rebar top layer and black bar lower (SDS and MS specimens), and e) intentional defects in the case of clad bars. These were in addition to a standard specimen for which all bars were straight and none of the above conditions were present (standard condition for MS specimens was with bars wire brushed). Three concrete mix designs, termed STD1 (high permeability), STD2 (intermediate permeability), and STD3 (permeability between that of STD1 and STD2), were employed. All specimens were tested outdoors with the SDS and FC being fully exposed and the MS and 3BTC sheltered (a second set of MS specimens was tested under controlled temperature and relative humidity (25^{o}C and 50 percent, respectively)). The following conclusions were reached:

1. The reinforcements other than black bar were classified into two groups as either improved performance or high performance, where alloys in the former category initiated corrosion during the project time frame and ones in the latter did not, at least in cases for specimens of the standard configuration (STD – all straight bars in the as-received condition without crevices and no simulated concrete cracks). Improved performers were 3Cr12, MMFX-2, and 2101 (black bar reinforced specimens were included in this grouping also for reference purposes), and the other alloys were high

performers. These alloys ranked according to time for corrosion to initiate as BB < 2101, < 3Cr12, MMFX-2.

2. No SDS specimens with 304 and clad or solid 316 bar, other than ones with black bar lower layer, initiated corrosion; and no macro-cell currents were detected during the exposure period. Test times for the 304 reinforced specimens were as long as 440 days and for the 316 ones 1,726 days. The MS and 3BTC specimens with these reinforcements exhibited both anodic and cathodic macro-cell current "spikes" to as high as 16 μA for 316 and 0.8 μA for 304; however, net mass loss associated with these was calculated as nil. In general, macro-cell current activity was less for 304 than for 316, in contrast to the normally perceived better corrosion resistance of the latter alloy. Also, macro-cell currents were less for specimens in the higher quality concrete (STD2) compared to the lower (STD1). Corrosion potentials remained relatively positive, and the macro-cell current activity was not considered indicative of corrosion initiation.

3. For improved performance and black bar reinforcements, time-to-corrosion, T_i, and the Cl^- concentration to initiate corrosion, C_T, were distributed over a range rather than being a discrete value. Chloride threshold for corrosion initiation of 3Cr12 and MMFX-2 reinforced SDS specimens was about four times greater than for black bar ones and slightly less than four times greater in the case of 2101. Weibull analysis of the $[Cl^-]$ data indicated that at two percent of bars being active, C_T for black bar was 1.0 kg/m^3 or 0.36 wt% cement and for 3Cr12 and MMFX-2 4.0 kg/m^3 or 1.44 wt% cement. On the other hand, there was little difference in T_i between each of the three improved performance reinforcements compared to black bar for STD1 MS specimens. For STD2 MS specimens, however, T_i for MMFX-2 and 2101 was from 3.4 to more than 5.7 times greater than for black bar (limited data precluded this determination for 3Cr12). For 3BTC specimens, this ratio for these same two alloys (MMFX-2 and 2101) in STD2 concrete was from 2.1 to 6.4. The results imply that the enhanced corrosion resistance that is derived from these reinforcements relative to black bar increases with increasing concrete quality.

4. Time-to-corrosion for STD1 MS specimens was shorter than for SDS specimens, and macro-cell currents for the former were an order of magnitude or more greater than for the latter. Apparently, the MS type specimen and exposure condition provided a more severe testing of the reinforcements than did the SDS. The finding that T_i for improved performance bars was about the same as for black bar in STD1 MS specimens but about four times greater in SDS ones (see Conclusion 3) may have resulted because of this.

5. The MS specimens exposed outdoors exhibited shorter T_i and greater macro-cell current activity than identical ones tested at constant temperature and relative humidity. The former condition is thought to have fostered a higher level of sorptive moisture and Cl^- transport such that the corrosion threshold was reached in a shorter time.

6. The FC specimens that were exposed in the tidal zone on the Intracoastal Waterway at Crescent Beach, Florida, with improved performance and black bar reinforcements, typically initiated corrosion within the first several days. This is thought to have resulted because of poor concrete quality and possibly cracks that provided direct water access to the reinforcement. With one exception, the high performance reinforcements have remained passive. The exception was a 316 reinforce column that was damaged during installation.

7. A ranking of these corrosion resistant reinforcements based on Cl^- threshold failed to correlate with results from previously performed short-term potentiostatic tests in synthetic pore solution to which chlorides were incrementally added. This calls into question the usefulness of this and perhaps other accelerated test methods for evaluating corrosion resistant alloys for service as reinforcements in concrete.

8. In specimens with lower layer black bars, corrosion of the black bars was often extensive and to the point that delaminations occurred along the plane of these bars. If a corrosion resistant steel upper bar layer is to be combined with a black bar lower one, the concrete should be of sufficient quality and with limited or no cracks such that Cl^- concentration at the lower bars remains below the black steel threshold for the design life of the structure.

9. Corrosion occurred at defects and unprotected embedded bar ends for stainless clad reinforcements. The likelihood that this attack or corrosion at clad defects will ultimately cause concrete cracking and spalling is uncertain but probably depends on corrosion morphology, geometry, and rate factors. Corrosion induced concrete cracking and spalling probably result in time if the surface area of the exposed core carbon steel and extent of attack exceed a certain value. Further research is needed to define this threshold.

10. Life-cycle cost analyses for corrosion resistant reinforcements should consider not only differences in C_T and macro-cell current but also the possibility that concrete cover can be reduced. This, in turn, could lower superstructure and, hence, substructure size and weight and lower initial cost

accordingly. Also, lower cover may reduce the number and width of concrete cracks, leading to less corrosion of top bars and to lower maintenance costs in the long-term.

11. An example analysis was performed that calculated T_i of a concrete structure reinforced with, first, black bar and, second, an improved performance rebar. The calculation was based on an effective Cl^- diffusion coefficient of 10^{-12} m^2/s, concrete cover 63 mm, surface $[Cl^-]$ 18 kg/m^3, and C_T for the corrosion resistant alloy as four times greater than for black bar (see Conclusion 3). The analysis yielded T_i for black bar as ranging from 17 to 24 years and for the corrosion resistant alloy from 43 to 86 years as the percentage of bars being active increased from two and 20 percent. Limitations of this analysis are that, first, the above input parameters for the calculation are mean values, whereas these are, in fact, distributed such that corrosion will initiate at some locations sooner than projected and, second, enhanced inward Cl^- migration along any concrete cracks was not considered. Further, corrosion should initiate sooner at concrete corners since inward Cl^- diffusion is from two directions here rather than just one. On the other hand, the above difference in C_T for black compared to the improved performance bar was based on data acquired from highly permeability concrete; however, this difference is expected to be greater for concrete with a Cl^- diffusion coefficient of 10^{-12} m^2/s.

12. The C_T and macro-cell current data indicate that the intended service life of major reinforced concrete bridge structures (75-100 years) can confidently be achieved with the solid high performance reinforcements that were investigated. This may be the case also for the clad reinforcements provided there is adequate control of surface defects and bar ends are protected. This same service life may result also with the improved performance bars provided design and construction quality control are good and concrete cracking is minimal but with a lesser degree of confidence and margin for error compared to the high performance reinforcements.

6.0. BIBLIOGRAPHY

[1] Virmani, Y.P, Jones, W.R., and Jones, D.H., *Public Roads,* Vol. 84(3), 1984, p. 96.

[2] Koch, G.H., Brongers, P.H., Thompson, N.G., Virmani, Y.P, and Payer, J.H., "Corrosion Costs and Prevention Strategies in the United States," Report No. FHWA-RD-01-156, Federal Highway Administration, Washington, DC, March, 2002.

[3] Yunovich, M, Thompson, N.G., and Virmani, Y.P., "Life Cycle Cost Analysis for Reinforced Concrete Bridge Decks," Paper No. 03309 presented at CORROSION/03, March 10-14, 2003, San Diego.

[4] Stratfull, R.F., Jurkovich, W.J., and D.L. Spellman, Transportation Research Record, Vol. 539, 1975, p. 50.

[5] Code of Federal Regulations, Section 650.305, "Frequency of Inspections," U.S. Government Printing Office, April 1, 2002 Revision, Washington, DC.

[6] Tutti, K., "Corrosion of Steel in Concrete", Report No. 4, Swedish Cement and Concrete Research Institute, Stockholm, 1982.

[7] Hausman, D.A., "Steel Corrosion in Concrete," *Materials Protection*, Vol. 6, No. 11, p. 19, 1967.

[8] Glass, G.K. and Buenfeld, N.R., "Chloride Threshold Levels for Corrosion Induced Deterioration of Steel in Concrete," Paper No. 3 presented at RILEM International Workshop on Chloride Penetration into Concrete, Oct. 15-18, 1995, Saint Rémy-les-Chevreuse.

[9] Sagűés, A.A., "Modeling the Effects of Corrosion on the Lifetime of Extended Reinforced Concrete Structures," *Corrosion*, Vol. 59, p. 854, 2003.

[10] Torres-Acosta, A.A. and Sagűés, A.A., "Concrete Cover Cracking with Localized Corrosion of the Reinforcing Steel," Proc. 5th CANMET/ACI Intl. Conf. on Durability of Concrete, SP-192, Ed. V.M. Malhotra (American Concrete Institute, Farmington Hills, MI), p. 591, 2000.

[11] Stafford, R.T., "Epoxy Coated Rebars," *Parking*, March-April, 1973, p. 39.

[12] Clifton, J.R., Beehgly, H.F., and Mathey, R.G., "Non-Metallic Coatings for Concrete Reinforcing Bars," Report No. FHWA-RD-74-18, Federal Highway Administration, Washington, DC, Feb., 1974.

[13] Virmani, Y.P. and Clemeña, G.G., "Corrosion Protection: Concrete Bridges," Report No. FHWA-RD-98-088, Federal Highway Administration, Washington, DC, Sept., 1998.

[14] Powers, R.G. and Kessler, R., "Corrosion Evaluation of Substructure, Long Key Bridge," Corrosion Report No. 87-9A, Florida Department of Transportation, Gainesville, FL, 1987.

[15] Powers, R.G., "Corrosion of Epoxy-Coated Rebar, Keys Segmental Bridges Monroe County", Report No. 88-8A, Florida Department of Transportation, Gainesville, FL, August, 1988.

[16] Zayed, A.M. and Sagűés, A.A., "Corrosion of Epoxy-Coated Reinforcing Steel in Concrete," Paper No. 386 presented at CORROSION/89, New Orleans, LA, April 21, 1989.

[17] Gustafson, D.P., "Epoxy Update," *Civil Engineering*, Vol. 58, No. 10, p. 38, 1988.

[18] Hartt, W.H., Powers, R.G., Leroux, V., and Lysogorski, D.K., "A Critical Literature Review of High-Performance Reinforcements in Concrete Bridge Applications," Report No. FHWA-HRT-04-093, Federal Highway Administration, Washington, DC, July, 2004.

[19] Hartt, W.H., Powers, R.G., Lysogorski, D.K., Liroux, V., and Virmani, Y.P., "Corrosion Resistant Alloys for Reinforced Concrete," Report No. FHWA-HRT-07-039, Federal Highway Administration, Washington, DC, July, 2007.

[20] ASTM C192-04, "Standard Practice for making and Curing Concrete Specimens in the Laboratory," Annual Book of Standards, American Society for Testing and Materials, West Conshohocken, PA.

[21] Kranc, S.C., Sagűés, A.A. and Presuel-Moreno, F. "Decreased Corrosion Initiation Time of Steel in Concrete Due to Reinforcing Bar Obstruction of Diffusional Flow," *ACI Materials Journal*, Vol. 99, No.1, p. 51, 2002.

[22] Yu, H. and Hartt, W.H. "Effect of Reinforcement and Coarse Aggregates on Chloride Ingress into Concrete and Time-to-Corrosion: Part I—Spatial Chloride Distribution and Implications," *Corrosion*, Vol. 63, p. 843, 2007.

[23] Yu, H., Himiob, R.J. and Hartt, W.H., "Effect of Reinforcement and Coarse Aggregates on Chloride Ingress into Concrete and Time-to-Corrosion: Part II—Spatial Distribution of Aggregates," *Corrosion*, 63, p. 924, 2007.

[24] Clemeña, G.G. and Virmani, Y.P., "Comparing the Chloride Resistances of Reinforcing Bars," *Concrete International*, p. 39, Nov., 2004.

[25] Sagüés, A.A., Kranc, S.C., Presuel-Moreno, F., Rey, D., Torres-Acosta, A., and Yao, L., "Corrosion Forecasting for 75-Year Durability Design of Reinforced Concrete," Report No. BA502 submitted to Florida Department of Transportation by University of South Florida, December 31, 2001.